The Pore-level Investigation of Phenomena Affecting the Recovery of Oil with Gas Assisted Gravity Drainage

by

© Hossein Khorshidian

A Thesis submitted to the

School of Graduate Studies

in partial fulfillment of the requirements for the degree of

Doctor of Philosophy

Faculty of Engineering and Applied Science

Memorial University of Newfoundland

May 2018

St. John's Newfoundland

ABSTRACT

Gas Assisted Gravity Drainage (GAGD) is an effective method of oil recovery that can be implemented injecting gas in the crest of reservoirs and producing oil from lower zones. GAGD is controlled by the interaction between capillary, gravitational and viscous forces, which depend on parameters of the operation, porous medium, and fluids. In this research, the performance of GAGD under various conditions was investigated by visualizing the flow of fluids at the pore-level to understand phenomena affecting the recovery of oil. A new pore network micromodel with an improved capillary continuity was developed that provides a transparent porous medium for studying the interplay between capillary, gravitational and viscous forces. The visualization of fluids' interfaces helped with the characterization of GAGD performance under various conditions. Results of the studies imply that the porous medium heterogeneities caused the gas-front to bypass oil in smaller pores surrounded by larger pores. The bypassed oil could flow in the form of thick films in fine capillaries of porous media upon a subsequent enhancement of the gas-oil capillary pressure due to the effect of gravity on the gas-oil differential density. In the presence of mobile water, a better GAGD performance was obtained under oil-wet conditions as the hydraulic continuity of oil under water-wet conditions can be arrested by the residual water in small pores and fine capillaries of a porous medium. Although the recovery of oil at earlier times after a gas-breakthough was higher under oil-wet conditions, extending the duration of GAGD resulted in a high oil recovery under water-wet conditions upon an effective reduction of the residual water saturation. In post-waterflood GAGD, increasing the production rate resulted in the instability of the gas-front and the reduction of oil recovery at gas-breakthrough because of viscous pressure

drops and capillary pressure associated with the flow of oil and water from trailing zones toward leading zones of the gas-front. Experimental results suggest that both oil-wet and water-wet reservoirs are excellent candidates for the implementation of post-waterflood GAGD. However, higher rate of oil drainage with less water production can be expected from early stages of the process in oil-wet reservoirs. Under water-wet conditions, although the production rate of oil is initially low, a very low residual oil saturation can be obtained after an effective reduction of the water saturation.

ACKNOWLEDGEMENTS

I would like to acknowledge my supervisors, Dr. Lesley James and Dr. Stephen Butt, for their enlightening guidance, kind assistance, constructive recommendations, and financial support in this research.

I would like to thank Petroleum Research Newfoundland and Labrador (PRNL), Research and Development Corporation of Newfoundland and Labrador (RDC), Hibernia Management and Development Company (HMDC), Natural Sciences and Engineering Research Council of Canada (NSERC), and Faculty of Engineering and Applied Science at Memorial University of Newfoundland for their financial support of this research.

I also would like to thank all members of Hibernia EOR Research Group who assisted me in this research.

Dedication

This thesis is dedicated to my beloved wife, Samaneh, and our kind parents, sisters and brothers for their endless love, kind passion and devotion.

Table of Contents

List of Tables

List of Figures

List of Symbols, Nomenclature or Abbreviations

Acronyms

EOR: Enhanced Oil Recovery

GAGD: Gas Assisted Gravity Drainage

OOIP: Original Oil in Place

Latin Letters

B: Pixel Blue Component Value

C_{go}: Mean Curvature at the Gas-Oil Interface (m^{-1})

g: Gravity Acceleration ($m.s^{-2}$)

G: Pixel Green Component Value

H: Vertical Distance (m)

i: Iteration Number

L: Vertical Length of a Film-Flow Path

N_B: Total Blue Pixels

N_R: Total Red Pixels

N_T: Total Pixel Number

N_W: Total White Pixels

P_{cgo}: Gas-Oil Capillary Pressure (Pa)

P_{cgo}^{f}: Gas-Oil Capillary Pressure in Gas-front (Pa)

P_{cgw}: Gas-Water Capillary Pressure in a Constricted Pore (Pa)

P_{cgw}^{L}: Gas-Water Capillary Pressure in leading Zones of Gas-front (Pa)

P_{cgw}^{T}: Gas-Water Capillary Pressure in Trailing Zones of Gas-front (Pa)

P_o: Oil Pressure (Pa)

P_g: Gas Pressure (Pa)

PV: Pore Volume (ml)

r: Radius of Curvature

ΔP_{vis}: Viscous Pressure Drop (Pa)

R: Pixel Red Component Value

S_{co}: Oil Spreading Coefficient

Sg: Gas Saturation

So: Oil Saturation

Sw: Water Saturation

T_G: Green Threshold Value

v: Average Displacement Velocity (m/sec)

X: Red and Blue Colour Calibration Parameter

ΔP_{vis}^{film}: Viscous Pressure Drop of Film Flow (Pa)

Greek Letters

$\Delta\rho_{go}$: Gas-Oil Differential Density ($kg.m^{-3}$)

$\Delta\rho_{gw}$: Gas-Water Differential Density ($kg.m^{-3}$)

μ_w: Water Viscosity (Pa.sec)

σ_{go}: Gas-Oil Interfacial Tension ($mN.m^{-1}$)

σ_{gw}: Gas-Water Interfacial Tension ($mN.m^{-1}$)

σ_{ow}: Oil-Water Interfacial Tension ($mN.m^{-1}$)

Φ: Micromodel Surface Porosity

Ψ: Half of the Cone Angle in a Conical Capillary

θ: Contact Angle

List of Appendices

Chapter 1 : Introduction and Overview

1.1. Gas Assisted Gravity Drainage

Primary oil recovery driven by the natural energy of reservoirs is often less than 20% due to the reduction of the reservoir pressure.[1] Therefore, a variety of improved and enhanced oil recovery methods have been developed to assist the production of oil, such as the waterflood (sometimes with the polymer or chemical additives) and gas injection (miscible or immiscible) processes. Main Objectives of oil recovery operations are to:

- repressurize the reservoir;
- increase the volumetric sweep efficiency; and
- minimize the residual oil saturation in the swept zone.[2]

The performance of an oil recovery method is affected by the characteristics of the rock and fluids in reservoirs, such as:

- the presence of faults, fractures, and pore-scale heterogeneities;
- the wettability and permeability of rocks;
- the composition, density, viscosity, and interfacial tension of fluids; and
- the relative permeability, and capillary pressures.[2]

In addition, operational parameters, such as the location of wells, production rates, the composition of injected fluids, and reservoir pressure can influence the performance of an oil recovery method.[3]

An oil reservoir is typically formed by trapping of oil in a porous and permeable formation (e.g., sandstone and carbonated rocks) that is sealed by an overlying formation

with a low permeability (e.g. shale and salt).[4] The presence of a seal above an oil reservoir provides a favourable geometry for a vertical gas injection from the crest of the reservoir to push the oil toward the production well without leaking into neighbouring formations. The injection of gas at the top of a reservoir is called Gas Assisted Gravity Drainage (GAGD), as schematically shown in Figure 1-1. The gas injection can help maintain the reservoir pressure[5] and control of a possible water encroachment from an active aquifer below the pay zone toward the production wells.[6] In addition, the injected gas may dissolve into the oil and improve the overall recovery factor due to increase of oil volume.[7] Field GAGD projects, such as Ryckman Creek, Overthrust Belt, Hawking Dexter, and West Hackberry resulted in high ultimate oil recoveries ranging from 50% to 90% of the original oil in place (OOIP).[6, 8]

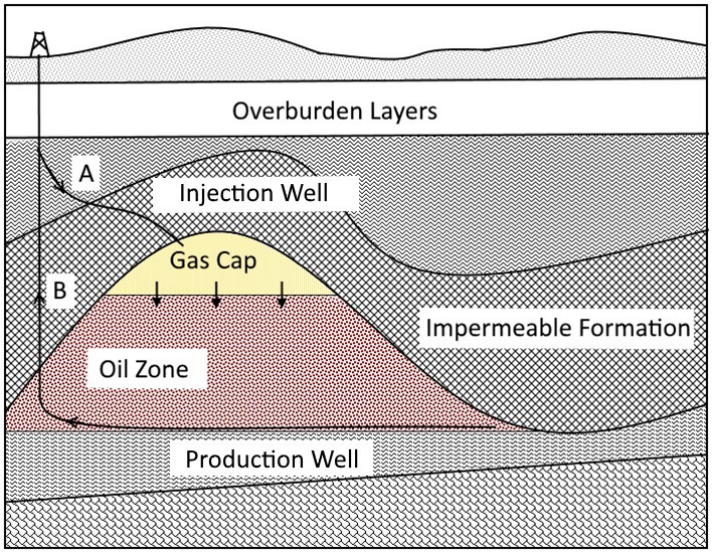

Figure 1-1. Schematic of Gas Assisted Gravity Drainage (A: injection well, B: production well).

A drainage process is mainly affected by the capillarity in porous media.[9] The capillary pressure is defined as the differential pressure between two fluids that form an interface in

a pore (or a capillary). In the displacement of oil by gas (two-phase flow), gas is often the non-wetting phase and oil is the wetting phase. The gas-oil capillary pressure (P_{cgo}) is defined by Eq. 1.1,[9]

$$P_{cgo} = P_g - P_o \tag{1.1}$$

where P_g is the gas pressure, and P_o is the oil pressure. Figure 1-2 shows a meniscus formed at the interface between oil and gas in a conical capillary. When gas displaces oil toward the corner of the capillary, the process is drainage. The reverse process is an imbibition, which is the displacement of a non-wetting phase by the wetting phase. The radius of curvature at the interface (r) can be calculated using Eq. 1.2,[9]

$$r = \frac{R}{\cos(\theta + \psi)} \tag{1.2}$$

where R is the diameter of the capillary where the interface is formed, ψ is the half of the cone angle, and θ is the contact angle.

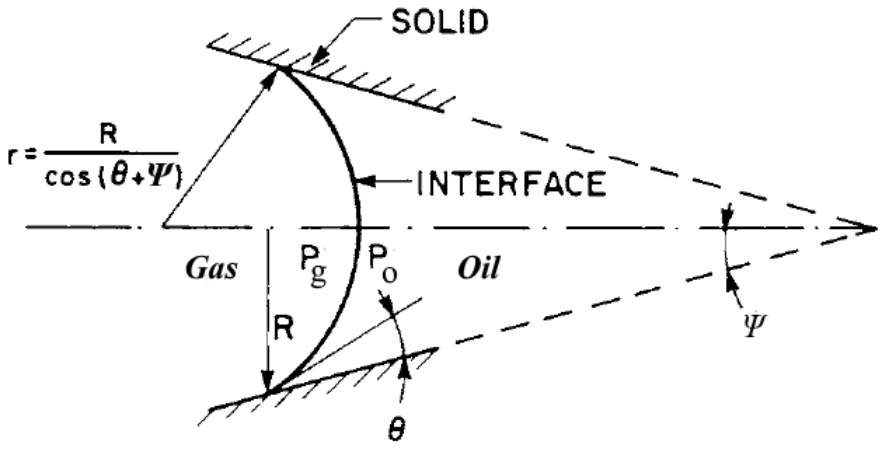

Figure 1-2. Gas-Oil Interface in a Conical Capillary (Adapted from Porous media: Fluid Transport and Pore Structure[9]).

The corresponding capillary pressure, based on the Young-Laplace equation,[9] can be shown by Eq. 1.3,

$$P_{cgo} = \frac{2\sigma_{go}R}{cos(\theta + \psi)} \tag{1.3}$$

where σ_{go} is the gas-oil interfacial tension. Eq. 1.3 implies that the gas-oil capillary pressure is higher when the gas-oil interfacial tension is greater, and the size of a pore and contact angle are smaller. The drainage of oil by gas is accompanied by a lower effort when the corresponding capillary pressure is lower. Therefore, the gas-front follows high permeable zones, larger pores and fractures as least resistant paths.[9] Reservoir heterogeneities negatively affect the stability of the gas-front. In GAGD, gravity counteract this instability.[10] The effect of gravity on the gas-oil differential density helps with the flow of the residual oil from undrained zones to lower elevations, promoting gas-oil differential pressure (capillary pressure) at geater elevations. However, viscous and capillary forces in trailing zones often create a resistant for the drainage of oil from higher to lower elevations. The balance between driving and resisting forces controlls the oil drainage rate.

In GAGD, capillary, gravitational, and viscous forces play important roles in the recovery of oil.[10] The presence of heterogeneties reduces the macroscopic sweep efficiency of the gas-front,[11] and gravity contributes to the stability of a gas-front. The microscopic sweep efficiency of the gas-front can also be reduced by the presence of pore-scale heterogeneities that promote the retention of oil in small pores surrounded by larger pores due to capillarity. Gravity drainage also improves the pore-scale sweep efficiency

overcoming capillary forces with the promotion of the gas-oil differential pressure at higher elevations.[12] Furthermore, gravity can help with the control the adverse mobility ratio of gas, viscous fingering under either immiscible or miscible conditions.[13] GAGD also be performed post-waterflood for displacing the waterflood residual oil, thus increasing the final recovery of oil.[14-17] The main priority of GAGD over horizontal gasfloods under immiscible conditions is the subsequent recovery of oil from regions initially bypassed with the gas-front. The bypassed oil may find an appropriate path to flow downward in the form of oil-films.

Oil-films may be found in forms of: a) a thick film that is formed in the corner of fine capillaries, and b) a thin film that is formed due to spreading on the surface of solid grains or water. The thick oil-film allows the flow of oil in the corner of fine capillaries (corner flow), and the mean curvature at the gas-oil interface (C_{go}) is proportional to the ratio between the gas-oil capillary pressure (P_{cgo}) and gas-oil interfacial tension (σ_{cgo}) as shown by Eq. 1-4.[9]

$$C_{go} = \frac{P_{cgo}}{2\sigma_{go}}. \tag{1-4}$$

Figure 1-3 shows the section view a fine path containing a thick oil-film where a gas-oil interface if formed. In a porous medium, these fine paths are surface irregularities of connected solid grains in permeable rocks. Figure 1-4 shows a microscopic image of a sandstone rock sample containing thick films of oil in capillary corners formed between solid grains and on their surface irregularities.

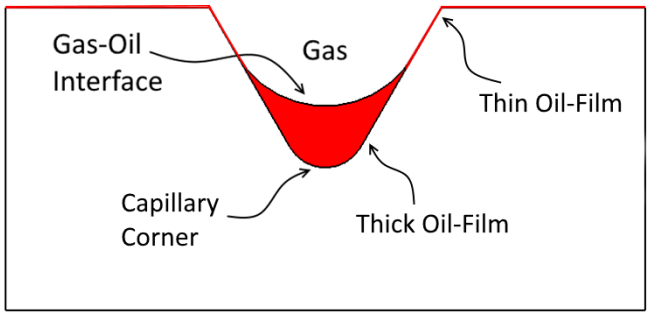

Figure 1-3. Schematic presentation of a thick oil-film in a capillary corner, and a thin oil-film on a smooth surface (red: oil).

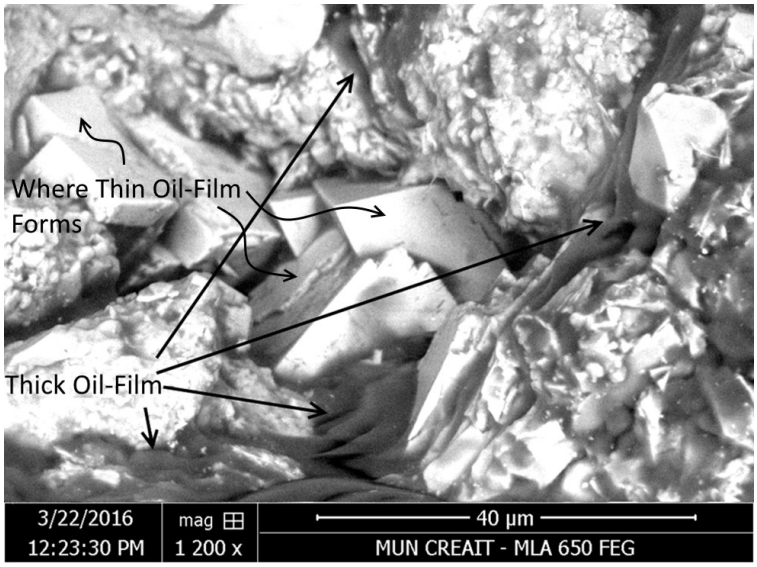

Figure 1-4. Thick oil-films on the surface irregularities of solid grains in a sandstone rock sample (Hibernia EOR Lab).

A thick oil-film cannot exist where the curvature of the gas-oil interface equals with the curvature of the surface (geometric constraint).[19] This discontinuity may occur at increased capillary pressures in a porous medium made from spherical solid grains with smooth surfaces.[18] In addition, the presence of water as the wetting phase in the corner of fine paths results in a geometric constraint when the gas-oil curvature equals with the oil-water curvature.[19, 20]

Under stong oil-wet conditions, the surface of solid grains can be covered with a thin layer of spreading oil after the rupture of a thick oil-film (Figure 1-3).[9] Under water-wet conditions, a thin layer of oil spreads over the water surface when the gas-water interfacual tension (σ_{gw}), is greater than the summation of gas-oil and oil-water interfacial tensions (σ_{go} & σ_{ow}). Under such conditios, the oil spreading coefficient (S_{co}) becomes positive as shown by Eq. 1-5. [21] Experiments showed that the rate of oil flow through thin oil-films is very low and unmeasurable,[18, 21] thus it cannot be accounted as an effective mechanism for an oil recovery operation.

$$S_{co} = \sigma_{gw} - \sigma_{ow} - \sigma_{go} \tag{1-5}$$

The gas-oil interface can be formed with great curvatures in the corner of fine paths. Therefore, the hydraulic continuity of residual oil between regions bypassed with the gas-front can be maintained by thick oil-films at increased gas-oil capillary pressures.[18] The effect of gravity on the gas-oil differential density is the main mechanism that contributes to the enhancement of the gas-oil capillary pressure at greater elevations reducing the hydrostatic pressure of oil at higher elevations.[12] Eventually, oil-occupied pores with smaller sizes can be drained when corresponding gas-oil capillary pressures are overcome.

Figure 1-5 presents mechanisms of GAGD oil recovery at the pore-level schematically. In Figure 1-5 (a), the gas-front displaced oil downward through the path of least resistance (larger pores). Figure 1-5 (b) shows that oil is bypassed in a pore containing small throats without maintaining a hydraulic communication to lower elevations. In this situation, the bypassed oil have no hydraulic communication with the gas-front as there is no fine path

for a downward flow of oil in the form of a thick film. In Figure 1-5 (c), a fine path maintained the hydraulic communication of the initially bypassed oil with the gas-front, thus reducing the hydrostatic pressure of oil at point 1. A further advancement of the gas-front causes a further reduction in the hydrostatic pressure of oil at point 1 (Figure 1-5 (d)). Consequently, the ultimate gas-oil capillary pressure at point 1 ($P_{cgo}{}^{1}$) can become higher than the gas-oil capillary pressure in the gas-front ($P_{cgo}{}^{f}$) due to effect of gravity (g) on gas-oil differential density ($\Delta\rho_{go}$) over a vertical distance of ΔH (Eq. 1.6)

$$P_{cgo}^{1} = P_{cgo}^{f} + \Delta\rho_{go} g H \,. \tag{1.6}$$

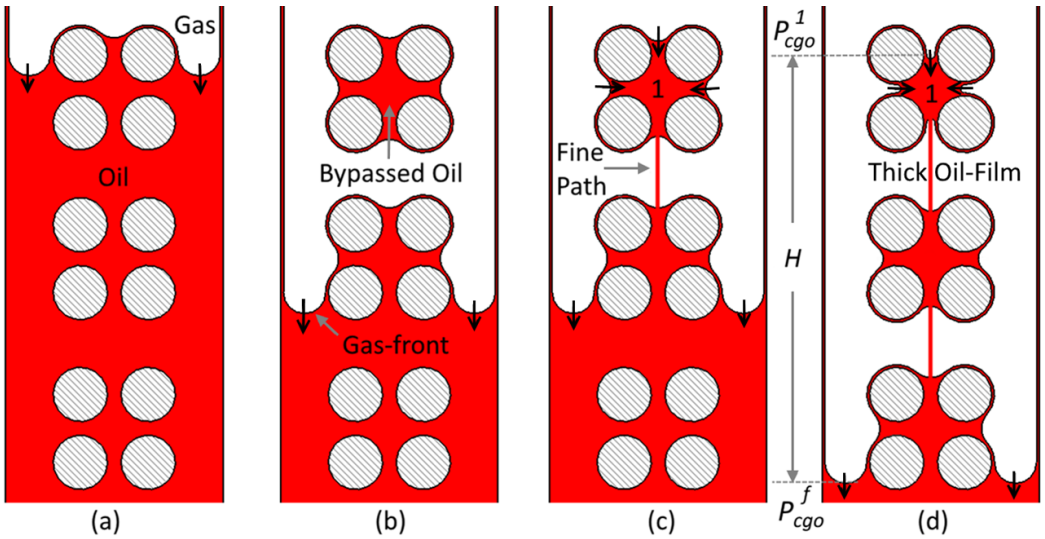

Figure 1-5. (a): The drainage of oil by gas through paths of least resistance. (b): The bypass and isolation of oil in a pore with small throat without any hydraulic continuity to lower elevations. (c): The bypassed oil maintained a hydraulic link with the gas-front through a fine path. (d): The reduction of oil hydrostatic pressure at higher elevations can result in the increase of the gas-oil capillary pressure and drainage of the oil in point 1 ($P_{cgo}{}^{f}$: gas-oil capillary pressure in the gas-front, $P_{cgo}{}^{1}$: gas-oil capillary pressure above the gas-front in point 1, H: vertical distance between point 1 and gas-front).

The hydrostatic pressure of oil at higher elevations is also affected by a viscous pressure drop along the path of the film flow. In Eq. 1.6, the effect of the viscous pressure drop is neglected. This can be valid when the time of GAGD process is sufficiently extended and the drainage rate is suffienctly low, so the hydrostatic pressure of oil at point 1 drops effectively. The gas-oil interface is more curved upon an increase of the gas-oil capillary pressure (Eq. 1.4), thus the gas-oil interface may ultimately enter a pore with small throats.

1.2. Research Objectives and Motivation

The vertical gas injection is one of the most effective oil recovery methods due to its high performance and wide applications. The injected gas can form a miscible or immiscible contact with oil. Although miscible gas injection always results in high recovery, it may not be a feasible option where there is a limited access to a rich gas source (i.e., offshore fields). Therefore, immiscible GAGD with a lean gas, e.g., natural gas produced from a neighbouring part of the field, might be considered as an oil recovery operation especially in a good pay zone where the block has maybe watered out or broken through limiting further economic oil production.

GAGD is a multiphase flow process in which the displacement of fluids' interfaces can be affected by the operational parameters, fluids properties, and porous media characteristics. The effect of wettability,[14-16, 22] heterogeneities,[23-25] interfacial tension between fluids,[14] and production rates[15, 26, 27] on GAGD performance have been studied in macromodels made from packs of glass beads and sands. Oil recovery factor obtained

from three-dimensional models have been correlated with dimensionless numbers such as the bond number, gravity number, and capillary number.[26] Zendehboudi et al.[28] suggested that the dimensionless numbers alone cannot predict the oil recovery factor. Therefore, a new model was developed based on the combination of dimensionless numbers and porous media permeability to characterize oil recovery data obtained from different experiments. However, experiments were conducted under two-phase conditions, without reflecting the effect of wettability that is an important parameter in a real gravity drainage process. In another attempt, Zendehboudi et al.[29] tried to include the effect of wettability in their gravity drainage investigations. However, experiments were conducted under two-phase conditions with two pairs of air-water and air-Varsol™ varying the contact angle in a porous medium made from glass beads. Therefore, their research result under two-phase conditions cannot be used in the evaluation of GAGD performance in oil-wet and water-wet porous media, which are meaningful terminologies under three-phase conditions. Grattoni et al.[30] developed dimensionless number criteria to correlate oil recovery factor for post-waterflood GAGD in a porous medium made from glass beads. Their model was successfully correlated with the total oil and water production, but not the oil recovery factor. It is to be noted that smooth glass beads results in the hydraulic discontinuity of a wetting and intermediate-wetting phase at increased capillary pressures.[18] In addition, the promotion of differential pressures between gas and other fluids can be limited in porous media with a short vertical height. Terwilliger et al.[31] developed an excellent experimental setup for conducting gravity drainage test with a sandpack having a vertical length of 240 cm. The performance of gravity drainage was successfully demonstrated and correlated with the drainage rate in their porous medium.

They suggested that increasing the production rate increased the residual oil saturation at a gas-breakthrough. Vizika and Lombard[14] developed a similar setup comprising a sandpack with a length of 50 cm for studying the effect of wettability on post-waterflood GAGD performance. They also varied gas-water and oil-water interfacial tensions to change the sign of the oil spreading coefficient. It has been found that the residual oil saturation along the length of porous medium was affected by both the state of wettability and interfacial tensions between fluids.

Although macromodels can generate useful data such as oil recovery curves, it may not provide a sufficient transparency to demonstrate fluids' interfaces in detail. GAGD research has been conducted in micromodels to study the displacement of fluids at the pore-level.[12, 17] A challenge in micromodel studies is that two-dimensional porous media may not represent all the characteristics of a reservoir rock effectively during GAGD processes. For instance, the hydraulic continuity of the residual wetting phase[11] in micromodels is weak as the pore space is formed in between separated solid grains. Therefore, a new pore network micromodel was developed, containing coarse pores covered by fine capillaries to visually investigate the multiphase flow of fluids in a transparent porous medium that can represent characteristics of a permeable rock. The objective of this research is to understand mechanisms that influence GAGD performance and recognize potential reservoir conditions where GAGD can be implemented successfully.

1.3. Development of the Micromodel

The characterization of reservoir rocks has been often perfromed with coreflood equipment[4] generating flow/pressure data under corresponding reservoir conditions. The obtained information, such as oil recovery, releative permeability and capillary pressure curves, are used in the evaluation of EOR methods, and reservoir simulations. One of the major problems accosiated with the coreflood experiments is the lack of the visualization of a multiphase flow process at macro-scales. For instance, pore-level events that promote/retard oil recovery cannot be inferred from data generated with a coreholder or centrifuge device. Micromodels have been made with a variaty of methods to be used in geo-science related investigations, specially study of enhance oil recovery methodologies. The transparency of micromodels can reveal phenomena affecting mechanisms of oil recovery (e.g., bypass & snap-off, and contribution of capillary, gravity and viscous forces in the displacement of oil).[9]

Micromodels can be made on the surface any trasnparent material such as glass,[32] plexiglas™,[33] polydimethylsiloxane,[34] and a transparent rock[35]. The first step in the micromodel fabrication is the etching of a workpiece. Depending on the micromodel material, the etching process can be perfromed with physical or chemical methodologies, as well as a combination of both methods. In physical methodologies, the surface of material is removed with a high kinetic energy, such as the laser ablation[36] and plasma etching[37]. In chemical etching, the surface of a workpiece is coated with a layer of material that can be removed by the lithography technique[38] or laser ablation[35]. Then, the exposed surface of the workpiece can then be etched with a corrosive chemical through a

wet[39] or dry[40] etching (chemical) process. In the reaction ion etching,[41, 42] the combination of physical and chemical etching methods has been implemented in the fabrication of microfluidic devices with a high resolution (1 μm). In the next step, the etched palte must be bonded to a blank plate. The bonding can be implemented thermally in an oven, chemically using an adhesive, or physically using plasma surface treatment.[43] In this research, the new pore network micromodel was developed using laser ablation on the surface of plexiglas™ for the ease of the process, fast prototyping and a low cost of fabrication. In addition, a thermal bonding process has been developed to seal the pore network that can withstand pore pressures up to 900 psig.

A CO_2 laser device (Trotec Speedy 300), which can engrave pores with a minimum width of 100 μm, was used for etching the pore network on the surface acrylic plates. The minimum width of an engraved zone depends on the laser beam diameter and the optic configuration of the device. The laser ablation creates greater depths and widths when higher energy is discharged per laser pulse. The discharged energy can be controlled by adjusting the power of the laser, and the movement speed of the laser probe. The laser parameters were characterized conducting engraving tests on the surface of an acrylic plate. Figure 1-6 presents results of characterization. Lowering laser power below 8 W resulted in no or poor engraving, and increasing the speed of the probe movement resulted in an inconsistency in the engraving. In addition, laser etching at high power and low speed resulted in melting of the plate due to a high energy ablation. Ultimately, high quality etching was obtained when the power and speed of the laser was adjusted between 8-12 W and 25-35 cm/sec, respectively. Figure 1-7 show the surface of a Plexiglas™

plate engraved with the laser power and speed of 10 w and 30 cm/sec, respectively. The optimal conditions resulted in an average penetration depth of 150 µm.

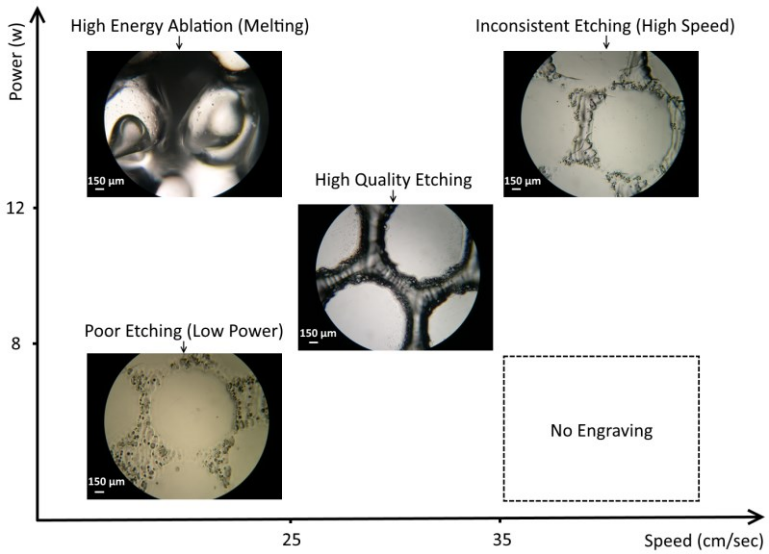

Figure 1-6. Characterization of laser parameters for engraving on the surface of acrylic plate.

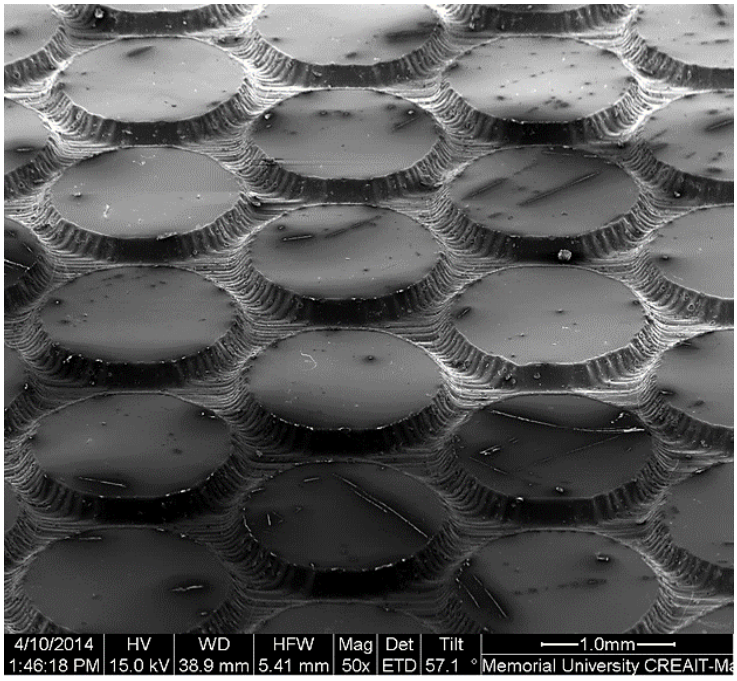

Figure 1-7. Engraved surface of an acrylic plate with optimized laser parameter.

Based on the capability of the CO_2 laser methodology, the average pore sizes in the developed micromodels was 500 μm. This is one order of magnitude greater than the average pores sizes in a Berea sandstone sample[44]. Although the enlargement of pore sizes scales down capillary forces in the micromodel compared to a real-rock porous medium, capillary forces still dominate gravitational forces. The capillary pressure for a pair of fluids with an interfacial tension of 50 mN/m in a pore with an average diameter of 500 μm can be up to 400 Pa. This can be compared with a hydrostatic pressure drop of 10 Pa/mm for the same pair of fluids with a differential density of 1 gr/ml. Therefore, a gravity drainage test can be successfully performed in the developed micromodel. The advantage of the pore size enlargement in the micromodel is achieving an effective interplay between capillary and gravitational forces in a porous medium with a limited vertical length (~ 20 cm). Etching real-size pores promotes capillary pressures. In such porous media, the length of the system must be sufficiently long, so gravity can create an effective hydrostatic pressure drop in the wetting phase. Otherwise, the drainage process over the length of porous medium is affected by the capillary end effect, which is the retention of a wetting phase in smaller pores of the porous medium when the gas-front breakthroughs at the outlet. A capillary barrier is normally used at the outlet of a such porous media (e.g. core-level experiments),[16] which induces the capillary pressure at a breakthrough. The variation in pore size distribution and enlargement of pores changes the residual saturation profile, which is an apparent phenomenon varying porous media with different pore size distribution and pore morphologies.

1.4. Design of Experiment

In this research the influence of the:

- porous media wettability (oil-wet and water-wet),
- porous media heterogeneity,
- gas-oil interfacial tension,
- gas injection rate, and the
- presence of mobile water (in post-waterflood GAGD)

on GAGD performance have been investigated through direct visualization of fluids' interfaces at the pore-level in newly developed micromodels.

Table 1.1 presents the experimental design in this research. In chapter 1, the effect of wettability has been studied at two levels of oil-wet and water-wet conditions in micromodels 1 and 2, respectively. The pattern of the micromodels 1 and 2 contains a simple array of circles with different sizes to create a heterogeneous porous medium (Figure A-1 in Appendix A). In chapter 3, we improved the micromodel using a thin sand section to design a coarse pore network, as well as including a network of fine paths to obtain a better capillary continuity in the porous medium. GAGD experiments have been conducted at irreducible water saturations and post-waterflood under oil-wet and water-wet conditions, respectively. GAGD performance at irreducible water saturations (oil-wet conditions) was evaluated in micromodels 3 and 4. Micromodel 3 comprises a coarse pore network superimposed by fine capillaries, thus having a strong capillary continuity. Micromodel 4 contains only the coarse pore network, thus providing a weak hydraulic continuity for a wetting phase during a multiphase flow process.

Table 1-1. Experimental Design for investigating GAGD in pore network micromodels.

Chapter Number	Studied Parameters	Levels	Micromodel ID in Main Tests	Micromodel ID in Repeated Tests
Chapter 2: GAGD at Irreducible Water Saturations	Wettability	Oil-wet	1	-
		Water-wet	2	-
Chapter 3: Development of the New Micromodel	Hydraulic Continuity (Irreducible Water Saturation)	Strong (Oil-wet)	3	5
		Weak (Oil-wet)	4	-
	Hydraulic Continuity (Post-waterflood)	Strong (Water-	6	-
Chapter 4: GAGD at Irreducible Water Saturations	Wettability	Oil-wet	3	5
		Water-wet	3	5
	Gas-Oil Interfacial Tension	CO_2	3	5
		C_3H_8	3	5
	Miscible GAGD	Water-wet	3	-
Chapter 5: Post-waterflood GAGD	Effect of Wettability	Oil-wet	6	3
		Water-wet	6	3
	Effect of Production Rate	Low Rate	6	-
		High Rate	6	-

In chapter 4, the effect of wettability (oil-wet vs. water-wet conditions) was studied conducting tests with CO_2 and C_3H_8 in a full-factorial scheme. Varying the gas type changed the gas-oil interfacial tension. Experiments were conducted in micromodel 3 and repeated in micromodel 5 (replicate of micromodel 3). In addition, an experiment was conducted in micromodel 3 to evaluate miscible GAGD performance under water-wet conditions. In chapter 5, another replicate of the improved micromodel was fabricated to perform post-waterflood GAGD experiments varying the state of wettability over two levels of oil-wet and water-wet conditions, as well as the production rate over two levels of low rate (0.2 ml/hr) and high rate (2.0 ml/hr) in a full-factorial scheme.

The associated error with the calculated saturation of fluids with the image analysis program is smaller than ±0.02 PV. This error was obtained comparing calculated data with measured volume using a precision pump. A detailed description of the implemented material balance can be found in Appendix B. This error is higher when a greater number of interfaces is formed between a fluid and other phases. For instance, the highest error belongs to the wetting phase when it is only around solid grains and smaller pores. Similarly, the associated error with the saturation of the intermediate wetting phase is highest when it occupies the center of pores as isolated droplets. This error is affected by the efficiency of the imaging system in the detection of boundaries at all interfaces between fluids with different colours. The efficiency of the imaging system is controlled by the utilized optic components. The qualitative and quantitative calibration methodologies are described in Appendix B.

When an experiment is conducted in a real-rock porous medium, the presence of salts in the aqueous phase may influence test results reacting with rock minerals. In addition, interfacial tensions between fluids can be affected by the presence of salts in water. Furthermore, the evaporation of water can lead to the precipitation of salts in porous media. In our micromodel experiments, the water evaporation are unremarkable, and the brine-mineral reactions are absent in a porous medium made from a polymer (acrylic). Also, the interfacial tensions between aqueous and non-aqueous fluids (deionized water – Varsol: 32 mN/m) is close to typical values between crude and water (30 – 35 mN/m). Therefore, deionized water was used as the aqueous phase in the performed experiments.

1.5. Overview

This thesis includes four chapters presenting the progress made during the research.

- Chapters 2 is a refereed conference proceeding presented at the 30th international symposiums of the Society of Core Analysts (SCA 2016).
- Chapter 3 has been submitted for publication in the Journal of Petroleum Science and Engineering.
- Chapters 4 is a refereed conference proceeding presented at the 31st international symposiums of the Society of Core Analysts (SCA 2017).
- Chapter 5 has been submitted for publication to the Journal of Energy & Fuels.

In Chapter 2, results of GAGD experiments performed in a typical micromodel at low (irreducible) water saturations are presented. The objective of this study was to investigate the effect of porous medium heterogeneities and wettability on the recovery of oil at pore-level. Results of Chapter 2 indicated that the effect of gravity on GAGD performance depends on the hydraulic continuity of the residual wetting phase in porous media. Therefore, micromodels must be improved for a better demonstration of the interaction between capillarity and gravity during a GAGD process. In Chapter 3, the procedure for the fabrication of the new micromodel is explained. The new micromodel effectively demonstrated the importance of the effect of hydraulic continuity on GAGD processes. In addition, an image processing methodology used for the calculation of fluids' saturations in micromodels was developed, and its detail is discussed in Appendix B. In Chapter 4, results of GAGD experiments performed in improved micromodels at irreducible water saturations are presented. In this study, the effect of wettability,

heterogeneities and miscibility on the recovery of oil are discussed. In Chapter 5, results of post-waterflood GAGD experiments are presented. The post-waterflood GAGD is a three-phase process, and the capillary, gravitational and viscous forces influenced the recovery of oil. The influence of these forces was investigated varying the porous media wettability and production rate. Chapter 6 presents the summary of the research. Additional information including images of micromodels and results of repeated experiments are presented in Appendices.

The main contributions and novelties of this research include the:

- design and development of an improved pore network micromodel for studying multiphase flow processes particularly GAGD;
- investigation of the effect of capillarity, gravity, and viscous forces on GAGD performance;
- studying the effect of wettability, miscibility, and production rates on GAGD oil recovery;
- visualization of phenomena affecting oil recovery during GAGD;
- development of an image processing program for calculating saturation of fluids;
- and, the design and development of an experimental setup for conducting GAGD experiment.

The result of investigation can be used to characterize GAGD perfromance under different wettability and operational conditions.

1.6. Co-authorship Statement

The authors of research papers in Chapters 2 to 5 are:

1. Hossein Khorshidian (student and first author)
2. Dr. Lesley James (corresponding author, principal investigator and academic supervisor)
3. Dr. Stephen Butt (academic supervisor).

The papers were written through contributions of all authors in the conception and design of the study, interpretation of data, and drafting the article.

Chapter References

1. Sandrea, I.; Sandrea, R., Global Oil Reserves-1: Recovery factors leave vast target for EOR technologies. *Oil and Gas Journal* **2007,** 105, (41), 44.
2. Lake, L. W., In *Enhanced Oil Recovery*. Old Tappan, NJ; Prentice Hall Inc.: USA, 1989.
3. Lake, L. W.; Venuto, P. B., A niche for enhanced oil recovery in the 1990s. *Oil & Gas Journal* **1990,** 88, (17), 62-67.
4. Amyx, J. W.; Bass, D. M.; Whiting, R. L., Fundamental Properties of Fluid-Permeated Rocks. In *Petroleum reservoir engineering: physical properties*. McGraw-Hill College: 1960; Vol. 1. Pp 36-132.
5. Shreve, D.; Welch Jr, L., Gas drive and gravity drainage analysis for pressure maintenance operations. *Petroleum Transactions, AIME* **1956**, 207, 136-143.
6. Clancy, J.; Gilchrist, R.; Cheng, L.; Bywater, D., Analysis of nitrogen-injection projects to develop screening guides and offshore design criteria. *Journal of petroleum technology* **1985,** 37, (06), 1,097-1,104.
7. Campbell, B. T.; Orr Jr, F. M., Flow visualization for co2/crude-oil displacements. *Society of Petroleum Engineers Journal* **1985,** 25, (05), 665-678.
8. Kulkarni, M. M.; Rao, D. N., In *Characterization of operative mechanisms in gravity drainage field projects through dimensional analysis*, Proceeding of the SPE Annual Technical Conference and Exhibition, September 24-27, 2006; Society of Petroleum Engineers: San Antonio, Texas, USA, 2006.
9. Dullien, F. A., In *Porous media: fluid transport and pore structure*, 2nd ed; Academic Press, Inc.: San Diego, Ca, USA, 1991.
10. Løvoll, G.; Méheust, Y.; Måløy, K. J.; Aker, E.; Schmittbuhl, J., Competition of gravity, capillary and viscous forces during drainage in a two-dimensional porous medium, a pore scale study. *Energy* **2005,** 30, (6), 861-872.
11. Rao, D. N.; Ayirala, S. C.; Kulkarni, M. M.; Mahmoud, T. N.; Paidin, W. R., *Development and Optimization of Gas-Assisted Gravity Drainage (GAGD) Process for Improved Light Oil Recovery*. United States. Department of Energy: 2006.

12. Kantzas, A.; Chatzis, I.; Dullien, F. In *Mechanisms of capillary displacement of the residual oil by gravity-assisted inert gas injection*, Proceeding of the SPE Rocky Mountain Regional Meeting, May 11-13, 1988; Casper, Wyoming, USA, 1988.
13. Rao, D. N.; Ayirala, S. C.; Kulkarni, M. M.; Sharma, A. P., In *Development of gas assisted gravity drainage (GAGD) process for improved light oil recovery*, Proceeding of the SPE/DOE Symposium on Improved Oil Recovery, April 17-21, 2004; Society of Petroleum Engineers: Tulsa, Oklahoma, USA, 2004.
14. Vizika, O.; Lombard, J., Wettability and spreading: two key parameters in oil recovery with three-phase gravity drainage. *SPE Reservoir Engineering* **1996,** 11, (01), 54-60.
15. Maroufi, P.; Rahmanifard, H.; Al-Hadrami, H.; Escrochi, M.; Ayatollahi, S.; Jahanmiri, A., Experimental investigation of wettability effect and drainage rate on tertiary oil recovery from fractured media. *Journal of Porous Media* **2012,** 15, (12).
16. Kantzas, A.; Chatzis, I.; Dullien, F. In *Enhanced oil recovery by inert gas injection*, Proceeding of the SPE Enhanced Oil Recovery Symposium, April 16-21, 1988; Society of Petroleum Engineers: Tulsa, Oklahoma, USA, 1988.
17. Catalan, L. J.; Dullien, F. A.; Chatzis, I., The effects of wettability and heterogeneities on the recovery of waterflood residual oil with low pressure inert gas injection assisted by gravity drainage. *SPE Advanced Technology Series* **1994,** 2, (02), 140-149.
18. Dullien, F. A.; Zarcone, C.; Macdonald, I. F.; Collins, A.; Bochard, R. D., The effects of surface roughness on the capillary pressure curves and the heights of capillary rise in glass bead packs. *Journal of Colloid and Interface Science* **1989,** 127, (2), 362-372.
19. Piri, M.; Blunt, M. J., Three-phase threshold capillary pressures in noncircular capillary tubes with different wettabilities including contact angle hysteresis. *Physical Review E* **2004,** *70*, (6), 061603.
20. Dong, M.; Dullien, F. A.; Chatzis, I., Imbibition of oil in film form over water present in edges of capillaries with an angular cross section. *Journal of colloid and interface science* **1995,** 172, (1), 21-36.

21. Blunt, M.; Zhou, D.; Fenwick, D., Three-phase flow and gravity drainage in porous media. *Transport in porous media* **1995,** *20*, (1-2), 77-103.
22. Mahmoud, T.; Rao, D. N. In *Range of operability of gas-assisted gravity drainage process*, Proceeding SPE Symposium on Improved Oil Recovery, April 20-23, 2008; Society of Petroleum Engineers: Tulsa, Oklahoma, USA, 2008.
23. Zendehboudi, S.; Chatzis, I., Laboratory investigation of free fall gravity drainage in fractured porous systems using unconsolidated macromodels. *Energy & Fuels* **2011,** 25, (5), 2356-2372.
24. Parsaei, R.; Chatzis, I., Experimental investigation of production characteristics of the gravity-assisted inert gas injection (GAIGI) process for recovery of waterflood residual oil: effects of wettability heterogeneity. *Energy & Fuels* **2011,** 25, (5), 2089-2099.
25. Rezaveisi, M.; Rostami, B.; Kharrat, R.; Ayatollahi, S.; Ghotbi, C., Experimental investigation of tertiary oil gravity drainage in fractured porous media. *Special Topics & Reviews in Porous Media: An International Journal* **2010,** 1, (2).
26. Sharma, A.; Rao, D. N., In *Scaled physical model experiments to characterize the gas-assisted gravity drainage EOR process*, Proceeding of the SPE Symposium on Improved Oil Recovery, April 20-23, 2008; Society of Petroleum Engineers: Tulsa, Oklahoma, USA, 2008.
27. Chatzis, I.; Ayatollahi, S., *In The effect of gas injection rate on the recovery of waterflood the residual oil under gravity assisted inert gas injection*, Proceeding of the Technical Meeting/Petroleum Conference of The South Saskatchewan Section, October 18 – 20, 1993; Petroleum Society of Canada: Regina, Canada, 1993.
28. Zendehboudi, S.; Chatzis, I.; Mohsenipour, A. A.; Elkamel, A., Dimensional analysis and scale-up of immiscible two-phase flow displacement in fractured porous media under controlled gravity drainage. *Energy & Fuels* **2011,** 25, (4), 1731-1750.
29. Zendehboudi, S.; Rezaei, N.; Chatzis, I., Effect of wettability in free-fall and controlled gravity drainage in fractionally wet porous media with fractures. *Energy & Fuels* **2011,** 25, (10), 4452-4468.

30. Grattoni, C.; Jing, X.; Dawe, R., Dimensionless groups for three-phase gravity drainage flow in porous media. *Journal of Petroleum Science and Engineering* **2001,** 29, (1), 53-65.
31. Terwilliger, P.; Wilsey, L.; Hall, H. N.; Bridges, P.; Morse, R., An experimental and theoretical investigation of gravity drainage performance. *Journal of Petroleum Technology* **1951,** 3, (11), 285-296.
32. McKellar, M.; Wardlaw, N., A method of making two-dimensional glass micromodels of pore systems. *Journal of Canadian Petroleum Technology* **1982,** 21, (04).
33. Cheng, J.-Y.; Wei, C.-W.; Hsu, K.-H.; Young, T.-H., Direct-write laser micromachining and universal surface modification of PMMA for device development. *Sensors and Actuators B: Chemical* **2004,** 99, (1), 186-196.
34. Karadimitriou, N.; Musterd, M.; Kleingeld, P.; Kreutzer, M.; Hassanizadeh, S.; Joekar-Niasar, V., On the fabrication of PDMS micromodels by rapid prototyping, and their use in two-phase flow studies. *Water Resources Research* **2013,** 49, (4), 2056-2067.
35. Song, W.; de Haas, T. W.; Fadaei, H.; Sinton, D., Chip-off-the-old-rock: the study of reservoir-relevant geological processes with real-rock micromodels. *Lab on a Chip* **2014,** 14, (22), 4382-4390.
36. Ben-Yakar, A.; Byer, R. L., Femtosecond laser ablation properties of borosilicate glass. *Journal of applied physics* **2004,** 96, (9), 5316-5323.
37. Vlachopoulou, M.; Tsougeni, K.; Kontakis, K.; Vourdas, N.; Tserepi, A.; Gogolides, E., Plasma etching technology for fabrication and surface modification of plastic microfluidic devices. *Pure and Applied Chemistry* **2010,** 86, (6).
38. Hines, D. R.; Siwak, N. P.; Mosher, L. A.; Ghodssi, R., MEMS Lithography and Micromachining Techniques. In *MEMS Materials and Processes Handbook*, Springer: 2011; pp 667-753.
39. Anoop Prakash, A.; Jency, J. G.; Mathew, M. C., A review of various wet etching techniques used in micro fabrication for real estate consumption. **2013**.

40. Madou, M. J., Fundamentals of microfabrication: the science of miniaturization. CRC press: 2002.
41. Chen, K.-S.; Ayón, A. A.; Zhang, X.; Spearing, S. M., Effect of process parameters on the surface morphology and mechanical performance of silicon structures after deep reactive ion etching (DRIE). *Journal of Microelectromechanical Systems* **2002,** 11, (3), 264-275.
42. Karadimitriou, N.; Joekar-Niasar, V.; Hassanizadeh, S.; Kleingeld, P.; Pyrak-Nolte, L., A novel deep reactive ion etched (DRIE) glass micro-model for two-phase flow experiments. *Lab on a Chip* **2012,** 12, (18), 3413-3418.
43. Mazurczyk, R.; Mansfield, C. D.; Lygan, M., Glass microstructure capping and bonding techniques. *Microfluidic Diagnostics: Methods and Protocols* **2013**, 141-151.
44. Chatzis, I.; Morrow, N. R.; Lim, H. T., Magnitude and detailed structure of residual oil saturation. *Society of Petroleum Engineers Journal* **1983,** 23, (02), 311-326.

Chapter 2 : The Role of Film Flow and Wettability in Immiscible Gas Assisted Gravity Drainage

This chapter is based on a paper prepared for presentation at the International Symposium of the Society of Core Analysts held in Snow Mass, Colorado, USA, 21-26 August 2016.

2.1. Abstract

Capillary and gravity forces control the residual saturation of liquid phases in Gas Assisted Gravity Drainage (GAGD). These forces are determined by properties of fluids and porous media. In this research, the effect of capillary and gravity forces on the film flow of oil has been investigated. Experiments were conducted under oil-wet and water-wet conditions to investigate the role of wettability on GAGD oil recovery. It has been observed that the residual oil saturation was affected by the state of wettability. In the water-wet micromodel, the irreducible water saturation, that was found in smaller pores, blocked potential pathways for the film flow of oil. Under oil-wet conditions, the majority of the residual oil was found in smaller pores and around the grains in the form of oil rings. In GAGD, the presence of corners and edges enabled a wetting phase to maintain strong hydraulic continuity between lower and higher elevations. We have observed a higher oil recovery in locations with stronger hydraulic continuity (i.e., edges of the pattern). However, the discontinuity of liquid films due to geometric constraints terminated the film flow at elevated capillary pressures.

2.2. Introduction

In Gas Assisted Gravity Drainage (GAGD) oil recovery process, the effect of gravity on the differential density between gas and oil causes the gas-oil capillary pressure to

increase above the gas-front.[1] Since GAGD is a drainage process, increasing the gas-oil capillary pressure increases the number of pores invaded by gas (non-wetting phase). Consequently, the ultimate oil recovery factor becomes higher draining oil from smaller pores of a porous medium. In order to enhance the capillary pressure above the gas-front, fine capillaries must exist through which a downward flow of oil in the form of thick films can occur.[2]

The role of the film flow in GAGD is schematically illustrated in Figure 2-1, which is a simple pattern having two pore bodies with different throat sizes. In Figure 2-1: A, oil (wetting phase) is displaced by gas (non-wetting phase) through the least resistant path (larger pore). The capillary pressure ahead of the gas-front is indicated by P_{cgo}^{f} (Figure 2-1B). Stable films of oil occupy the corners of the pattern where gas-oil interfaces with small radii (higher capillary pressure) can be formed. The radius of a gas-oil interface at higher elevations is smaller where the capillary pressure is higher. The capillary pressure above the gas-front, P_{cgo}, is calculated by Eq. 2.1,

$$P_{cgo}^{l} = P_{cgo}^{f} + \Delta\rho_{go} g H \tag{2.1}$$

where $\Delta\rho_{go}$ is the gas-oil differential density, g is the gravity acceleration, H is the elevation of the gas-oil interface above the gas-front. When an oil-occupied pore, which was initially uninvaded by gas, is located at a sufficient vertical distance (H_1 in Figure 2-1: C) from the gas-front, gas can enter the pore from the center of its throat, and oil can be drained through the corners (Figure 2-1: D). Similarly, gas may enter the smaller throat (Figure 2-1: E) when the gas-front moves further downward. However, the roundness of the capillary corners (geometric constraint[3]) may not allow oil and gas to form a highly

curved interface with a small radius corresponding to the capillary pressure that must be overcome for the drainage of the pore with a small throat. Therefore, the continuity of the thick oil-films is terminated, and the residual oil in the pore with the smaller throat may not be recovered (Figure 2-1: F).

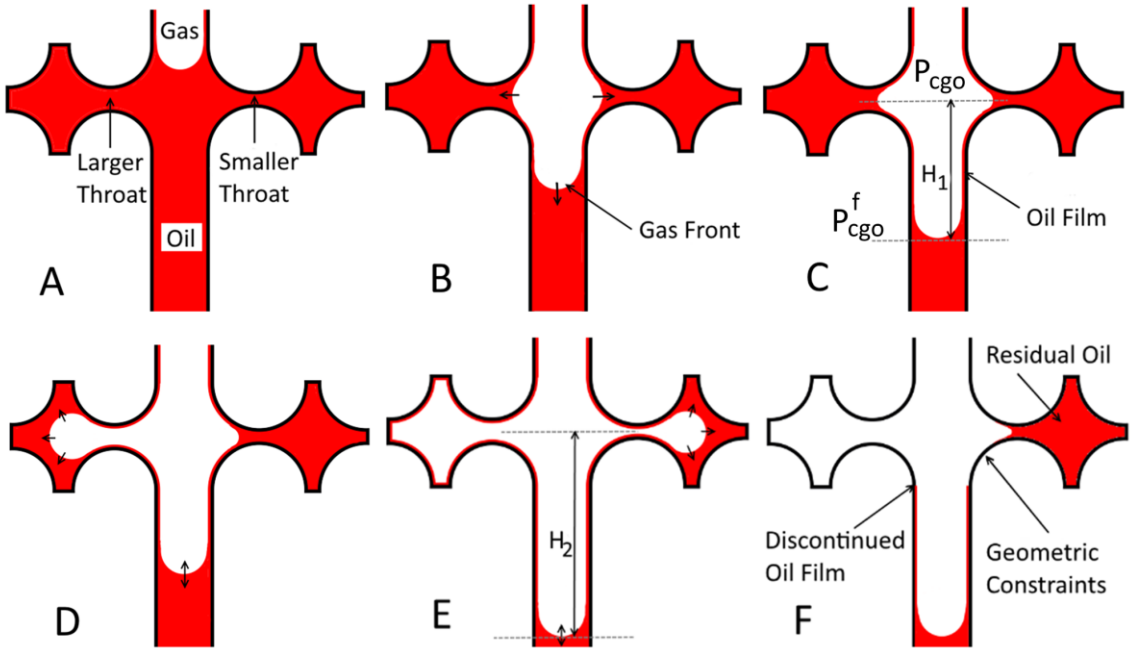

Figure 2-1. Oil drainage above the gas-front through film flow in capillary corners. A-C: Advancement of the gas-front through path of least resistance. D: Drainage of an oil-occupied pore above the gas-front. E: Drainage of another oil-occupied pore due to further enhancement of the gas-oil capillary pressure. F: Rupture of oil-film at elevated capillary pressure due to geometric constraints.

The presence of water in capillary corners of a water-wet medium can also affect the maximum obtainable gas-oil capillary pressure.[3-5] The presence of a thick oil-film on water is possible when the curvature of the gas-oil interface is smaller than the curvature of the oil-water interface. Otherwise, thin layers of oil may form over the water surface

due to a geometric constraint created by water.[3] Oil may spread over the surface of water when the gas-water interfacial tension is greater than the summation of the gas-oil and oil-water interfacial tensions.[7] It has been argued that the rate of oil flow in the form of thin films is unremarkable and may not be accounted for oil recovery processes.[5, 6]

An important parameter of a porous medium that influences GAGD performance is the state of wettability. Chatzis et al.[8] suggested that highest oil recovery can be obtained from water-wet porous media when oil can spread over the water surface. Vizika and Lombard studied the effect of the wettability on the residual oil saturation conducting post-waterflood GAGD in a 50 cm long sandpack.[9] The residual oil saturation under water-wet conditions was lower than oil-wet conditions when oil could spread over the surface of water. In addition, i-butanol was added in water to prevent the spreading of oil by reducing the gas-water interfacial tension. Adding i-butanol in water reduced the oil-water interfacial tension as well, which helped with an easier drainage of water by oil under water-wet conditions. Consequently, oil occupied smaller pores of the water-wet porous medium, thus leading to an increase of the residual oil saturation. Under oil-wet conditions, lowering the oil-water interfacial tension helped with a better drainage of oil by reducing capillary forces at oil-water interfaces that contribute to the rentention of oil in oil-occupied pores with entries blocked by water. It has been also observed that GAGD in porous media made by glass beads resulted in higher recovery of oil under oil-wet conditions compared to water-wet conditions irrespective of spreading conditions of oil.[10, 11] Therefore, GAGD performance might be better correlated with the interfacial tension between fluids rather than the spreading condition of oil.

In this research, the influence of wettability on GAGD performance was studied using oil-wet and water-wet pore network micromodels. The micromodel allows the detailed visualization of the gas, oil and water interfaces during GAGD. The mechanisms that affected the recovery of oil in GAGD are presented in this paper.

2.3. Experimental Details

A 256 x 64 mm (LxW) pore network micromodel was fabricated in the Hibernia EOR Laboratory at Memorial University. Figure A-1 in appendix A shows the micromodel pattern. The presence of smaller pore network at the bottom of the pattern played the role of a capillary barrier, which contributed to the attenuation of the capillary end effect during GAGD. The micromodel pattern, which contains pore bodies with sizes of 1000 to 1600 μm, and pore throats with sizes of 200 to 800 μm, was etched on an acrylic plate wirg an average depth of 150 μm. The laser etched plate was then bonded to a blank plate in an oven at a temperature of 130°C. The pore volume (PV) and porosity of the micromodel are 1.25 ml and 0.52, respectively. A pump (Quizix 20K series) and three custom floating piston accumulators were used to inject oil (red dyed Varsol), water (blue dyed deionized water), and gas into the micromodel under a constant pressure for establishing the initial oil saturation. The fluids were produced with constant rates using another pump and accumulator. GAGD experiments were conducted under oil-wet and water-wet conditions in two separate micromodels. The water-wet conditions was prepared by flushing a clean micromodel with a solution, which leaves a layer of hydrophilic silica gel on the acrylic surface without affecting its permeability.

In the oil-wet micromodel, oil saturation was established in two steps. A fully oil saturated micromodel, which was aged 24 hrs to ensure strongly oil-wet conditions, was flooded by 2 PV of water at 10 ml/hr from bottom to top of the micromodel, and then, 2 PV of oil was injected into the micromodel at 3 ml/hr from top to bottom (gravity stabilized). In the water-wet micromodel, 2 PV of oil was injected into a fully water saturated micromodel from top to bottom at 3 ml/hr. GAGD tests were conducted by connecting the top port of micromodels to CO_2 under a constant pressure of 1.7 bar (25 psig), and producing fluids with a constant rate of 0.1 ml/hr (temperature: 24°C). The implemented rate of production resulted in the domination of capillary forces over viscous forces. We have observed that the gas-front finds larger pores to displace oil, and oil was bypassed in smaller pores surrounded by larger pores as normal in a gravity drainage process in reservoirs containing light oil. The gas-water, oil-water and gas-oil interfacial tensions under experimental conditions are 72, 32, and 22 mN/m, respectively. This resulted in the spreading of oil over water surface. The duration of experiments was approximately 68 hrs.

A Canon 6D camera and Canon EF 100mm f/2.8 USM macro lens were used to capture micromodel images in order to calculate the saturation of fluids during GAGD experiments. An in-house image analysis program was used to calculate the saturation of fluids evaluating the colour of each individual pixel not accounting for any variation in the depth of pores (two-dimensional image processing). The pixels were categorized as red, blue, or white, based on their colours to calculate oil saturation and recovery factor.

2.4. Result and Discussion

The processed images of oil-wet and water-wet micromodels are shown in Figure 2-2 & Figure 2-3. The original images of oil-wet and water-wet micromodels are given in Appendix A. It was observed that the injected gas initially invaded larger pores rather than smaller pores, as expected in a drainage process. Therefore, gas-fingers were formed in the gas-front, which could bypass oil and water in smaller pores surrounded by larger pores. Consequently, bypassed oil-occupied zones (groups of pores) were created above the gas-front (Figure 2-2: B & C and Figure 2-3: B & C). Under both wettability conditions, a further drainage of oil from bypassed regions was obtained after a gas-breakthrough. The gas pressure at both sides of the micromodel were measured at 25.00 ± 0.02 psig, as the implemented rate of production (0.1 ml/hr) created an unmeasurable pressure gradient along the length of the micromodel.

Thick oil-films formed on rough surfaces and in corners of the pattern played an important role in the recovery of the bypassed oil. The additional oil recovery after a gas-breakthrough occurred via the film flow through the surface roughness created by laser beam at the bottom of the engraved pore network. The bypassed oil at higher elevations flowed toward neighbouring regions gradually. The increase of the oil saturation in a region caused oil to fill spaces (pore throats) between separated solid grains, thus developing a hydraulic link with a new zone. Consequently, oil could continue to flow in the direction of gravity toward a new destination at lower elevations. The drainage of oil continued in a stepwise from zones at greater elevations toward the bottom of the pattern.

In the oil-wet micromodel, the residual oil was observed in smallest pores and in the form of rings around solid grains as shown in Figure 2-2: D. In the water-wet micromodel, water initially occupied most of the small pores and around solid grains. Final residual oil is shown trapped in the small to medium-sized pores, as well as around the solid grains upon reduction of the water saturation. In the performed experiments, paths of gravity drainage were mainly formed through smaller pores, where the capillary continuity of oil could be maintained. Under water-wet conditions, smaller pores were often occupied by water, thus blocking a downward flow of residual oil to lower elevations.

The micromodel images after GAGD in Figure 2-2 and Figure 2-3 indicate that zones near the vertical edges (margins) of the pattern contain less residual oil and water compared to other regions in the middle of the pattern. The hydraulic continuity of oil and water in corners formed by vaertical edges of the pattern was stronger than central regions. Under oil-wet conditions, oil used the vertical margins of the pattern to drain effectively. Under water-wet conditions, however, the presence of the residual water in smaller pores and capillary corners created a constraint that limited the increase of the capillary pressure at gas-oil interfaces. Therefore, residual oil saturation under water-wet conditions was higher than oil-wet conditions.

Figure 2-4 shows GAGD oil recovery in micromodels as a function of the injected gas volume (or produced fluids). It is shown that the film flow mechanism after gas-breakthrough resulted in a higher additional oil recovery factor in the oil-wet micromodel compared to the water-wet micromodel. Film flow contributes to an additional 6% and

2% oil recovery post gas-breakthrough under oil-wet and water-wet conditions, respectively.

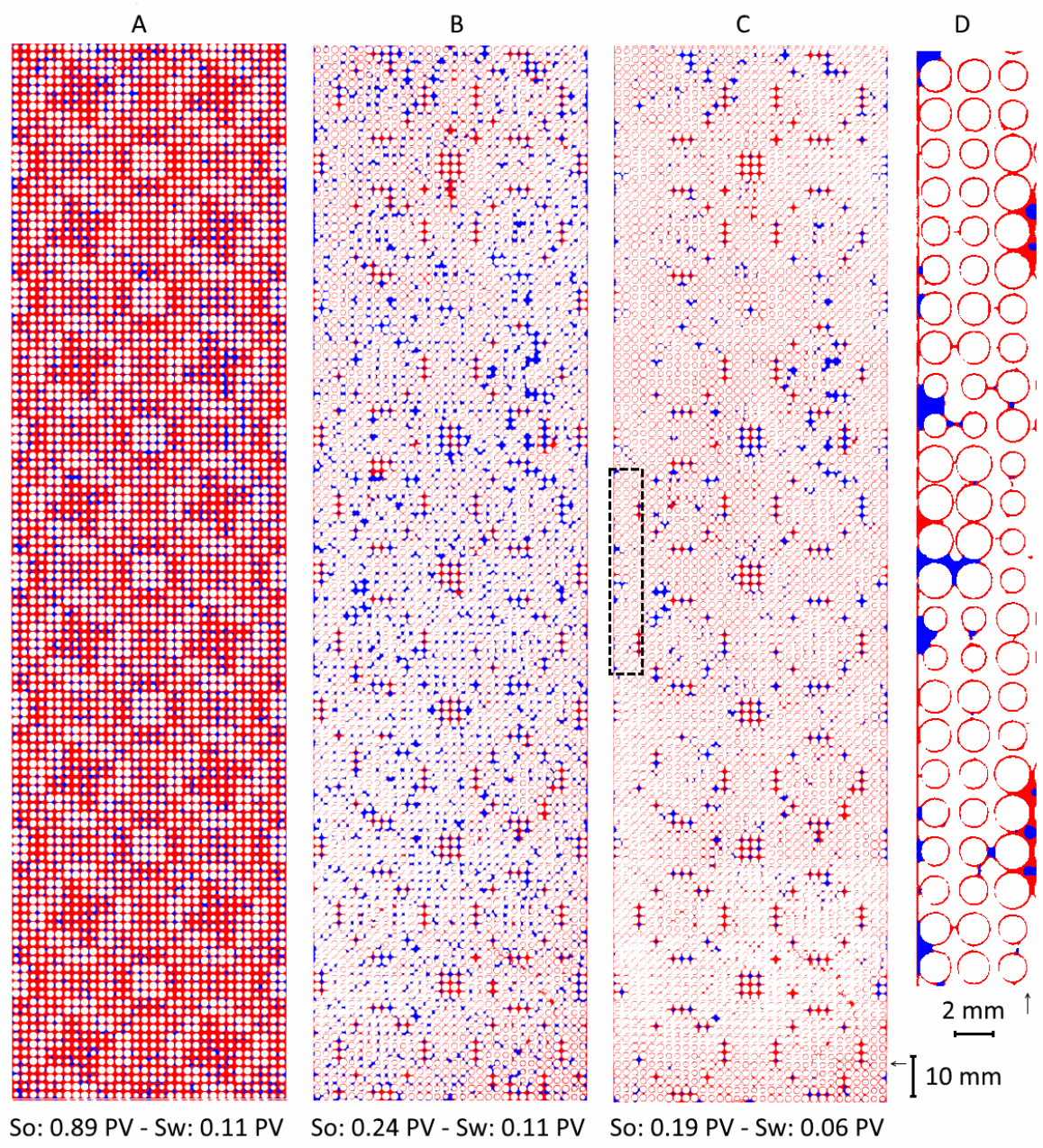

Figure 2-2. GAGD in oil-wet micromodel. A: initial oil saturation. B: After gas-breakthrough (8 hrs). C: After 5.4 PV gas injection (68 hrs). D: Magnified image of a zone in the micromodel margin (red: oil, blue: water, So: oil saturation, Sw: water saturation).

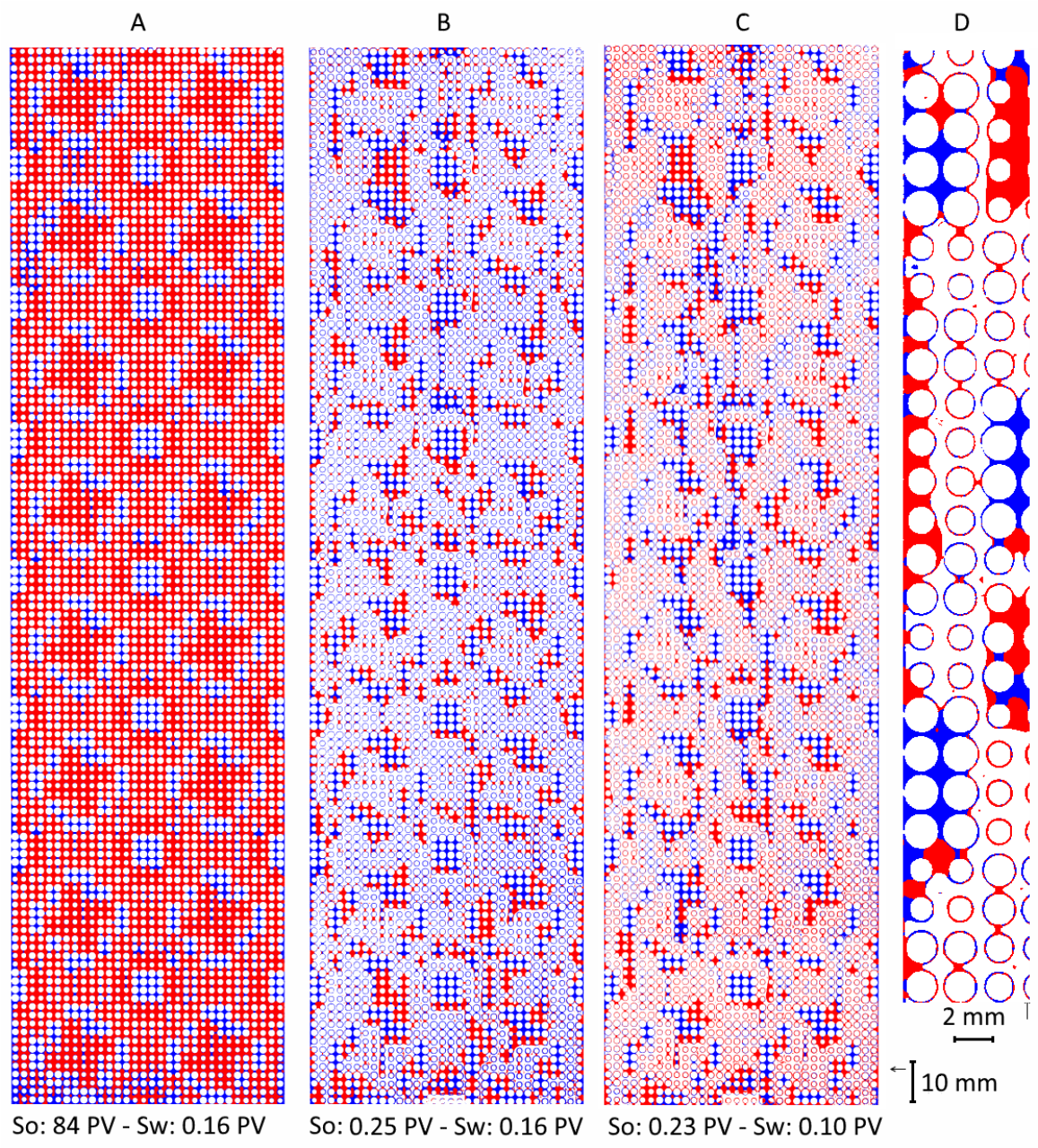

Figure 2-3. GAGD in water-wet micromodel. A: Initial oil saturation. B: After gas-breakthrough (8 hrs). C: After 5.3 PV gas injection (67 hrs). D: Magnified image of a zone in the micromodel margin (red: oil, blue: water, So: oil saturation, Sw: water saturation).

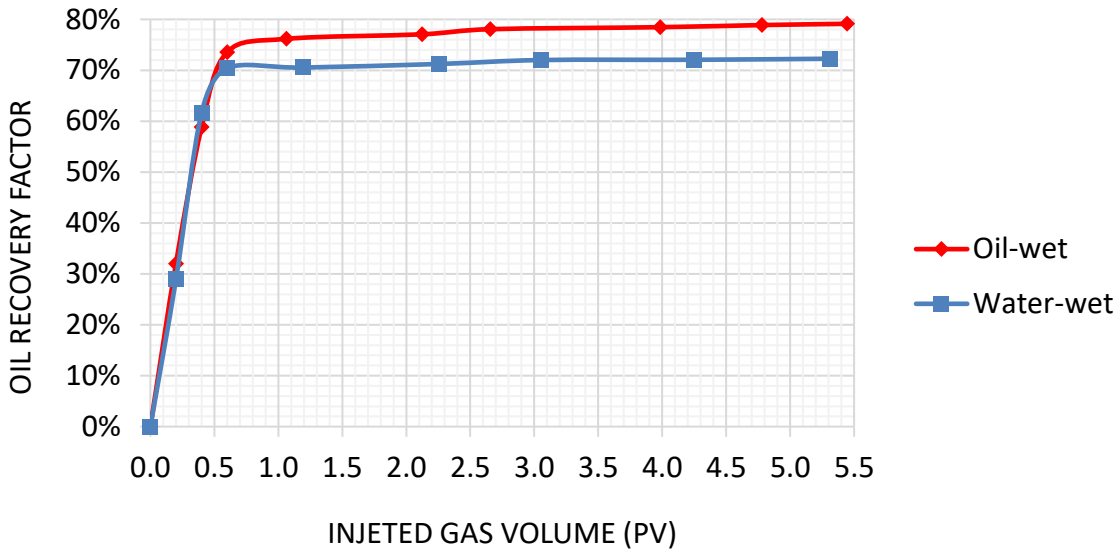

Figure 2-4. Oil recovery curve in oil-wet and water-wet micromodels vs. pore volume of the injected gas.

The evaporation of oil and water with CO2 under corresponding experimental conditions were analyzed, and the result is reported in Appendix A. The analysis indicates that the evaporation played an insignificant role in the reduction of the oil and water saturation, and drainage via the film flow was the main mechanism that contributed to the production of fluids after a gas-breakthrough.

The pore sizes of the fabricated micromodel are one order of magnitude larger than the typical pore sizes of a sandstone rock. According to Eq. 2.1, the gas-oil capillary pressure above the gas-front is determined by: 1) the breakthrough capillary pressure in the gas-front and 2): the hydrostatic pressure of oil above the gas-front. The enlargement of pore sizes lowers the breakthrough capillary pressures, as well as the capillary pressures that must be overcome for the drainage of a bypassed pore. Therefore, the enlargement of the pore sizes can reduce the capillary pressures with the same scaling factor. This may help

with the recovery of the bypassed oil in a medium with a limited vertical length as gravitational forces remained natural.

In this experiment, the result of GAGD in micromodel was affected by a weak capillary continuity of the porous medium. Future works should include a closer examination of GAGD oil recovery mechanisms in an improved micromodel with added surface roughness to enhance the hydraulic continuity and film flow of oil. We are developing a new micromodel with a dual pore network containing coarse and fine capillaries. The presence of fine capillaries can improve the capillary continuity of the micromodel, and the residual oil saturation can better represent GAGD performance.

2.5. Chapter Conclusions

The GAGD research in micromodels showed that gravity and capillary forces control the final residual oil saturation in an immiscible vertical gas injection process. It has been found that the post-GAGD residual oil saturation was affected by the state of wettability and pore sizes. The gas-front bypassed the smaller oil-occupied pores due to the presence of pore-scale heterogeneities. The film flow of oil helped with the recovery of the bypassed oil. The presence of water in the water-wet micromodel hindered the hydraulic continuity of oil between regions at higher and lower elevations, thus reducing the maximum achievable gas-oil capillary pressure. In the presence of the residual water, the oil recovery factor under oil-wet conditions was higher than water-wet conditions due to a better hydraulic continuity of oil in the oil-wet porous medium.

Chapter References

1. Khorshidian, H.; James, L.; Butt, S., In *Corner Oil Film Elevation above the Gas-Oil Interface in Water-Wet Capillaries*. Presented at the International Symposium of the Society of Core Analysts, August 16-21, 2015; St. John's, Newfoundland and Labrador, Canada, 2015.
2. Dullien, F. A., In *Porous media: fluid transport and pore structure*, 2nd ed; Academic Press, Inc.: San Diego, Ca, USA, 1991.
3. Piri, M.; Blunt, M. J., Three-phase threshold capillary pressures in noncircular capillary tubes with different wettabilities including contact angle hysteresis. *Physical Review E* **2004,** 70, (6), 061603.
4. Dong, M.; Dullien, F. A.; Chatzis, I., Imbibition of oil in film form over water present in edges of capillaries with an angular cross section. *Journal of colloid and interface science* **1995,** *172*, (1), 21-36.
5. Blunt, M.; Zhou, D.; Fenwick, D., Three-phase flow and gravity drainage in porous media. *Transport in porous media* **1995,** *20*, (1-2), 77-103.
6. Dullien, F.; Lai, F. S.; Macdonald, I., Hydraulic continuity of residual wetting phase in porous media. *Journal of colloid and interface science* **1986,** *109*, (1), 201-218.
7. Dumore, J.; Schols, R., Drainage capillary-pressure functions and the influence of connate water. *Society of Petroleum Engineers Journal* **1974,** *14*, (05), 437-444.
8. Chatzis, I.; Kantzas, A.; Dullien, F. In On the investigation of gravity-assisted inert gas injection using micromodels, long Berea sandstone cores, and computer-assisted tomography, SPE Annual Technical Conference and Exhibition, October 2-5, 1988; Society of Petroleum Engineers: Houston, Texas, USA, 1988.
9. Vizika, O.; Lombard, J., Wettability and spreading: two key parameters in oil recovery with three-phase gravity drainage. *SPE Reservoir Engineering* **1996,** 11, (01), 54-60.

10. Caubit, C.; Bertin, H.; Hamon, G. In *Three-phase flow in porous media: wettability effect on residual saturations during gravity drainage and tertiary waterflood*, Proceeding of SPE Annual Technical Conference and Exhibition, September 26-29, 2004; Society of Petroleum Engineers: Houston, Texas, USA, 2004.
11. Paidin, W. R.; Rao, D. N. In Physical Model Experiments to Evaluate the Effect of Wettability and Fractures on the Performance of the Gas-assisted Gravity Drainage (GAGD) Process. Presented in the Society of Core Analysts Symposium, September 10-12, 2007; Calgary, Canada, 2007.

Chapter 3：Demonstrating the Effect of Hydraulic Continuity of the Wetting Phase on the Performance of Pore Network Micromodels during Gas Assisted Gravity Drainage

This chapter is based on a paper prepared for publication in the Journal of Petroleum Science and Engineering.

3.1. Abstract

The flow of fluids during oil recovery processes can be visualized in pore network micromodels that represent the porous nature of reservoir rocks. In a permeable rock, pores are formed in spaces between connected solid grains with various sizes and shapes. The surface roughness and irregularities of solid grains create networks of fine capillaries in conjunction with coarse pores. These fine capillaries can maintain films of a wetting phase in regions occupied by a non-wetting phase. In two-dimensional micromodels, the pore network is formed between separated solid grains, and the hydraulic communication of the wetting phase between regions separated by the non-wetting phase is terminated. In this paper, we present a simple procedure for the fabrication of oil-wet and water-wet micromodels that provide the wetting phase with strong hydraulic continuity. The new micromodel contains a pattern of coarse pores covered by fine capillaries without affecting its visualization capabilities. The performance of micromodels with and without fine capillaries was evaluated with the gas assisted gravity drainage (GAGD) experiments under oil-wet and water-wet conditions. The experimental results show that the presence of fine capillaries improved of the hydraulic continuity of a residual wetting phase. The

new micromodel effectively demonstrated the interaction between capillary and gravitational forces in gravity drainage processes.

3.2. Introduction

3.2.1. Pore Network Micromodels

Oil recovery processes have been studied in various porous media representing reservoir rocks. A three-dimensional pore space is created in macromodels, made from sand-packs and glass beads,[1-4] without restrictions in the size of the system but with limited visualization capabilities. Two-dimensional pore network micromodels allow a clear visualization of interfaces between fluids during multiphase flow processes. A variety of oil recovery methods have been studied in micromodels, such as gravity drainage,[5-7] miscible gasflood,[8, 9] polymer-flooding,[10, 11] vapour extraction[12] and water alternating gas injection[13, 14]. Image processing and analysis tools have also been developed to quantify and evaluate the saturation of fluids in micromodels[15, 16]. The visualization of fluid flow in micromodels helps with the interpretation of core experiment data[17, 18] and development of mathematical models for multiphase flow processes in porous media[19-21].

Micromodels have been manufactured with various methodologies. In wet etching processes, transparent substrates, such as glass[22-24] and calcite,[25] are coated with materials that can be removed with lithography or laser ablation techniques to create a designed pore network pattern. The pattern is then etched with a particular depth by contacting the exposed surface of substrates with corrosive fluids. Then, the created flow channels are sealed bonding an etched substrate to a blank plate. Pore network chips with small

dimensions have also been fabricated with the dry etching of glass[26] and silicon substrates[27, 28] using the reactive-ion technology. Glass plates in large dimensions can be directly etched with CO_2 laser.[5] The laser may leave undesired fractures due to thermal expansion of ablated zones.[29, 30] However, laser etching was successfully implemented on the surface of borosilicate and quartz glasses keeping the substrates hot during engraving.[31] Acrylic (poly methyl methacrylate) plates can also be etched with lasers without forming cracks in engraved zones when laser parameters are optimized.[32, 33] In this work, acrylic (Plexiglas™) plates were etched by CO_2 laser for the fabrication of micromodels because of a low cost and simplicity of the procedure.

3.2.2. Hydraulic Continuity of a Wetting Phase in a Porous Medium

During a multiphase flow process in a porous medium (e.g. drainage and imbibition) a differential pressure exists at the interface between wetting and non-wetting fluids called capillary pressure.[34] The capillary pressure is directly proportional to the interfacial tension between two fluids and inversely proportional to the size of a pore where the displacement of their interface occurs.[35] The capillary pressure controls final saturations of fluids during an immiscible displacement.[36] In a drainage process, a non-wetting phase requires a lower pressure to displace a wetting phase through larger pores, so the residual wetting phase is often bypassed in smaller pores surrounded by larger pores and fractures.[6, 19, 37] A subsequent increase of the differential pressure between the non-wetting and wetting phases allows the entry of the non-wetting phase into bypassed zones. However, a path must be available for the flow of the wetting phase toward a new zone.

Dullien and colleagues for the first time showed that in a synthetic porous medium made from glass beads, the lack of these fine paths on the surface of solid grains can impact results of capillary pressure curves during drainage and imbibition processes.[36, 38] They made two columns from glass beads, with smooth surfaces and with scratched surfaces, and found that adding fine capillaries on the surface of solid grains helped with the reduction of the residual wetting phase in a drainage process. It was also discussed that the flowrate of the wetting phase on the surface of smooth glass beads in the form of thin films was too low and unmeasurable. However, the presence of fine paths helped with the flow of the residual wetting phase in the form of thick films with a measurable rate. Therefore, the residual wetting phase could practically flow between regions bypassed with the non-wetting phase when the capillary pressure was increased sufficiently.[36, 38] In permeable rocks, such as sandstone, fine capillaries are formed through irregularities existing on the surface of connected solid grains as shown in Figure 3-1.

The investigation of the gas assisted gravity drainage (GAGD) process in sandstone showed that a high recovery of a waterflood residual oil could be obtained under water-wet conditions when a capillary barrier was used at the bottom of the medium.[39] The capillary barrier increased the differential pressure between gas and liquid phases (i.e., oil and water) as the gas phase required a higher pressure to flow through the barrier compared to liquid phases. Consequently, a further recovery of oil from initially bypassed zones was possible due to a subsequent increase in the capillary pressure at interfaces between gas and liquid phases when the gas-front reached to the capillary barrier. The enhancement of the capillary pressure is possible in regions with a hydraulic link to the

capillary barrier. This link at high saturations of gas is maintained through fine paths of the porous medium. The hydraulic continuity of the residual wetting phase in a porous medium is terminated at increased capillary pressures due to geometric constraints of fine capillaries. [40, 41] In the presence of three phases, the hydraulic continuity of the intermediate-wetting phase can also be affected by the saturation of the wetting phase in capillary corners (e.g., flow of oil in the corner of a water-wet capillary).[42]

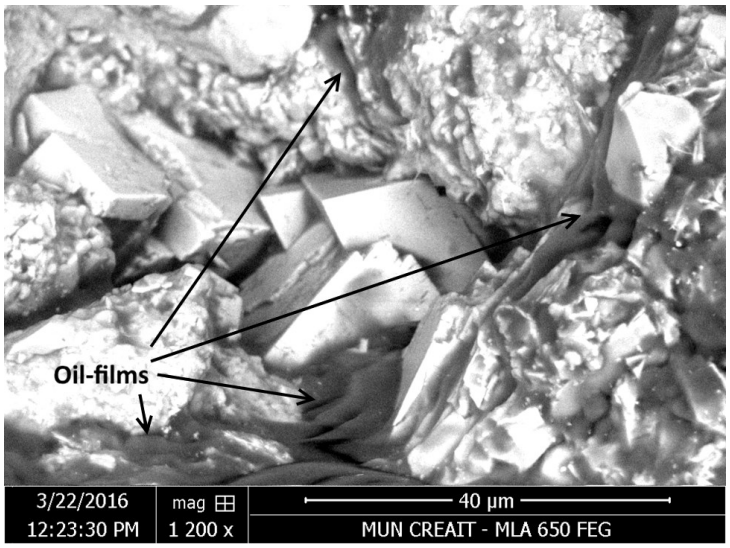

Figure 3-1. Oil-films on the surface irregularities of solid grains in sandstone rock (Hibernia EOR Lab).

Micromodels with heterogeneous[43] and dual-permeability[44] pore networks have been fabricated for visualizing oil recovery processes at the pore-level. In such micromodels, the pore network was formed between separated solid grains without fine paths connecting zones with different pore sizes. Although a thin film of the wetting phase may cover the smooth surfaces of plates between solid grains, the rate of flow through thin films is low and may not be accounted for an oil recovery process. The objective of this

work is to develop a new micromodel that contain fine and coarse pore network in parallel, maintaining the transparency of the medium. This improvement is demonstrated by GAGD experiments under oil-wet and water-wet micromodels at irreducible and post-waterflood conditions, respectively.

3.3. Theory

The influence of fine capillaries on a vertical displacement of oil by gas in an oil-wet medium is schematically shown in Figure 3-2. The interface between oil and gas in a pore is curved because of the capillary effect. The mean curvature at an interface between oil and gas, C_{go}, can be calculated by Eq. 3.1,[36]

$$C_{go} = \frac{P_{cgo}}{2\sigma_{go}} \tag{3.1}$$

where P_{cgo} is the gas-oil capillary pressure, and σ_{go} is the gas-oil interfacial tension. The curvature at the oil and gas interface is greater when oil is displaced through smaller pores, thus a higher gas-oil capillary pressure must be overcome. The gas-front prefers to displace oil through larger pores where is the path of least resistance (the curvature at gas-oil interface is smaller). Figure 3-2: a & b show that the gas-front bypasses an oil-occupied pore with small throats, and the residual oil was left isolated above the gas-front. In this situation, any subsequent variation of the gas-oil capillary pressure in the gas-front, P_{cgo}^{f}, may no longer contribute to the recovery of the bypassed oil. In addition, the hydrostatic pressure of oil in the bypassed pore is no longer affected by the vertical distance between the gas-front and the bypassed zone.

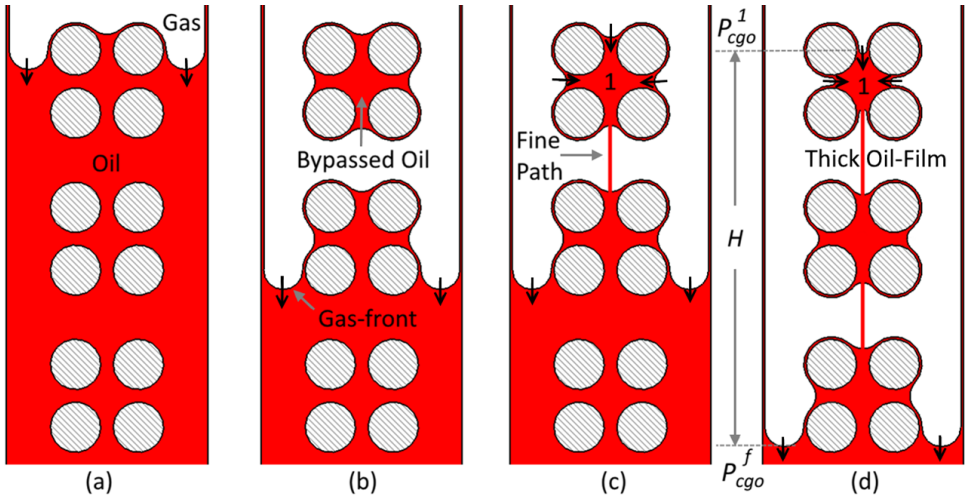

Figure 3-2. (a): The drainage of oil by gas through paths of least resistance. (b): The bypass and isolation of oil in a pore with small throat without any hydraulic continuity to lower elevations. (c): The bypassed oil maintained a hydraulic continuity with the gas-front through a fine path. (d): The reduction of oil hydrostatic pressure at higher elevations can result in the increase of the gas-oil capillary pressure and drainage of the oil in point 1 (P_{cgo}^{f}: gas-oil capillary pressure in the gas-front, P_{cgo}^{1}: gas-oil capillary pressure above the gas-front in point 1, H: vertical distance between point 1 and gas-front).

In Figure 3-2: c, the bypassed pore maintained its hydraulic continuity with the gas-front through a fine path. This path allows a downward flow of the bypassed oil as gravity can reduce the oil pressure at higher elevations. Therefore, the curvature of the gas-oil interface at point 1 is increased upon an elevation of the gas-oil differential pressure or capillary pressure. In Figure 3-2: d, the distance between the bypassed pore and gas-front is further increased. Consequently, gas can enter the bypassed pore upon a sufficient elevation of the gas-oil capillary pressure. The contribution of gravity in the enhancement of the gas-oil capillary pressure above the gas-front at point 1, P_{cgo}^{1}, is shown in Eq. 3.2,

$$P_{cgo}^{1} = P_{cgo}^{f} + \Delta\rho_{go} g H \tag{3.2}$$

where $\Delta\rho_{go}$ is the gas-oil differential density, and H is the distance between gas-front and point 1. In Eq. 3.2, it is assumed that the saturation of oil in point 2 is invariant, and the drainage process is performed at a low rate so the reduction of the oil pressure in point 1 is unaffected by the viscous pressure drop in the fine path.

The viscous pressure drop associated with the flow of oil in fine paths may prevent a rapid discharge of the bypassed pore into the gas-front. Therefore, the distance between a bypassed pore and gas-front may increase. However, the bypassed oil can eventually flow through a fine path toward a new destination at a lower elevation gradually. This process continues until an equilibrium establishes between capillary and gravity forces. Another parameter that can restrict the flow of oil from higher to lower elevations is the geometry of a fine path. A fine path, depending on its corner geometry, may allow a limited increase of the gas-oil capillary pressure beyond which the hydraulic continuity of oil through thick films is terminated. Eventually, the irreducible residual oil may be found in capillary corners around solid grains and pores with small throats.

3.4. Development of Pore Network Micromodels

3.4.1. Fabrication Procedure

The coarse pore network of micromodels was designed as a bitmap image with a resolution of 2000 dot per inch (DPI) and was engraved on the surface of an acrylic plate (Plexiglas™) using CO2 laser (Trotec Speedy 300™). The main parameters of the laser are the speed and power. A good quality of etching was obtained setting the power and speed of the laser between 8-12 W and 25-35 cm/sec, respectively. Figure 3-3 shows a

microscopic image from the surface of an acrylic plate etched with a power of 10 W and speed of 30 cm/sec that resulted in the penetration depths ranging from 140 ± 5 μm (in small pores) to 160 ± 5 μm (in large pores).

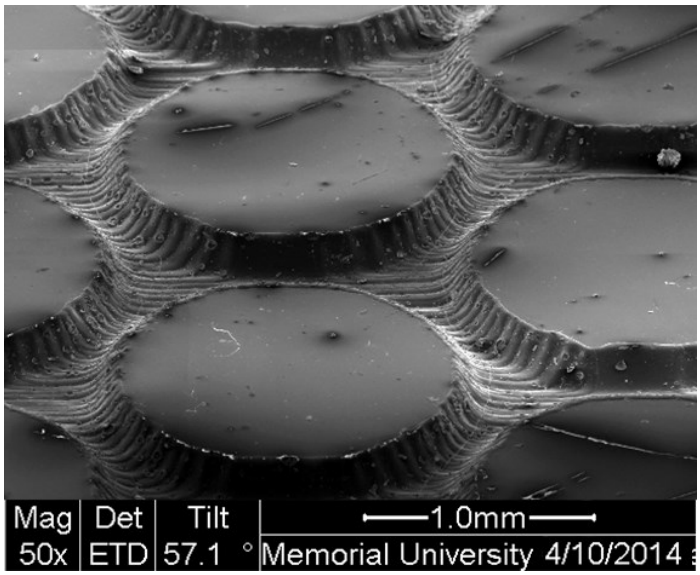

Figure 3-3. A laser etched acrylic plate under scanning electronic microscope.

The micromodel without fine capillaries was fabricated bonding a laser etched plate (containing the coarse pore network) with a blank plate. Two plates were bonded in an oven at a temperature of 130°C after 48 hrs. In the micromodel with fine capillaries, the blank plate was replaced by a plate containing fine scratches created with a grit 60 sandpaper. The width of fine capillaries ranges from 40 ± 5 μm to 120 ± 5 μm, and their depth ranges from 20 ± 5 μm to 40 ± 5 μm. These fine capillaries can improve the hydraulic continuity of the wetting phase covering coarse pores of micromodels. Fine capillaries created by finer sandpapers were dissipated during thermal bonding, and using coarser sandpapers impacts the micromodel visibility. An image of a region in micromodel containing both coarse pores and fine capillaries is shown in Figure 3-4.

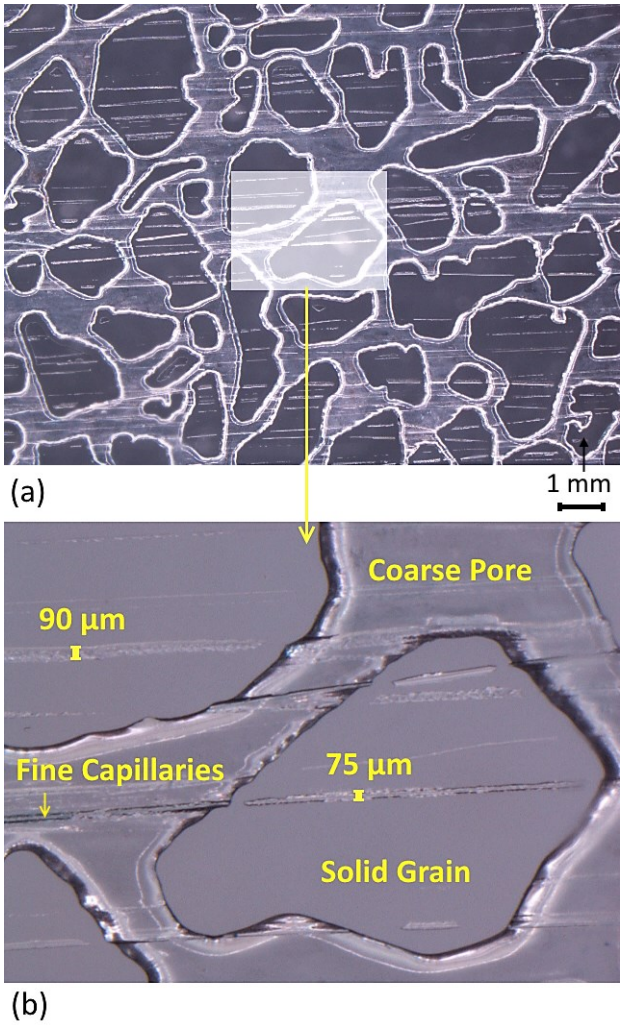

Figure 3-4. (a): Image of a zone in micromodel under a microscope showing coarse pores covered by fine capillaries. (b): Magnified image of the indicated zone.

A custom fitting was also designed and manufactured from stainless steel for the flow of test fluids (Figure 3-5). Each fitting contains two ports that allow circulation of fluids at the top and bottom parts of micromodels. Acrylic micromodels can be re-used by cleaning with hexane and water to remove non-aqueous and aqueous fluids, respectively. The solvents can be removed and dried with the flow of compressed air. It is noted that

acetone, alcohols, and toluene dissolve the acrylic and therefore cannot be used for the cleaning of micromodels.

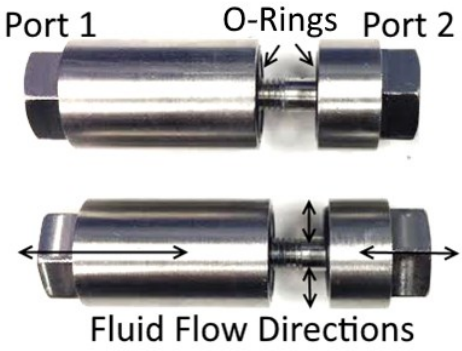

Figure 3-5. Custom designed fittings for micromodel.

3.4.2. Micromodel Wettability

A fresh acrylic micromodel becomes strongly oil-wet without affecting its transparency when contacted with a clear oil such as Varsol™. Acrylic absorbs oil, thus aging a clean micromodel with oil for 1 hr prior to an experiment ensures strong oil-wet conditions. The deposition of hydrophilic material on the surface of polymers provides a water-wet condition. A commercially available solution containing nano-silica gel[45] was injected into a clean micromodel to prepare a strongly water-wet condition. The solution was removed with the flow of compressed air, and a thin layer of the hydrophilic material was cured on the surface of pores without affecting the visibility and permeability of micromodels. Images of a pattern under oil-wet and water-wet conditions are shown in Figure 3-6: a & b, respectively (note films of red oil (a) and blue water (b) in the fine capillaries of the oil-wet and water wet micromodels). The colour intensity of wetting phase films in fine capillaries due to a low thickness is unremarkable. Images of

micromodels were recorded using Canon 6D camera and Canon EF 100 mm f/2.8 USM lens.

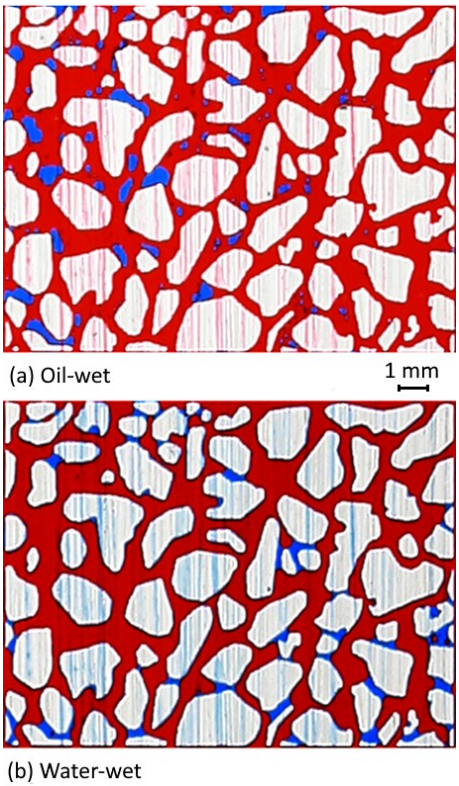

Figure 3-6. Image of a pattern in (a) oil-wet and (b) water-wet micromodels showing films of wetting phases in fine capillaries. Images were sharpened to better show fine capillaries (unprocessed images, red: oil, blue: water, white: grains, pattern size: 16×12 mm).

3.5. Experimental Detail

3.5.1. Porous Medium

The performance of oil-wet micromodels with and without fine capillaries was evaluated with GAGD experiments under various conditions. Figure 3-7 shows the coarse pore network of micromodels formed by repeating of a heterogeneous pattern (Figure 3-6) that

is designed based on a magnified image of a thin sand section. The width of pores ranges from 0.15 to 1.30 mm, and the average depth of pores is 0.15 mm. The pore sizes were designed in a range that can be engraved with the laser device. In addition, horizontal and vertical channels (width: 1 mm) were placed between the repeated pattern to play the role of large heterogeneities in the central region of the micromodel. This zone mimics a particular form of heterogeneity where matrices are surrounded by fractures. The width of fractures is larger than sizes of pore that are in contact with fractures. Therefore, it is expected that the gas-front follows the fractured network when capillary forces are dominant. The difference between different zones of the micromodel also helps us to demonstrate the influence of the pore-level heterogeneities on GAGD perfromance. The permeability of the developed micromodel is measured at 24 Darcy, and the porosity of the pattern is 0.48.

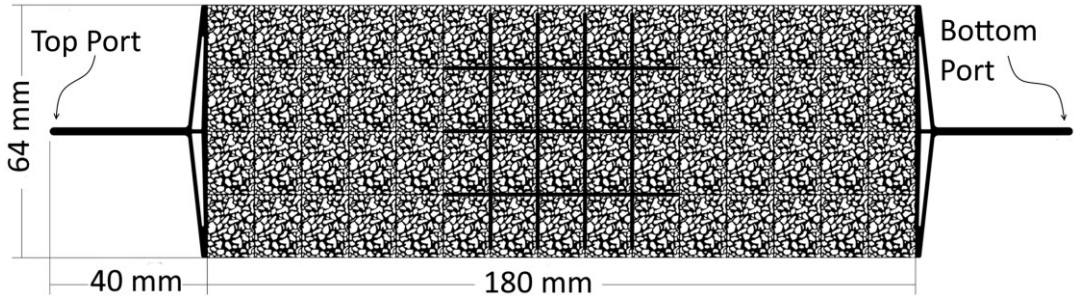

Figure 3-7. The coarse pattern of micromodel designed for GAGD experiments and the pathways for the injection and production of test fluids.

The range of capillary pressure between air and water (surface tension: 72 mN/m) in the fabricated micromodel under water-wet conditions is approximately from 500 to 1000 Pa. This range is approximately 20 times smaller than the range of capillary pressure

measured with the same pair of fluids in a sandstone[46]. In addition, the gradient of pressure drop due to gravity is approximately 10 Pa/mm, and the gradient of the viscous pressure drop when air displaces water with an average gas-front velocity of 100 mm/hr is approximately 1 Pa/mm (in zones with a permeability of 24 Darcy). Although pore sizes in the fabricated micromodel are one order of magnitude larger than permeable rocks (e.g., sandstone), the domination of capillary forces in the gas-front over gravitational and viscous forces can be maintained. In addition, the length of the micromodel pattern (180 mm) is sufficient to allow the drainage of a wetting phase from smaller pores toward the micromodel bottom due to an interaction between gravity and capillarity.

3.5.2. Image Analysis

The saturations of fluids were quantified with an in-house developed image processing and analysis program. The image analysis program evaluates the intensity of red, blue and green components in every pixel of a micromodel image cropped to contain the pattern area. Consequently, the saturation of oil (red pixels), water (blue pixels) and gas were calculated. The image processing parameters were calibrated with respect to the volumetric data recorded by a pump, and the uncertainty associated with the saturation of fluids is ± 0.02 PV. The image analysis methodology is discussed in detail in the Appendix B. A code was also provided that can be modified and used for other applications.

3.5.2. Experimental Design

The design of the experiment is shown in Table 3-1. GAGD tests were conducted at irreducible water saturations under oil-wet conditions in micromodels with and without fine capillaries (tests 1 and 2) at a production rate of 0.1 ml/hr. In addition, a GAGD test was repeated in a duplicate of micromodel with fine capillaries (test 3) to examine the reproducibility of data. Furthermore, a post-waterflood GAGD experiment was conducted in a water-wet micromodel with fine capillaries (test 4). Different micromodels were used for conducting GAGD experiments. The pore volume (PV) of micromodels was measured by mass balance as shown in Table 3-1. The gas phase in tests 1-3 was CO_2 (pressure: 3 bars), and in test 4 was air (pressure: 4 bars). All experiments were performed at a temperature of 24°C. No swelling and evaporation of oil was observed when equilibrated with CO_2 and air under corresponding conditions of experiments. Therefore, all experiments were under immiscible conditions. The interfacial tension between test fluids (red dyed Varsol™, blue dyed deionized water, air and CO_2) was measured using the VINCI IFT 700 apparatus as shown in Table 3-1. The oil-water interfacial tension was 31.5 ± 0.8 mN/m.

Table 3-1. The experimental design and test parameters.

Test ID	Capillary Continuity	Micromodel Pore Volume (ml)	Gas	Pressure (Bars)	Production Rate (ml/hr)	Gas-Oil Interfacial Tension	Gas-Water Interfacial Tension
1	Strong	0.940	CO_2	3.0	0.1	22.1 ± 0.4	71.8 ± 1.6
2	Weak	0.855					
3	Strong	0.840					
4	Strong	0.850	Air	4.0	0.2	24.8 ± 0.4	71.5 ± 1.2

3.5.3. Experimental Setup

Figure 3-8 shows the piping and instrumentation diagram of a setup developed for conducting GAGD experiments in micromodels. Test fluids were stored in accumulators and delivered to a micromodel using a pump (Quizix 20K) for establishing the initial saturations of fluids. The initial oil saturation in micromodels under oil-wet conditions (test 1-3) was established in two steps. In the first step, a fully oil-saturated micromodel (aged for 1 hr) was flooded by 10 PV of water from its bottom port at 1 ml/min. In the second step, 10 PV of Varsol™ oil was injected from the top port of micromodels at 5.00 ml/min to lower the water saturation to an irreducible level. The initial oil saturation under water-wet conditions was established by injecting 10 PV of oil at 7.50 ml/min into a fully water-saturated micromodel followed by a waterflood process. The waterflood was performed with a production rate of 2 ml/hr, and it was terminated at a water-breakthrough. The piping of the experimental setup was designed to perform the waterflood from the bottom port, thus stabilizing the oil displacement by gravity. GAGD experiments were initiated injecting gas from the top port of micromodels under a constant pressure and producing fluids with a constant rate from the bottom port of micromodels (see Table 3-1). The tubing and fittings at the upstream of micromodels were cleaned prior to gas injection to avoid the entry of any trapped oil or water during GAGD experiments.

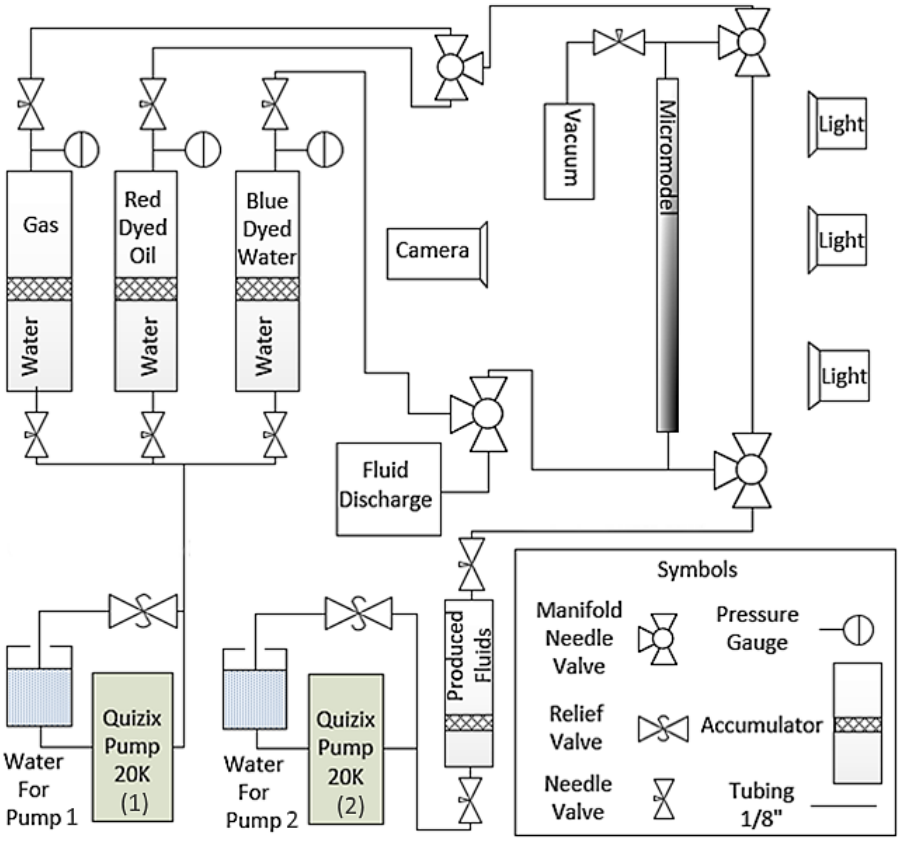

Figure 3-8. Schematic of GAGD setup showing piping and instrumentation diagram.

3.6. Results and Discussion

The result of GAGD experiments under oil-wet conditions in micromodel with fine capillaries is shown in Figure 3-9, and in micromodel without fine capillaries is shown in Figure 3-10. The comparison of the initial and final saturations of fluids before and after GAGD in two micromodels indicates that the fine capillaries significantly influenced the recovery of oil. Although the initial oil saturation in both micromodels was 0.89 PV, the residual oil saturation after 12 hrs in micromodel with fine capillaries was 0.21 PV (oil recovery factor: 76%) compared to 0.40 PV in micromodel without fine capillaries (oil recovery factor: 55%). The repeated GAGD experiment in the duplicate of micromodel with fine capillaries resulted in an initial oil saturation of 0.88 PV and a residual oil

saturation of 0.25 PV (oil recovery factor: 72%). Unprocessed images of micromodel during the repeated experiment is shown in Figure 3-11.

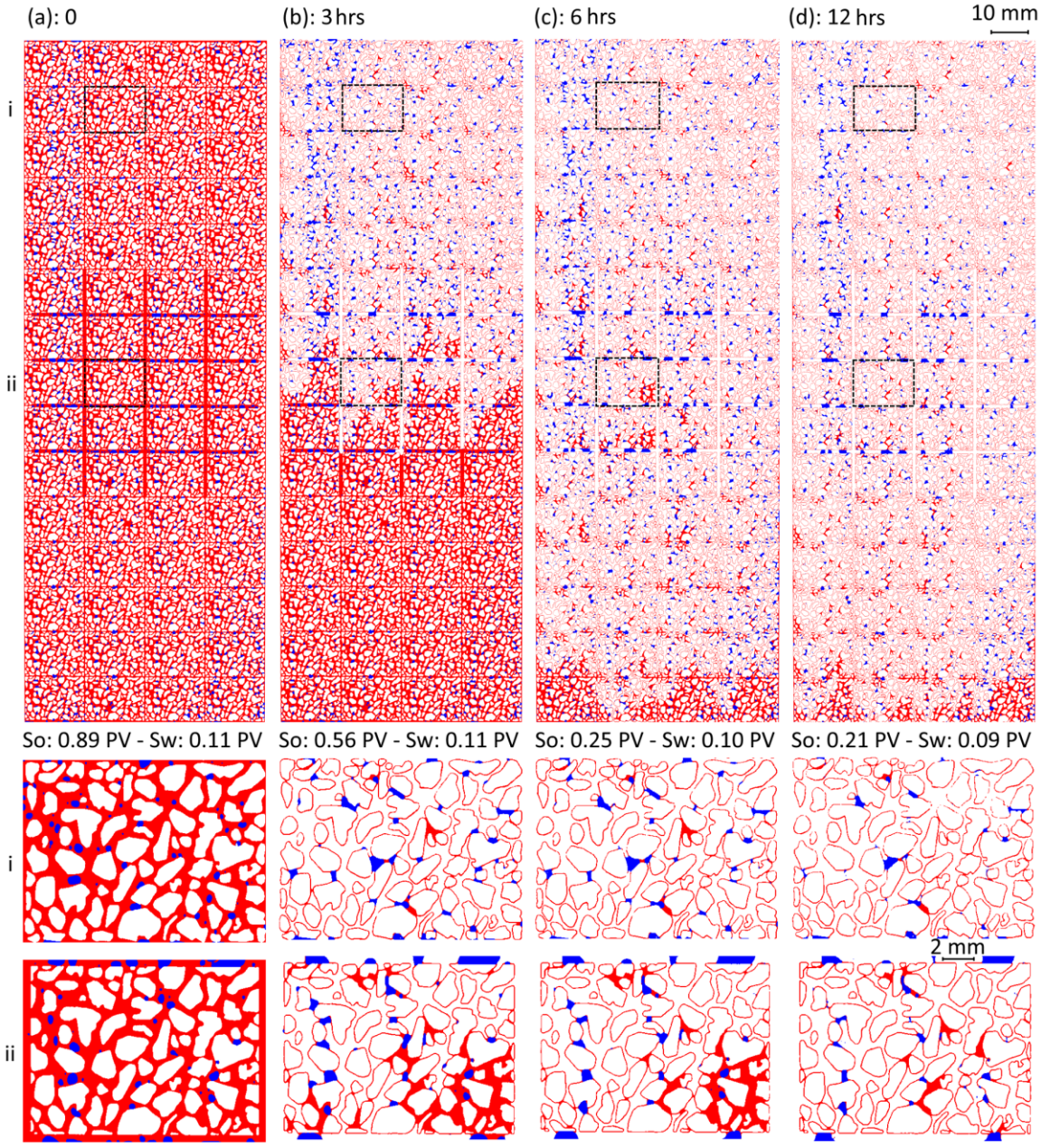

Figure 3-9. Images of oil-wet micromodel with fine capillaries during GAGD in test 1. (a): Prior to gas injection. (b): After 3 hours. (c): Gas-breakthrough. (d): After 12 hrs. (i & ii): Magnified images of the indicated zones (processed images, red: oil, blue: water, So: oil saturation, Sw: water saturation).

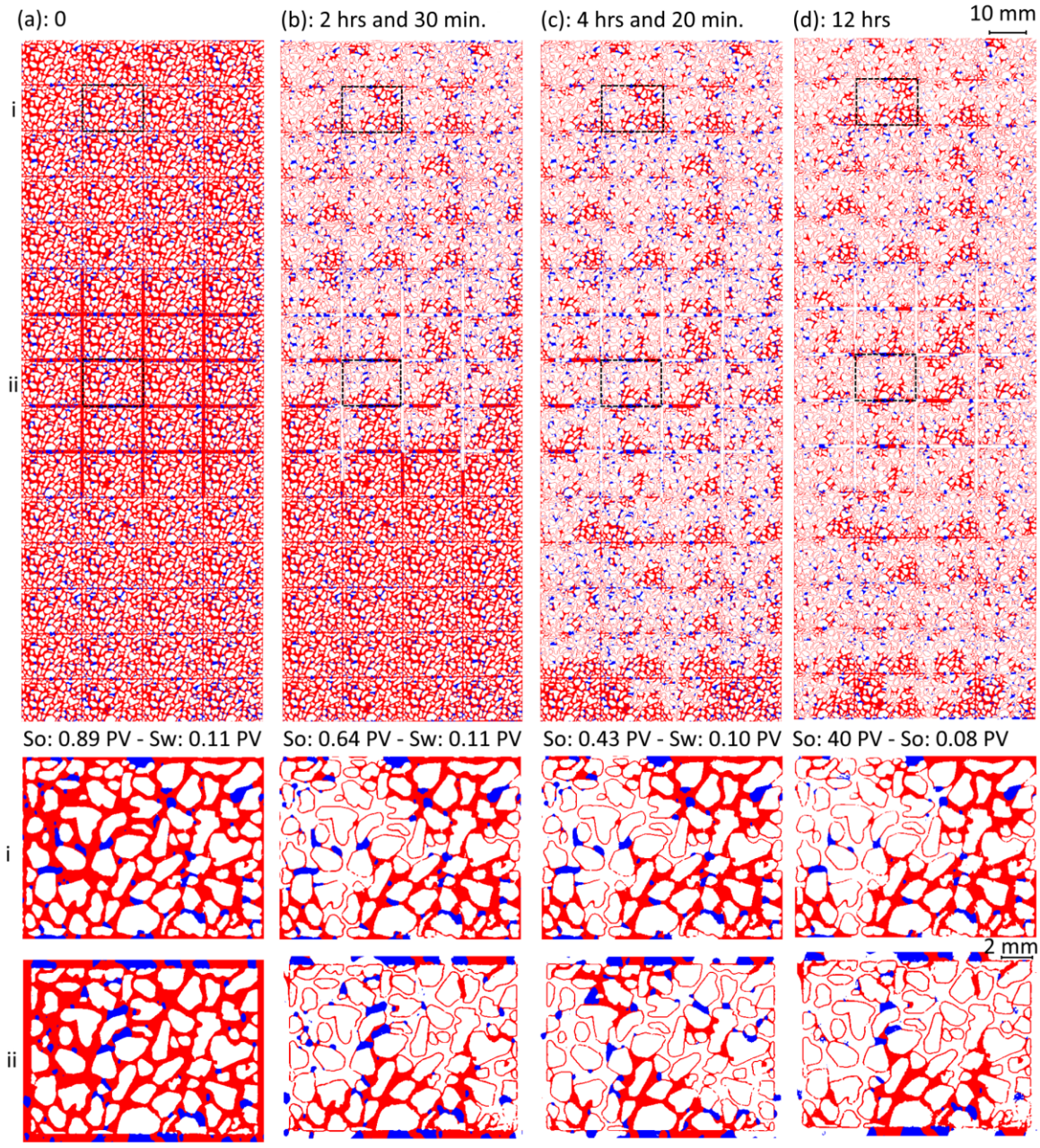

Figure 3-10. Images of oil-wet micromodel without fine capillaries during GAGD in test 2. (a): Prior to gas injection. (b): After 2 hrs & 30 min. (c): Gas-breakthrough. (d): After 12 hrs. (i & ii): Magnified images of the indicated zones (processed images, red: oil, blue: water, So: oil saturation, Sw: water saturation).

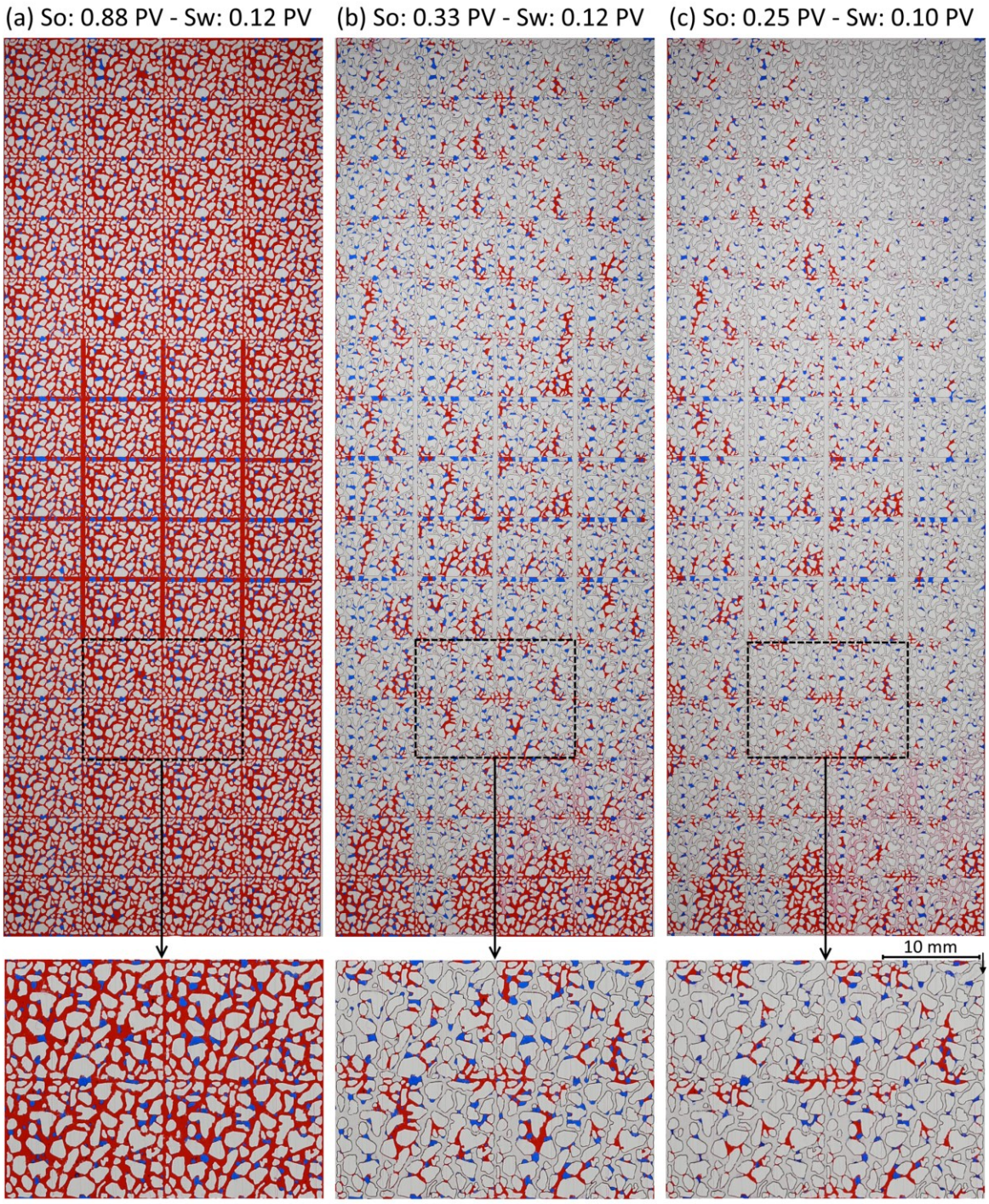

Figure 3-11. Images of oil-wet micromodel with fine capillaries during GAGD in test 3. (a): Prior to gas injection. (b): Gas-breakthrough. (c): After 12 hrs (unprocessed images, red: oil, blue: water, So: oil saturation, Sw: water saturation).

The average gas-front velocity in micromodel with fine paths was 30 mm/hr (gas-breakthrough time: 6 hrs) and in micromodel without fine paths was 40 mm/hr (gas-breakthrough time: 4 hrs and 20 minutes). The presence of heterogeneities in micromodels caused gas to bypass oil in in small pores surrounded by large pores, particularly in the fracture-matrix region, as expected in a drainage process. In micromodel with fine capillaries a subsequent enhancement of the gas-oil capillary pressure at higher elevations helped with the recovery of the bypassed oil. However, in micromodel without fine capillaries the bypassed oil was unable to maintain an effective hydraulic continuity to lower elevations, thus resulting in a higher residual oil saturation. A slight reduction of the residual oil saturation in the micromodel without fine capillaries occurred after the gas-breakthrough. The pattern of the micromodel formed straight corners in vertical boundaries of the pattern, which provided fine paths for the film flow of the residual oil. However, the residual oil in bypassed pores away from the vertical margins of the pattern was unable to drain because of a capillary discontinuity.

The image of micromodels (Figure 3-9: d and Figure 3-10: d) were divided into 15 equal sections along the vertical axis (size of divisions: 64×12 mm) to calculate the residual oil saturation of each division with respect to their elevations as shown in Figure 3-12. The calculated residual oil saturations were plotted against the vertical distance between the center of each division and the bottom of the pattern. In both micromodels, a higher oil saturation was retained in the zones near the bottom of the pattern. The entry of gas into the outlet path of micromodels, which is 2 mm wide, dropped the gas-oil capillary pressure dramatically. Consequently, a higher residual oil saturation was retained at the

bottom of the pattern in both micromodels due to the capillary end effect. The residual oil saturation in micromodel with fine capillaries decreased at higher elevations. However, in micromodel without fine capillaries, no clear trend in the reduction of the residual oil saturation was observed, and the bypassed oil was retained with higher saturation. The reducing trend of the oil saturation in micromodel with fine capillaries is similar to the curves obtained during gravity drainage experiments in sand-packs[21] and sandstone[46].

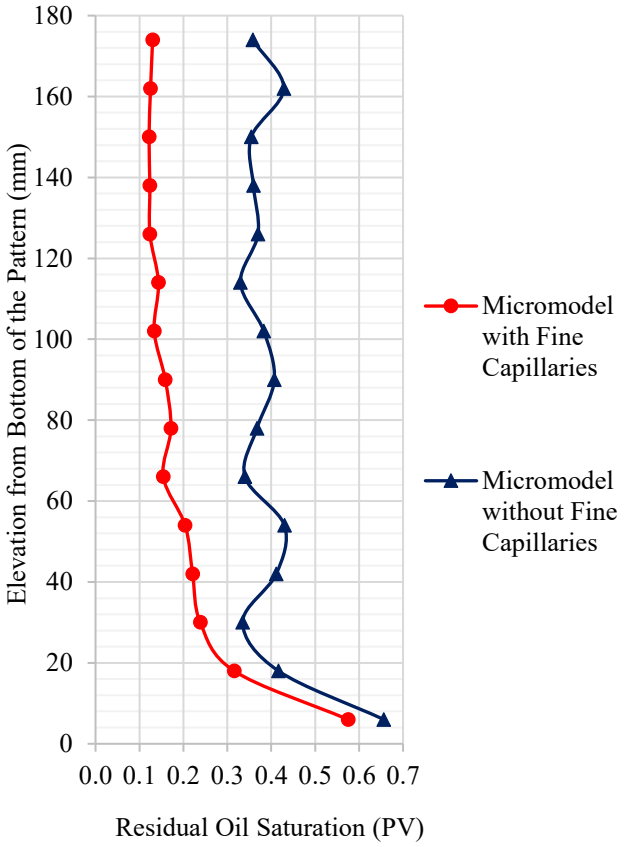

Figure 3-12. The residual oil saturation in micromodels with and without fine capillaries vs. the distance from the bottom of the pattern (tests 1 & 2 after 12 hrs).

Figure 3-13 shows results of post-waterflood GAGD experiments in a micromodel with fine capillaries under water-wet conditions. In the waterflood, the path of breakthrough

was formed in smaller pores, as excepted in an imbibition process (Figure 3-13:a). Therefore, waterflood residual oil was surrounded by water in the body of larger pores. In post-waterflood GAGD, the waterflood oil-blobs were able to reconnect upon the drainage of their surrounding water. The connected oil-blobs created an oil-bank ahead of the gas-front that displaced water. It was observed that the residual water was retained in smaller pores, and the majority of oil was bypassed with gas. The hydraulic continuity of bypassed oil (intermediate-wetting phase) in both coarse and fine pore network was initially hindered by the presence of the residual water (wetting phase) in small pores, fine paths and around solid grains (Figure 3-13: b). The residual water in smaller pores used fine paths to flow from higher toward lower elevations (Figure 3-13: c). Subsequently, oil used opened spaces in the coarse pore network as well as fine paths to flow downward upon the reduction of the water saturation. An effective reduction of the oil saturation was observed after 33 hrs, particularly from upper zones of the micromodel (Figure 3-13: d). It was also observed that the presence of large heterogeneities in central regions of the micromodel contributed to the bypass of oil and water with high saturations. It is speculated that the saturation of the residual oil from these zones can be reduced with the continuation of the experiment when the saturation of the residual water at higher elevations is effectively reduced.

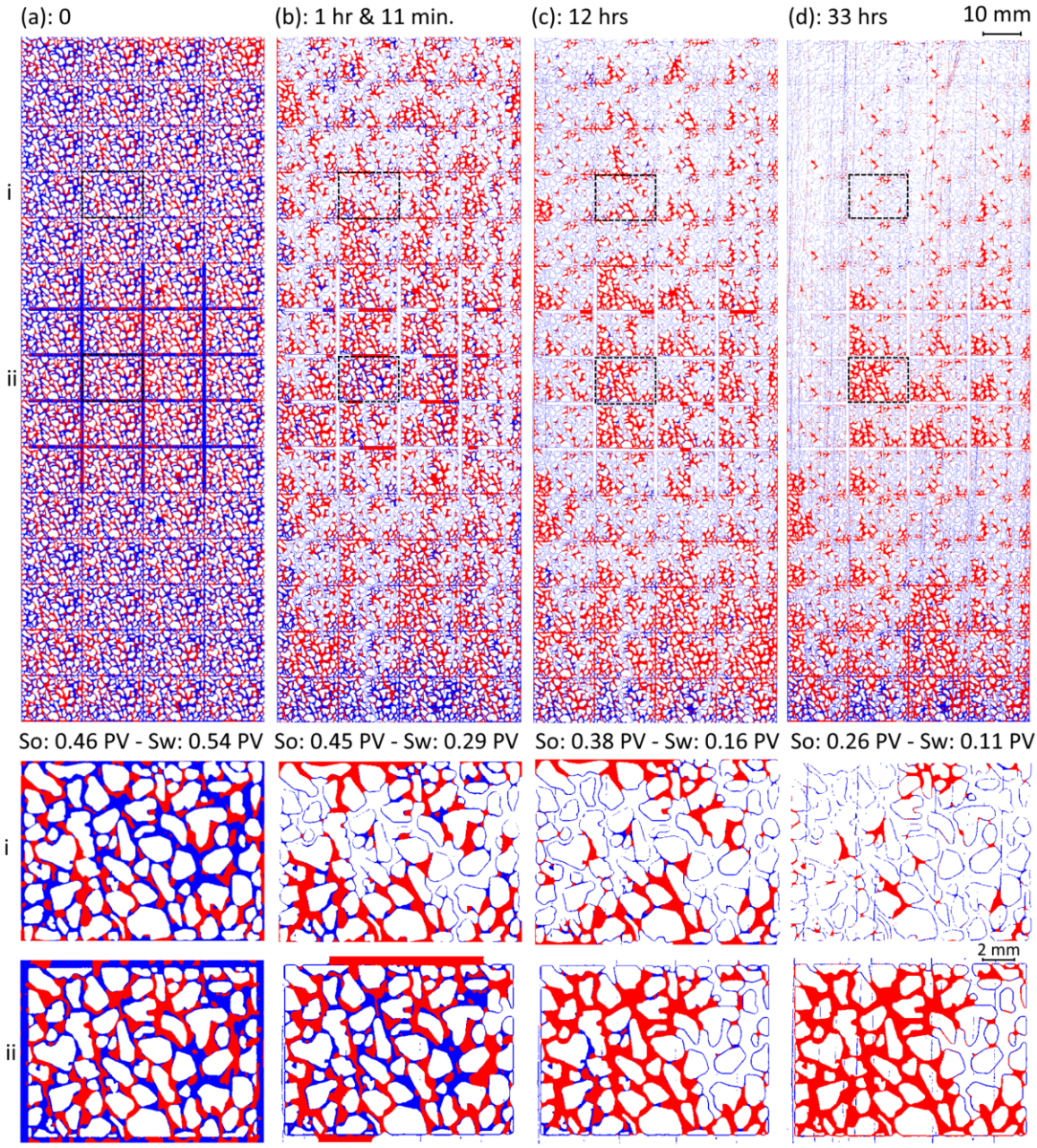

Figure 3-13. Images of water-wet micromodel with fine capillaries during post-waterflood GAGD in test 4. (a): Prior to gas injection. (b): Gas-breakthrough. (c): After 12 hrs. (d): After 33 hrs. (i & ii): Magnified images of the indicated zones (processed images, red: oil, blue: water, So: oil saturation, Sw: water saturation).

The current work demonstrated a concept for improving the hydraulic continuity of a residual wetting phase in transparent porous media. The new micromodel is a platform for the fabrication transparent porous media that provides strong hydraulic continuity for fluids similar to a real-rock porous medium. The transparency and improved capillary continuity can be utilized for studying phenomena affecting the releative permeability of fluids.

3.7. Chapter Conclusions

A new micromodel has been developed to study oil recovery processes in a porous medium containing a coarse pore network covered by fine capillaries. Results of GAGD experiments in micromodels showed that the presence of fine capillaries contributed to a significant reduction of the residual wetting phase saturation by improving its hydraulic continuity. However, in the micromodel without fine capillaries the drainage of the wetting phase was restricted as the coarse pore network is formed between separated solid grains leading to a hydraulic discontinuity. The current work demonstrated a concept for improving the hydraulic continuity of a residual wetting phase in transparent porous media. The new micromodel provides a strong platform for investigating the relative permeability of fluids in various oil recovery processes.

Chapter References

1. Vizika, O.; Lombard, J., Wettability and spreading: two key parameters in oil recovery with three-phase gravity drainage. *SPE Reservoir Engineering* **1996,** 11, (01), 54-60.
2. Meszaros, G.; Chakma, A.; Jha, K.; Islam, M. In *Scaled model studies and numerical simulation of inert gas injection with horizontal wells*, SPE Annual Technical Conference and Exhibition, September 23-26, 1990; Society of Petroleum Engineers: New Orleans, Louisiana, USA, 1990.
3. Zendehboudi, S.; Chatzis, I., Laboratory investigation of free fall gravity drainage in fractured porous systems using unconsolidated macromodels. *Energy & Fuels* **2011,** 25, (5), 2356-2372.
4. Parsaei, R.; Chatzis, I., Experimental investigation of production characteristics of the gravity-assisted inert gas injection (GAIGI) process for recovery of waterflood residual oil: effects of wettability heterogeneity. *Energy & Fuels* **2011,** 25, (5), 2089-2099.
5. Zareh, N.; Kharrat, R.; Ghazanfari, M., An Experimental Investigation of the Effect of Fracture Dip Angle on Oil Recovery and Drainage Rate in Free Fall Gravity Drainage in Fractured Reservoirs Using a Glass Micromodel (A Pore Level Investigation). *Petroleum Science and Technology* **2013,** 31, (4), 355-367.
6. Catalan, L. J.; Dullien, F. A.; Chatzis, I., The effects of wettability and heterogeneities on the recovery of waterflood residual oil with low pressure inert gas injection assisted by gravity drainage. *SPE Advanced Technology Series* **1994,** 2, (02), 140-149.
7. Kantzas, A.; Chatzis, I.; Dullien, F. In *Mechanisms of capillary displacement of the residual oil by gravity-assisted inert gas injection*, Proceeding of the SPE Rocky Mountain Regional Meeting, May 11-13, 1988; Casper, Wyoming, USA, 1988.
8. Campbell, B. T.; Orr Jr, F. M., Flow visualization for co2/crude-oil displacements. *Society of Petroleum Engineers Journal* **1985,** 25, (05), 665-678.

9. Oren, P. E.; Pinczewski, W. V., The effect of wettability and spreading coefficients on the recovery of waterflood residual oil by miscible gasflooding. *SPE Formation Evaluation* **1994,** 9, (02), 149-156.
10. Buchgraber, M.; Clemens, T.; Castanier, L. M.; Kovscek, A., A microvisual study of the displacement of viscous oil by polymer solutions. *SPE Reservoir Evaluation & Engineering* **2011,** 14, (03), 269-280.
11. Aktas, F.; Clemens, T.; Castanier, L.; Kovscek, A. R. In *Viscous Oil Displacement via Aqueous Associative Polymers*, SPE symposium on improved oil recovery, April 20-23, 2008; Society of Petroleum Engineers: Tulsa, Oklahoma, USA, 2008.
12. James, L.; Rezaei, N.; Chatzis, I., VAPEX, Warm VAPEX and hybrid VAPEX-The state of enhanced oil recovery for in situ heavy oils in Canada. *Journal of Canadian Petroleum Technology* **2008,** 47, (04).
13. Sohrabi, M.; Tehrani, D.; Danesh, A.; Henderson, G., Visualization of oil recovery by water-alternating-gas injection using high-pressure micromodels. *SPE Journal* **2004,** 9, (03), 290-301.
14. Dong, M.; Foraie, J.; Huang, S.; Chatzis, I., Analysis of immiscible water-alternating-gas (WAG) injection using micromodel tests. *Journal of Canadian Petroleum Technology* **2005,** 44, (02).
15. Meybodi, H. E.; Kharrat, R.; Araghi, M. N., Experimental studying of pore morphology and wettability effects on microscopic and macroscopic displacement efficiency of polymer flooding. *Journal of Petroleum Science and Engineering* **2011,** 78, (2), 347-363.
16. Chang, L.-C.; Tsai, J.-P.; Shan, H.-Y.; Chen, H.-H., Experimental study on imbibition displacement mechanisms of two-phase fluid using micro model. *Environmental Earth Sciences* **2009,** 59, (4), 901-911.
17. Chatzis, I.; Dullien, F., Dynamic immiscible displacement mechanisms in pore doublets: theory versus experiment. *Journal of Colloid and Interface Science* **1983,** 91, (1), 199-222.
18. Morrow, N. R.; Lim, H. T.; Ward, J. S., Effect of crude-oil-induced wettability changes on oil recovery. *SPE Formation Evaluation* **1986,** 1, (01), 89-103.

19. Lenormand, R.; Zarcone, C.; Sarr, A., Mechanisms of the displacement of one fluid by another in a network of capillary ducts. *Journal of Fluid Mechanics* **1983,** 135, 337-353.
20. Oren, P. In *Pore-scale network modelling of waterflood residual oil recovery by immiscible gas flooding*, SPE/DOE Improved Oil Recovery Symposium, April 17-20, 1994; Society of Petroleum Engineers: Tulsa, Oklahoma, 1994.
21. Vizika, O.; Avraam, D.; Payatakes, A., On the role of the viscosity ratio during low-capillary-number forced imbibition in porous media. *Journal of colloid and interface science* **1994,** 165, (2), 386-401.
22. McKellar, M.; Wardlaw, N., A method of making two-dimensional glass micromodels of pore systems. *Journal of Canadian Petroleum Technology* **1982,** 21, (04).
23. de Haas, T. W.; Fadaei, H.; Guerrero, U.; Sinton, D., g. *Lab on a Chip* **2013,** 13, (19), 3832-3839.
24. Wan, J.; Tokunaga, T. K.; Tsang, C.-F.; Bodvarsson, G. S., Improved glass micromodel methods for studies of flow and transport in fractured porous media. *Water resources research* **1996,** 32, (7), 1955-1964.
25. Song, W.; de Haas, T. W.; Fadaei, H.; Sinton, D., Chip-off-the-old-rock: the study of reservoir-relevant geological processes with real-rock micromodels. *Lab on a Chip* **2014,** 14, (22), 4382-4390.
26. Karadimitriou, N.; Joekar-Niasar, V.; Hassanizadeh, S.; Kleingeld, P.; Pyrak-Nolte, L., A novel deep reactive ion etched (DRIE) glass micro-model for two-phase flow experiments. *Lab on a Chip* **2012,** 12, (18), 3413-3418.
27. Gunda, N. S. K.; Bera, B.; Karadimitriou, N. K.; Mitra, S. K.; Hassanizadeh, S. M., Reservoir-on-a-Chip (ROC): A new paradigm in reservoir engineering. *Lab on a Chip* **2011,** 11, (22), 3785-3792.
28. Mao, P.; Han, J., Fabrication and characterization of 20 nm planar nanofluidic channels by glass–glass and glass–silicon bonding. *Lab on a Chip* **2005,** 5, (8), 837-844.

29. Chung, C.; Lin, S., CO2 laser micromachined crackless through holes of Pyrex 7740 glass. *International Journal of Machine Tools and Manufacture* **2010,** 50, (11), 961-968.
30. Allcock, G.; Dyer, P.; Elliner, G.; Snelling, H., Experimental observations and analysis of CO2 laser-induced microcracking of glass. *Journal of applied physics* **1995,** 78, (12), 7295-7303.
31. Yen, M.-H.; Cheng, J.-Y.; Wei, C.-W.; Chuang, Y.-C.; Young, T.-H., Rapid cell-patterning and microfluidic chip fabrication by crack-free CO2 laser ablation on glass. *Journal of Micromechanics and Microengineering* **2006,** 16, (7), 1143.
32. Cheng, J.-Y.; Wei, C.-W.; Hsu, K.-H.; Young, T.-H., Direct-write laser micromachining and universal surface modification of PMMA for device development. *Sensors and Actuators B: Chemical* **2004,** 99, (1), 186-196.
33. Kim, M.; Sell, A.; Sinton, D., Aquifer-on-a-Chip: understanding pore-scale salt precipitation dynamics during CO 2 sequestration. *Lab on a Chip* **2013,** 13, (13), 2508-2518.
34. Adamson, A. W.; Gast, A. P., Capillarity. In *Physical chemistry of surfaces*. 6th ed; John Wiley & Sons, Inc.: New York, USA, 1997; pp 4-43.
35. Tiab, D. and Donaldson, E. C., Capillary Pressure. In *Petrophysics: theory and practice of measuring reservoir rock and fluid transport properties*. 4th ed; Gulf Professional Publishing; Waltham, Ma, USA, 2015; pp 279-311.
36. Dullien, F. A., Capillarity in Porous Media. In *Porous media: fluid transport and pore structure*, 2nd ed; Academic Press, Inc.: San Diego, Ca, USA, 1991; pp 118-232.
37. Er, V.; Babadagli, T.; Xu, Z., Pore-scale investigation of the matrix− fracture interaction during CO2 injection in naturally fractured oil reservoirs. *Energy & Fuels* **2009,** 24, (2), 1421-1430.
38. Dullien, F. A.; Zarcone, C.; Macdonald, I. F.; Collins, A.; Bochard, R. D., The effects of surface roughness on the capillary pressure curves and the heights of capillary rise in glass bead packs. *Journal of Colloid and Interface Science* **1989,** 127, (2), 362-372.

39. Kantzas, A.; Chatzis, I.; Dullien, F. In *Enhanced oil recovery by inert gas injection*, Proceeding of the SPE Enhanced Oil Recovery Symposium, April 16-21, 1988; Society of Petroleum Engineers: Tulsa, Oklahoma, USA, 1988.
40. Khorshidian, H.; James, L. A.; Butt, S. D., In *The Role of Film Flow and Wettability in Immiscible Gas Assisted Gravity Drainage*. Presented at Society of Core Analysts 30st Symposium, August 21-26, 2016; Snowmass, Colorado, USA, 2016.
41. Piri, M.; Blunt, M. J., Three-phase threshold capillary pressures in noncircular capillary tubes with different wettabilities including contact angle hysteresis. *Physical Review E* **2004,** 70, (6), 061603.
42. Dong, M.; Dullien, F. A.; Chatzis, I., Imbibition of oil in film form over water present in edges of capillaries with an angular cross section. *Journal of colloid and interface science* **1995,** 172, (1), 21-36.
43. Chatzis, I.; Morrow, N. R.; Lim, H. T., Magnitude and detailed structure of residual oil saturation. *Society of Petroleum Engineers Journal* **1983,** 23, (02), 311-326.
44. Buchgraber, M.; Al-Dossary, M.; Ross, C.; Kovscek, A. R., Creation of a dual-porosity micromodel for pore-level visualization of multiphase flow. *Journal of Petroleum Science and Engineering* **2012,** 86, 27-38.
45. http://lotusleafcoatings.com Hydrophil. (January),
46. Terwilliger, P.; Wilsey, L.; Hall, H. N.; Bridges, P.; Morse, R., An experimental and theoretical investigation of gravity drainage performance. *Journal of Petroleum Technology* **1951,** 3, (11), 285-296.

Chapter 4 : Pore-Level Study of the Effect of Miscibility and Wettability on Oil Recovery during Gas Assisted Gravity Drainage

This chapter is based on a paper prepared for presentation at the International Symposium of the Society of Core Analysts held in Vienna, Austria, 28 August to 1 September 2017.

4.1. Abstract

The effect of the gas-oil interfacial tension and wettability on the performance of gas assisted gravity drainage (GAGD) process was investigated at the pore-level to explore conditions leading to high oil recovery. This work extends the previous investigation of GAGD parameters, i.e., the contribution of film flow and wettability that we presented in 2015 and 2016. GAGD experiments were conducted in a new micromodel with an improved capillary continuity to reflect mechanisms of oil recovery effectively. The result of experiments showed that the heterogeneities of the porous medium caused the gas-front to bypass oil in small pores surrounded by large pores. The subsequent drainage of bypassed pores was possible where the gas-oil capillary pressure was sufficiently increased due to a reduction in the hydrostatic pressure of oil. The strong hydraulic continuity of oil in an oil-wet porous medium compared to a water-wet porous medium contributed to a low residual oil saturation under immiscible conditions. In water-wet micromodels, a near-complete oil recovery was obtained under miscible conditions as no interface between oil and gas was formed, and no oil was bypassed when the miscible displacement was developed.

4.2. Introduction

Gas Assisted Gravity Drainage (GAGD) is an effective method of oil recovery influenced by the reservoir rock and fluids' properties, such as the state of wettability,[1,2] heterogeneities,[3,4] and interfacial tension between the fluids[5,6]. During GAGD, the entry of gas into an oil-occupied pore occurs when the gas-oil capillary pressure is sufficiently increased.[7] The capillary pressure between two phases is directly proportional to their interfacial tension and inversely proportional to the pore size. The gas-oil capillary pressure in larger pores is lower so drainage of oil initially begins from larger pores.[8] Consequently, the gas-front may bypass smaller oil-occupied pores that are surrounded by larger pores.[4] In gas-invaded zones, thick films of oil may be retained in fine capillaries of a porous medium formed around the rock grains and on their rough surfaces. In the gravity drainage, these fine capillaries provide the wetting phase with continuous paths to maintain strong hydraulic continuity linking the bypassed pores to pores at lower elevations.[9] Under such conditions, the hydrostatic pressure of oil in bypassed pores decreases at higher elevations from the gas-front. Therefore, the local gas-oil capillary pressure in a bypassed pore at greater elevations can be higher than the gas-oil capillary pressure in the gas-front when a hydraulic communication between the bypassed pore and gas-front is maintained.[10] The fine capillaries of a porous medium, depending on their length and geometry, contribute to a limited increase of the gas-oil capillary pressure beyond which the hydraulic continuity of oil is terminated.[10,11]

The reduction of the gas-oil interfacial tension decreases the gas-oil capillary pressure at the gas-oil interface. Therefore, a better GAGD performance might be expected with a

reduction in capillary forces allowing gravitational forces to drain the liquid more easily. Although, the injection of a rich gas reduces the gas-oil differential density by dissolving in oil, the reduction of the oil viscosity and the swelling of oil can help with GAGD perfromance decreasing viscous forces and increasing oil saturation,

In GAGD, the stability of the gas-front, in addition to heterogeneities of the porous medium, is controlled by the gas-oil interfacial tension. The gas-front normally bypasses oil when gas-oil interfaces in larger pores (leading zones) surround smaller oil-occupied pores (trailing zones). Figure 4-1 schematically shows the drainage of oil with gas in a porous medium containing large and small pore.

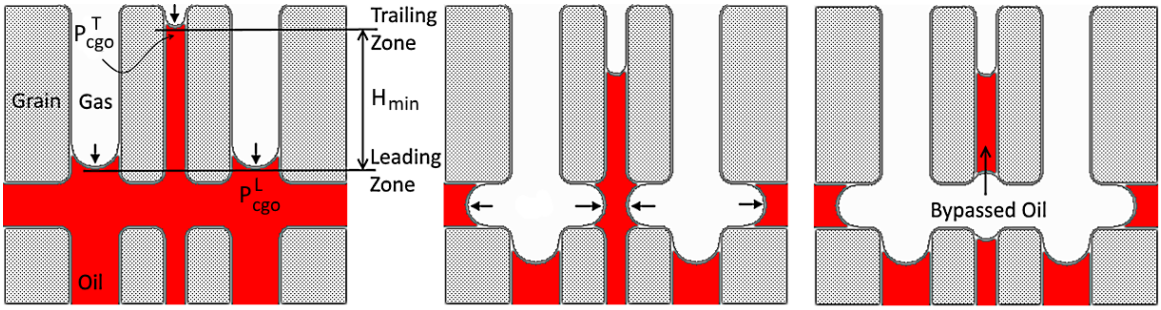

Figure 4-1. Schematic representation of the bypass of oil with leading zones in the gas-front

When the viscous forces are negligible (at low production rates), the minimum vertical distance (H_{min}) between the leading and trailing gas-oil interfaces prior to the bypass of oil can be calculated by Eq. 4.1,[7]

$$H_{min} = \frac{P^T_{cgo} - P^L_{cgo}}{\Delta\rho_{go} g} \tag{4.1}$$

where $P_{cgo}{}^{T}$ and $P_{cgo}{}^{L}$ are the gas-oil capillary pressure in the trailing and leading zones respectively, and $\Delta\rho_{go}$ is the gas-oil differential density. In a system with a fixed pore size distribution, decreasing the gas-oil interfacial tension lowers differentiations of gas-oil capillary pressure in various pore sizes (the numerator in Eq. 4.1). Therefore, a reduction of the gas-oil interfacial tension and an increase of the gas-oil differential density can stabilize the gas-front and eventually reduce the size of a bypassed zone (Figure 4-1: c). A further reduction of the gas-oil interfacial tension may lead to a miscible oil displacement depending on oil and gas composition, temperature and injection pressure.[12] Under miscible conditions, in addition to a direct oil displacement, the extraction of oil by gas and swelling of oil volume are the main mechanisms of the oil recovery.[13, 14]

In our previous work, the effect of wettability on the GAGD performance was studied in a micromodel with a weak capillary continuity. In this work, a new micromodel with improved capillary continuity has been developed to investigate the effect the gas-oil interfacial tension on the GAGD performance under oil-wet and water-wet conditions to identify the effect of wettability on residual oil saturations varying the gas-oil interfacial tensions.

4.3. Experimental Detail

A new pore network micromodel with an improved capillary continuity was fabricated bonding two acrylic (Plexiglas®) plates containing coarse pores and fine capillaries. The coarse pore network (Figure 4-2) was made by repeating a designed pattern (Figure 4-3) comprising pore sizes in the range of 150 - 1300 μm. The designed pore network was

etched by CO_2 laser on an acrylic plate, and the depth of etching was in the range of 140 - 160 μm. Another plate of the micromodel was scratched with a grit 60 sandpaper to form fine capillaries covering the coarse pore network from the top port to the bottom port. The porosity of the designed pattern is 0.48, and the pore volume (PV) of the micromodel is 0.940 ± 0.005 ml.

The pore sizes of the micromodel are one order of magnitude larger than the pore sizes in a sandstone. The magnification of the pore structure reduces the capillary forces compared to the gravitational forces. This helps us to study the interaction of capillary and gravitational forces in a system with limited height (vertical length). In addition, fluid saturations were quantified via image analysis and error due to resolution is less relative to larger pores. The image analysis methodology was developed in-house to evaluate the colour of pixels (red: oil and blue: water) in the recorded pictures during an experiment. The fluid saturation and recovery factor can be calculated with respect to the total number of pixels (with red, blue and white colours) and micromodel porosity. The uncertainty associated with the calculated saturations is ± 0.02 PV.

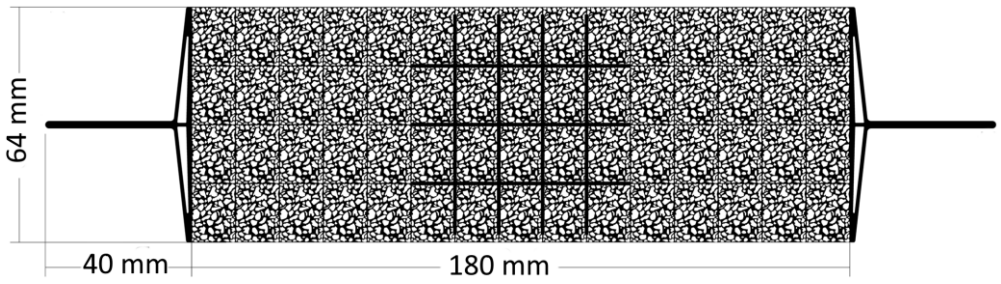

Figure 4-2. Designed pore network of micromodel.

The wettability of the micromodel was varied from a strongly oil-wet condition to a strongly water-wet condition as described in the previous work.[10] Figure 4-3: a & c show images of the repeated pattern in the oil-wet and water-wet micromodels, respectively (note films of the wetting phase in narrow fine capillaries).

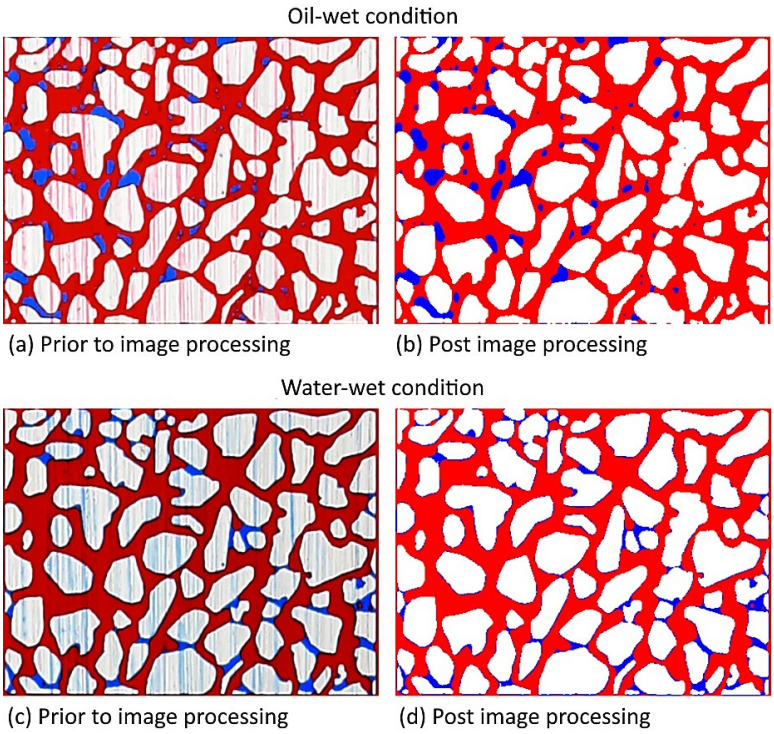

Figure 4-3. The repeated pattern of micromodel prior and after image processing (red: oil - blue: water, pattern size: (16×12 mm)

GAGD tests were conducted at 24°C injecting CO_2 and C_3H_8 (99% purity) under fixed pressure (4.0 bars in immiscible tests and 8.4 bars in a miscible test) from the top port of the micromodel. A precision piston pump (Quizix 20K series) was used to produce fluids from the bottom port of the micromodel at a constant rate (0.1 ml/hr in immiscible tests and 0.3 ml/hr in a miscible test). The initial oil and water saturations under the oil-wet

condition was established by injecting 5 PV water (blue dyed) into a fully oil-occupied micromodel at a flowrate of 5 ml/min followed by injecting 10 PV of oil (red dyed Varsol™ without dissolved gas) at a flowrate of 5 ml/min to establish a low water saturation. Under water-wet conditions, the fully water-occupied micromodel is flooded by 10 PV of oil at a flowrate of 5 ml/min.

Table 4-2 shows the interfacial tension between test fluids at the corresponding conditions measured with the VINCI IFT 700 apparatus. Table 4-3 also shows the composition of oil (Varsol™) measured with Agilent 7890 distillation system. In addition, equilibrium swelling of oil volume when contacted by C_3H_8 and CO_2 was measured at test conditions (4.0 bars and 24°C) using a chamber contaning three-phase (Figure C-5 in Appendix C). The volume of oil in equilibrium with C_3H_8 was increased by 32 ± 1%, but water volume was unchanged. In addition, no significant swelling and evaporation of oil and water was observed when contacted with CO_2. The density of live oil containing C_3H_8 at equilibrium was measured at 0.705 ± 0.001 g/ml using Anton Paar DMA-HPM density apparatus. The reduction of oil density was accounted in the calculation of final oil recovery factor in tests performed with C_3H_8.

Table 4-1. Interfacial tensions between fluids under experiment conditions (temperature: 24°C).

Bulk Fluid	Drop Fluid	Pressure (bar)	IFT (mN/m)
C_3H_8	Water	4.0	63.4±1.2
C_3H_8	Water	8.4	47.3±1.2
C_3H_8	Oil	4.0	15.8±0.2
C_3H_8	Oil	8.4	Miscible
CO_2	Water	4.0	71.3±1.8
CO_2	Oil	4.0	21.8±0.3
Oil	Water	4.0	31.5±0.8

Table 4-2. Composition of Varsol™ oil

Component	Composition
C9	8%
C10	27%
C11	38%
C12	25%
C13	2%
Sum	100%

4.4. Results and Discussions

The GAGD experimental results are presented in Table 4-3 showing the variation of fluids' saturation and final oil recovery. The average residual oil saturation in GAGD tests performed using CO_2 at the time of the gas-breakthrough was 0.29 PV in the oil-wet micromodel, and 0.34 PV in the water-wet micromodel. The average residual oil saturation after 2 PV production (total test duration: 19 hrs) was 0.21 PV and 0.30 PV under oil-wet and water-wet conditions, respectively. Similar results were obtained when experiments were repeated. The difference in the initial positioning of the residual water saturation was the major source of variation in results of repeated experiments (images of micromodels during repeated experiments are available in Appendix C).

Figure 4-4 and Figure 4-5 show the micromodel images during GAGD tests performed with CO_2 in the oil-wet and water-wet micromodels, respectively. In both wettability conditions, the bypass of oil with gas-fronts occurred in pores where a higher gas-oil capillary pressure must be overcome compared to their neighbouring pores (e.g. smaller pores surrounded by larger pores, and pores with entries blocked by residual water).

Micromodel images indicate that the size of bypassed regions (saturation of the residual oil) under water-wet conditions was larger than oil-wet conditions.

Table 4-3. Summary of experimental results

Wettability	Oil-wet				Water-wet				
Injected Gas	CO_2		C_3H_8		CO_2		C_3H_8		Miscible
Replication	1	2	1	2	1	2	1	2	1
Initial Oil Saturation (PV)	0.91	0.86	0.84	0.79	0.83	0.74	0.75	0.75	0.76
Initial Water Saturation (PV)	0.09	0.14	0.16	0.21	0.17	0.26	0.25	0.25	0.24
Oil Saturation at Breakthrough (PV)	0.27	0.31	NA	0.28	0.36	0.34	0.33	0.33	NA
Water Saturation at Breakthrough (PV)	0.09	0.14	NA	0.21	0.17	0.26	0.25	0.25	NA
Final Oil Saturation (PV)	0.22	0.19	0.20	0.24	0.32	0.30	0.27	0.31	< 0.01
Final Water Saturation (PV)	0.07	0.11	0.13	0.20	0.17	0.24	0.25	0.25	0.24
Final Oil Recovery Factor (% OOIP)	76%	78%	84%	80%	61%	59%	76%	72%	> 99%

OOIP: Original Oil in Place. NA: Data Not Available.

In the oil-wet micromodel, additional recovery from initially bypassed pores was obtained after the gas-breakthrough via the film flow mechanism. The fine capillaries maintained the hydraulic continuity of oil between zones at different elevations and provided continuous paths for the flow of oil-films. Therefore, a low residual oil saturation was obtained due to an effective increase of the gas-oil capillary pressure at higher elevations.

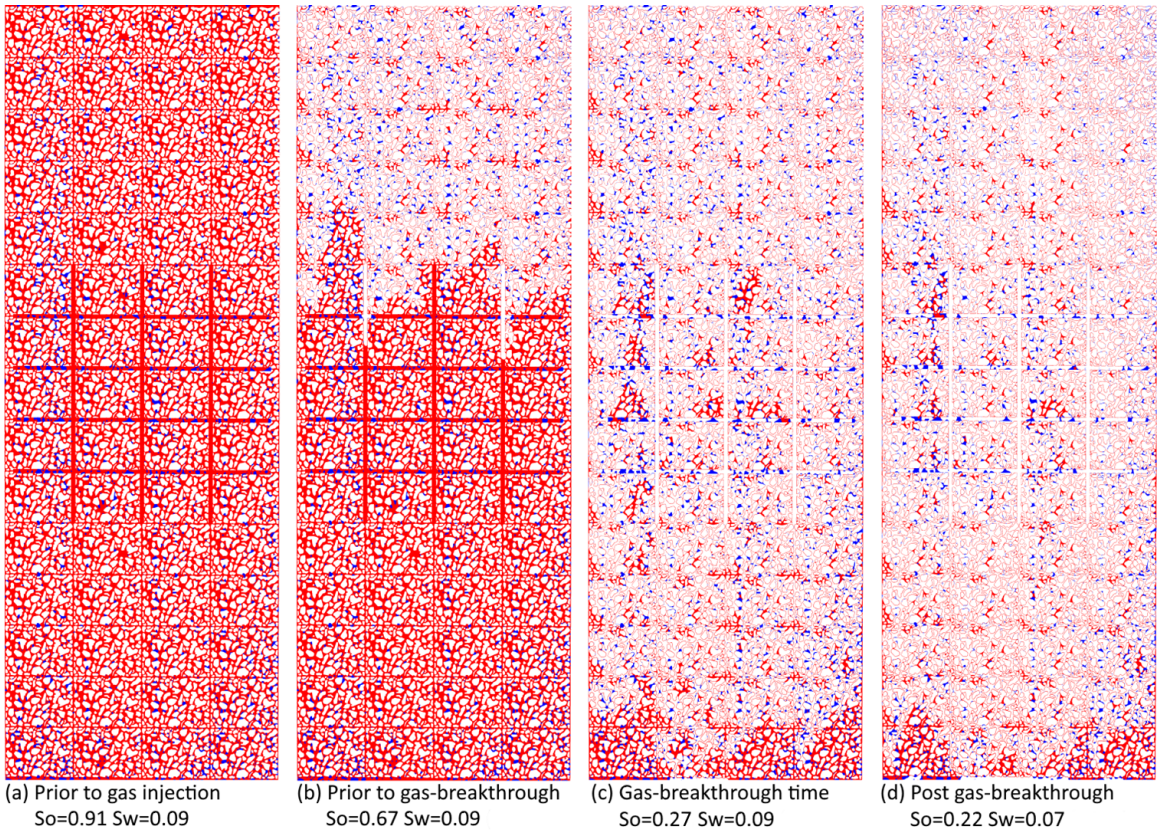

Figure 4-4. Immiscible GAGD experiment performed with CO_2 under oil-wet conditions (processed images, red: oil, blue: water, So: oil saturation, Sw: water saturation, pattern size: 64×185 mm).

Figure 4-6: a shows the final state of the residual oil saturation in the oil-wet micromodel. In addition to small pores and around the solid grains, the residual oil was also found in the pores with entries blocked by water. Under such conditions (Figure 4-6: a), the cumulative capillary pressure that must be overcome to displace the water-blob and oil-water interface was high, and may lead to the retention of oil depending on the size of the pore and geometry of local fine capillaries. Figure 4-6: b shows the final residual oil in the water-wet micromodel that is retained in larger pores compared to the oil-wet micromodel. Under water-wet conditions, paths of the oil drainage were often blocked by the presence of water in smaller pores. In addition, the presence of water around the solid

grains and corners of the fine capillaries restricted the hydraulic continuity of oil for an effective increase of the gas-oil capillary pressure. Consequently, the flow of oil in the form of thick films in water-wet media was restricted and resulted in a slight reduction of the residual oil saturation (0.04 PV) at the end of the experiment (15 hrs after a gas-breakthrough).

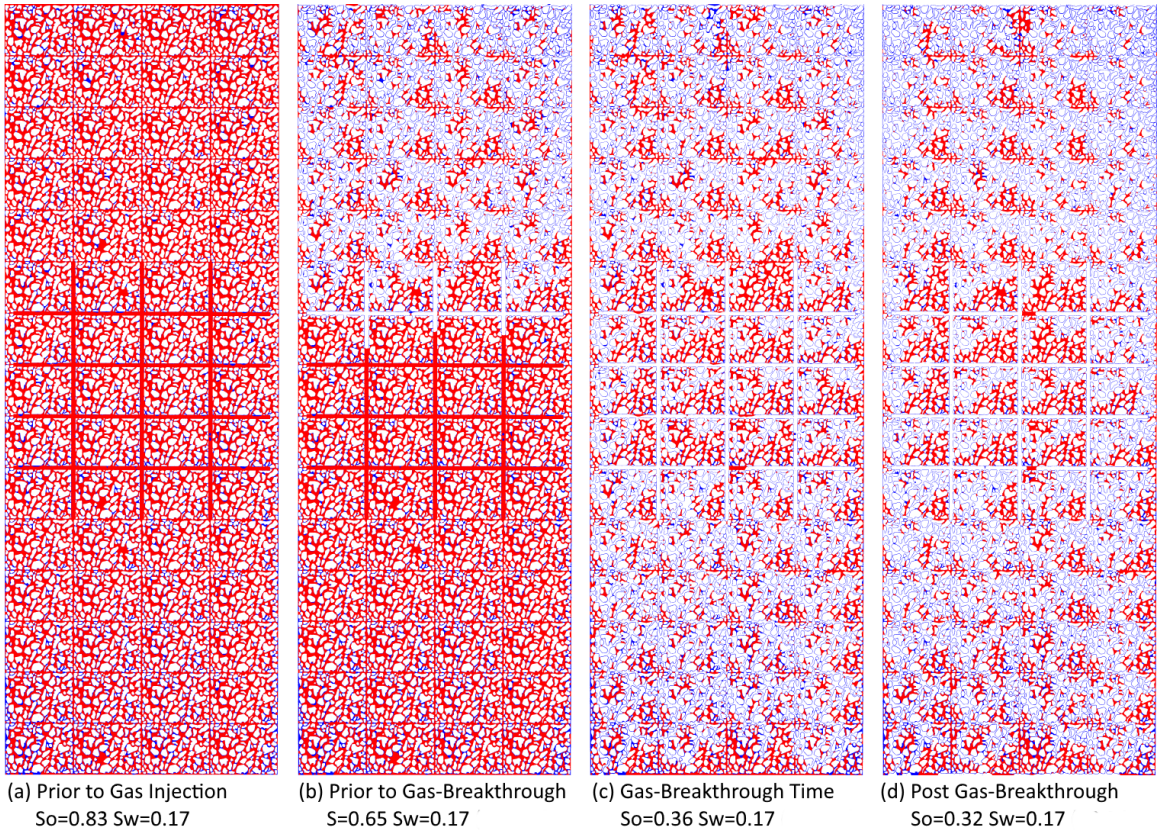

Figure 4-5. Immiscible GAGD experiment performed with CO_2 under water-wet conditions (processed images, red: oil, blue: water, So: oil saturation, Sw: water saturation, pattern size: 64×185 mm).

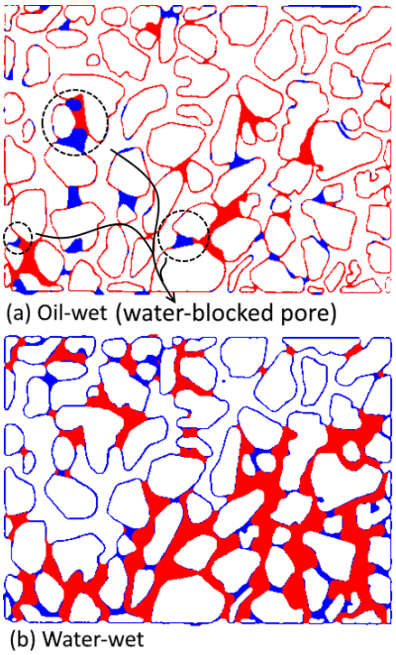

Figure 4-6. Residual oil (red) and water (blue) in oil-wet and water-wet conditions (processed images, pattern size 11×15 mm).

The central region of the pore network contains wide channels forming a larger scale of heterogeneity, i.e., fracture and matrices. During GAGD, the leading edge of the gas-front was formed in wide channels causing the bypass of oil in matrices with a higher saturation. Under oil-wet conditions, the bypassed oil was subsequently recovered from matrices because of the strong hydraulic continuity of oil. However, in the water-wet micromodel, the subsequent drainage of the bypassed oil from matrices was low as the hydraulic continuity of oil (intermediate-wetting phase) was weak.

The immiscible GAGD experiments were also performed with C_3H_8 (propane) to study the influence of a reduced gas-oil interfacial tension on GAGD performance. Figure 4-7: a & b show the oil-wet and water-wet micromodels after 2 PV production, respectively. The final residual oil saturation under oil-wet conditions was approximately unaffected

by the gas type. Under the water-wet condition, the variation of the gas type resulted in a slight reduction (0.02 PV) of the residual oil saturation mainly in the central region of the micromodel containing matrices and fractures.

In the oil-wet micromodel, because of the strong hydraulic continuity of oil, the residual oil saturation in bypassed zones was effectively reduced when the vertical distance between these zones and the gas-front (or the outlet port) was sufficiently increased. Ultimately, the residual oil saturation was similar for both gas types. In the water-wet micromodel, the hydraulic continuity of oil was weak. Therefore, reducing the size of bypassed zones, with the reduction of the 'gas-oil interfacial tension' to 'gas-oil differential density' ratio, could decrease of the final residual oil saturation particularly in the fractured region of the micromodel. The injection of C_3H_8 instead of CO_2 improved the final oil recovery factor due to swelling of the residual oil volume. It is speculated that the implementation of GAGD under reservoir conditions (elevated pressure and temperature) increases the solubility of gas (e.g. CO_2) in oil. In heavy oil reservoirs, the solubility of gas results in the swelling of oil and a reduction of the oil viscosity in gas-invaded zones. The swelling of oil increases its saturation and reduces the gas-oil interfacial tension, which reduce capillary forces that contribute to the retention of the residual oil. In addition, the reduction of the oil viscosity decreases viscous forces that retard the flow of oil. Consequently, a better GAGD performance can be expected when the injected gas can dissolve in oil. In addition, the solubility of CO_2 in residual water and oil can be considered as an effective mechanism for the sequestration purposes.

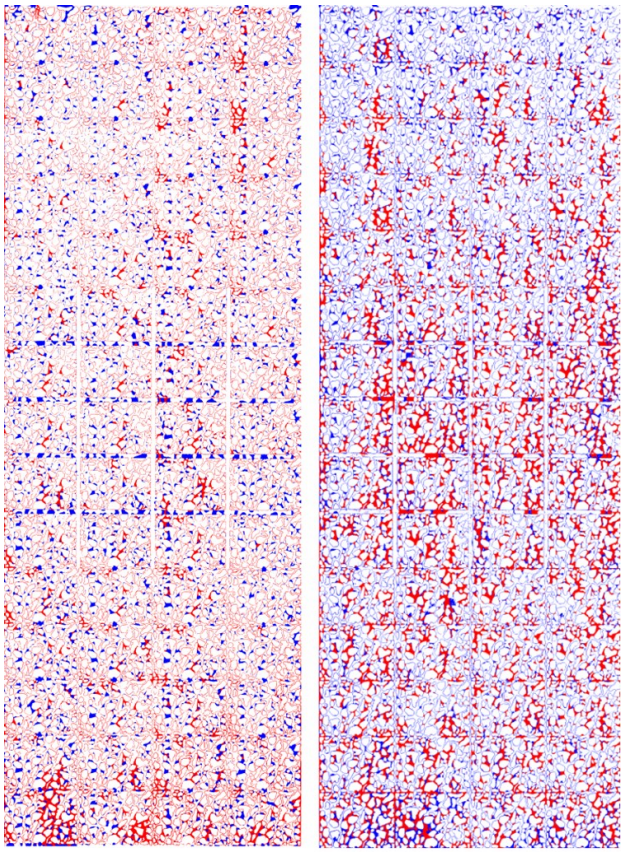

Figure 4-7. Results of immiscible GAGD tests performed with C_3H_8 (pressure: 4 bars, production rate: 0.1 ml/hr) under oil-wet and water-wet conditions (processed images, red: oil, blue: water, So: oil saturation, Sw: water saturation).

An additional GAGD test was performed in a water-wet micromodel by injecting C_3H_8 at 8.4 bars to develop a miscible oil displacement. The miscible gas injection, stabilized by gravity, resulted in an oil recovery factor of more than 99% (Figure 4-8). The small volume of the unrecovered oil was found in zones surrounded by water. In a miscible displacement, a region of swelled oil containing a high concentration of dissolved gas was developed between the gas and oil. A fully-developed transition zone formed without an interface with gas on top and with oil on the bottom. Consequently, a high recovery of oil

was obtained by eliminating capillarity. The miscible oil displacement was stabilized by gravity with the lowest density of gas being on top and increasing in the direction of gravity.

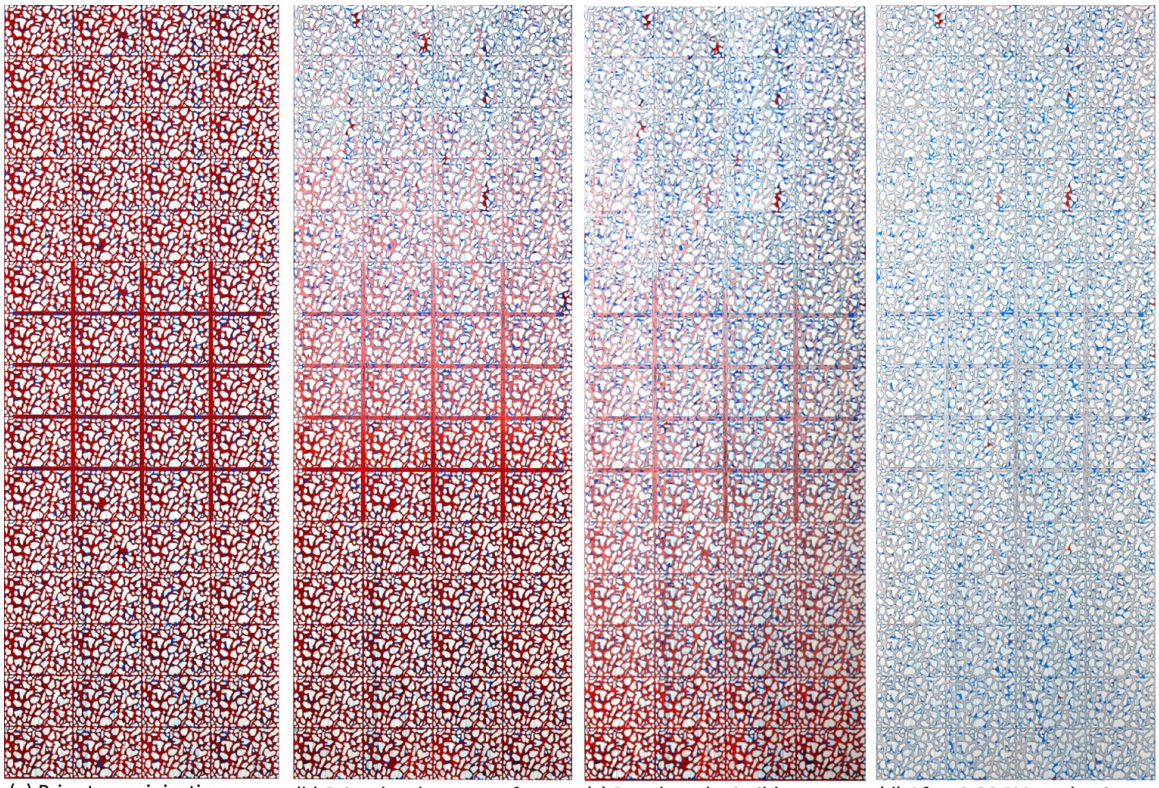

Figure 4-8. Miscible GAGD experiment performed with C_3H_8 in water-wet conditions (unprocessed images, red: oil, blue: water – pink: oil with dissolved gas)

The GAGD experimental results in micromodels with improved capillary continuity showed that high oil recovery was obtained under oil-wet conditions. Under water-wet conditions, the positive influence of the gravitational force on the immiscible displacement of oil was limited by the presence of residual water. Miscible gas-oil displacement is an effective process for obtaining a high oil recovery under all wettability

conditions. The saturation of the residual water is an imprtant parameter affecting the performance of GAGD. Under oil-wet conditions, the residual water-blobs blocked the entry of pores. It is also speculated that reducing the oil-water contact angle lowers the negative effect of the capillarity at oil-water interfaces on the drainage of oil. Under water-wet conditions, the presence of water arrested the continuity and flow of oil in the porous medium. Therefore, the reduction of the residual water saturation and improving the geometry of fine capillaries can provide a better condition for the recovery of oil under water-wet conditions.

4.5. Chapter Conclusions

During immiscible GAGD processes, heterogeneities of porous media caused the gas-front to bypass oil in smaller pores surrounded by larger pores. Under oil-wet conditions, the strong hydraulic communication of oil contributed to an additional oil recovery from initially bypassed regions where the gas-oil capillary pressure was effectively increased. However, under water-wet conditions, the presence of residual water in smaller pores and around the solid grains restricted the flow of oil from bypassed zones, and the residual oil was retained at higher saturations. A reduction in the ratio of the ‘gas-oil interfacial tension’ and ‘gas-oil differential density’ slightly improved the GAGD performance in the water-wet micromodel where the hydraulic continuity of oil was weak. A high oil recovery can be obtained with the downward displacement of oil under miscible conditions eliminating the capillarity at gas-oil interfaces in a heterogeneous porous medium.

Chapter References

1. Vizika, O.; Lombard, J., Wettability and spreading: two key parameters in oil recovery with three-phase gravity drainage. *SPE Reservoir Engineering* **1996,** 11, (01), 54-60.
2. Caubit, C.; Bertin, H.; Hamon, G. In *Three-phase flow in porous media: wettability effect on residual saturations during gravity drainage and tertiary waterflood*, Proceeding of SPE Annual Technical Conference and Exhibition, September 26-29, 2004; Society of Petroleum Engineers: Houston, Texas, USA, 2004.
3. Parsaei, R.; Chatzis, I., Experimental investigation of production characteristics of the gravity-assisted inert gas injection (GAIGI) process for recovery of waterflood residual oil: effects of wettability heterogeneity. *Energy & Fuels* **2011,** 25, (5), 2089-2099.
4. Catalan, L. J.; Dullien, F. A.; Chatzis, I., The effects of wettability and heterogeneities on the recovery of waterflood residual oil with low pressure inert gas injection assisted by gravity drainage. *SPE Advanced Technology Series* **1994,** 2, (02), 140-149.
5. Blunt, M.; Zhou, D.; Fenwick, D., Three-phase flow and gravity drainage in porous media. *Transport in porous media* **1995,** 20, (1-2), 77-103.
6. Rao, D., Gas injection EOR-A new meaning in the new millennium. *Journal of Canadian Petroleum Technology* **2001,** 40, (02).
7. Dullien, F. A., Capillarity in Porous Media. In *Porous media: fluid transport and pore structure*, 2nd ed; Academic Press, Inc.: San Diego, Ca, USA, 1991; pp 118-232.
8. Lenormand, R., Liquids in porous media. *Journal of Physics: Condensed Matter* **1990,** 2, (S), SA79.
9. Dullien, F. A.; Zarcone, C.; Macdonald, I. F.; Collins, A.; Bochard, R. D., The effects of surface roughness on the capillary pressure curves and the heights of capillary rise in glass bead packs. *Journal of Colloid and Interface Science* **1989,** 127, (2), 362-372.

10. Khorshidian, H.; James, L. A.; Butt, S. D., In *The Role of Film Flow and Wettability in Immiscible Gas Assisted Gravity Drainage*. Presented at Society of Core Analysts 30st Symposium, August 21-26, 2016; Snowmass, Colorado, USA, 2016.
11. 11. Piri, M.; Blunt, M. J., Three-phase threshold capillary pressures in noncircular capillary tubes with different wettabilities including contact angle hysteresis. *Physical Review E* **2004,** 70, (6), 061603.
12. Helfferich, F. G., Theory of multicomponent, multiphase displacement in porous media. *Society of Petroleum Engineers Journal* **1981,** 21, (01), 51-62.
13. Bahralolom, I. M.; Orr Jr, F. M., Solubility and extraction in multiple-contact miscible displacements: comparison of N2 and CO2 flow visualization experiments. *SPE Reservoir Engineering* **1988,** 3, (01), 213-219.
14. Campbell, B. T.; Orr Jr, F. M., Flow visualization for co2/crude-oil displacements. *Society of Petroleum Engineers Journal* **1985,** 25, (05), 665-678.

Chapter 5 : The Pore-level Investigation of the Influence of Wettability and Production Rate on the Recovery of Waterflood Residual Oil with Gas Assisted Gravity Drainage (GAGD) Process

This Paper was submitted for publication to the journal of Energy & Fuels.

5.1. Abstract

Gas assisted gravity drainage (GAGD) is an oil recovery mechanism that can be implemented after waterflood to enhance the recovery of oil. The performance of post-waterflood GAGD is affected by a variety of parameters that determine the balance between capillary, gravitational and viscous forces. In this research, the influence of the wettability, heterogeneities, and production rate on the recovery of oil have been studied at the pore-level to recognize phenomena affecting mechanisms of oil recovery through visualizing fluids' interfaces in a newly designed micromodel containing a coarse pore network covered by fine capillaries. Experimental results show that regions with high oil saturation (oil-bank) were formed ahead of the gas-front in both oil-wet and water-wet micromodels when the production rate was low. Under oil-wet conditions, the size of the oil-bank was greater, and the recovery of oil initiated prior to a gas-breakthrough. Under water-wet conditions, the flow of the residual oil after a gas-breakthrough was initially restricted by the presence of the residual water in small pores and fine capillaries. However, high oil recovery was finally obtained upon an effective reduction of the water saturation extending the time of the process. Under both wettability conditions, increasing the drainage rate contributed to the instability of gas-fronts and early gas-breakthroughs without a remarkable oil recovery. The experimental result implies that although the oil

production characteristics under oil-wet and water-wet conditions are different, both the wettability states are potential for the implementation of post-waterflood GAGD.

5.1. Introduction

Gas Assisted Gravity Drainage (GAGD) is an effective mechanism of oil recovery that can be implemented in potential reservoirs, such as anticlines, pinch-outs and thick pay zones, injecting gas from top zones and producing oil from lower zones.[1, 2] Field GAGD operations have resulted in high oil recovery up to 90%.[3] GAGD is a multiphase flow process that is controlled by capillary, gravitational and viscous forces.[4] These forces are affected by operational parameters (e.g. gas type, pressure, and production rate), characteristics of a reservoir rock (e.g. pore size distributions, heterogeneities, wettability), and properties of fluids (e.g. viscosity, interfacial tension and density).[2]

In a two-phase drainage process, a non-wetting phase (e.g. gas) can enter a pore occupied by a wetting phase (e.g. oil) when the corresponding differential pressure or capillary pressure is overcome.[5, 6] In the drainage of oil by gas, the gas-oil capillary pressure is higher when the gas-oil interfacial tension and the average curvature of the gas-oil interface are greater.[6, 7] The latter increases by the reduction of the gas-oil contact angle and pore sizes.[6] Based on Darcy's law,[8] the flow of a fluid in a porous medium is accompanied by greater viscous pressure drop when the viscosity and flowrate are higher, and the porous medium permeability is smaller.

The drainage of oil with gas occurs in a capillary fingering domain when the relative intensity of capillary forces is greater than viscous forces.[9] Under such conditions, the

gas-front forms and propagates through larger pores where the capillary pressure and viscous pressure drop to overcome are lower.[10] The gas-oil capillary pressure in the gas-front fluctuates due to a variation of pore sizes in the breakthrough path.[6] When the gas-front passes through smaller pores on its leading zones, the frontal capillary pressure increases. This helps with an additional drainage of oil overcoming capillary and viscous forces associated with the flow of the residual oil from trailing zones.[11] In a vertical gas injection, gravity also plays a remarkable role in the stability of the gas-front. The gas-oil capillary pressure in trailing zones of the gas-front (small pores) is higher than leading zones (large pores) upon a reduction of the oil hydrostatic pressure at higher elevations.[10] The effect of gravity on the gas-oil differential density promotes the gas-oil differential pressure (or capillary pressure) at higher elevations. The distance between trailing and leading zones of the gas-front depends on the balance between the hydrostatic pressure gradient, viscous pressure drop and variations of capillary pressure in different pore sizes.[12] For instance, in a fractured medium, the distance between gas-fronts in fracture and matrix is greater when the oil viscosity is higher, matrix permeability is lower, fracture aperture is wider, and production rate is higher.[13]

During a drainage processes. the bypass of oil (wetting phase) with gas (non-wetting phase) often occurs in smaller pores that are surrounded by larger pores.[12] The hydraulic communication of the residual oil in bypassed regions with neighbouring zones may be terminated at high capillary pressures depending on the characteristics of a porous medium. In a reservoir rock, the porous medium is formed in spaces between connected solid grains with rough surfaces. The surface irregularities of solid grains create networks

of fine capillaries that maintain thick films of wetting phase in regions invaded by the non-wetting phase.[14] Under such conditions, the hydraulic continuity of the residual oil between bypassed regions is maintained. Therefore, the bypassed residual oil may still flow downward through thick films formed in fine paths toward a new region or gas-front at lower elevations. The driving force for the film flow of oil between two regions after a gas-breakthrough is gravity.

The rate of drainage through thick layers of oil-films between two regions is also affected by parameters that create a resistance to the film flow of the wetting phase, such as the geometry of fine capillaries, oil saturation, and oil viscosity.[15] In GAGD, the downward flow of oil through fine paths continues until a balance between the gravity of capillary forces is developed. The drainage of oil from a bypassed region depends on the availability of a fine path with proper geometry that can maintain the hydraulic continuity of oil to lower elevations of a porous medium.[16] The elevation of the gas-oil capillary pressure, which increases the curvature of the gas-oil interface, may lead to the discontinuity of oil-films depending on the corner geometry of fine capillaries.[17] The contribution of gravity to the enhancement of the gas-oil capillary pressure in porous media having fine paths with rounded corners is limited.

GAGD can also be implemented after a waterflood process for a further recovery of oil.[18, 19] Post-waterflood GAGD is a three-phase flow process, and the state of contacts between fluids is affected by their interfacial tensions and the porous medium wettability.[20] In a water-wet porous medium, thick layers of oil-film can be formed in capillary corners between the water surface and gas when the curvature of the gas-oil interface is smaller

than the curvature of the oil-water interface.[17, 21, 22] The rate of the oil flow in the form of thick films, in addition to the geometry of capillary corners, oil viscosity and oil saturation, is affected by the saturation of water.[21, 23] At high gas-oil capillary pressures, when the presence of a thick layer of oil on the surface of water is geometrically limited,[17] a thin layer of oil-film spreads over the water surface. A thin oil-film covers the water surface when the gas-water interfacial tension is greater than the sum of the gas-oil and oil-water interfacial tensions (positive spreading coefficient).[24] However, thin oil-films play an insignificant role in the recovery of oil as the rate of oil flow through these layers is practically unmeasurable.[14, 22] In addition, high oil recovery was obtained with GAGD at connate water saturations irrespective of the spreading condition of oil.[25]

The recovery of oil with post-waterflood GAGD is influenced by the wettability of porous media.[26-30] Experiments in sandstone and unconsolidated sand packs showed that high oil recovery was obtained under water-wet conditions.[26, 30] The recovery of oil under oil-wet conditions was also observed to be higher than water-wet conditions when post-waterflood GAGD was performed in macromodels made from glass beads or unconsolidated sands.[28, 29] The performance of post-waterflood GAGD, in addition to the wettability of a porous medium, is influenced by a variety of parameters, such as:

- the use of a capillary barrier at the outlet of porous media that promotes capillary pressures between gas and liquid phases and eliminates the retention of fluids at the bottom of the porous media,[12, 30]

- heterogeneities in porous media that often affect GAGD performance negatively by increasing the saturation of bypassed oil,[12, 31]
- the vertical length of porous media that may affect the contribution of gravity to the recovery of oil,[22, 32] and formation of an oil-bank ahead of a gas-front,[33]
- the hydraulic continuity of the residual wetting phase in fine capillaries of porous media that also affects the contribution of gravity to the recovery of oil,[14, 34]
- interfacial tensions and contact angles between fluids that affect the capillary pressure at fluids' interfaces,[2]
- the duration of the experiments that determines the volume of the produced oil drained through the film flow mechanism,[30]
- and the production rate that often negatively affects GAGD performance prior to a gas-breakthrough.[29, 35, 36]

The visualization of fluids' interfaces in micromodels provided insights about phenomena affecting the displacement of fluids during multiphase flow processes.[37-42] In this research, the influence of the wettability and production rate on oil recovery have been studied at the pore-level. In micromodels, the pore network is often formed between separated solid grains. This may lead to a hydraulic discontinuity of oil and water during a gravity drainage, thus affecting the performance of the process.[19] We developed a new micromodel that contained a coarse pore network covered by fine capillaries. The fine capillaries improved the hydraulic continuity of the residual oil and water that might be bypassed with gas in the coarse pore network.[16] The bypassed oil and water use the corners of the fine paths to flow from higher to lower elevations at elevated capillary

pressures. Results of the pore-level investigation can be used to evaluate mechanisms affecting post-waterflood GAGD processes.

5.2. Experimental Detail

An experimental setup (Figure 5-1) was developed for running GAGD tests in micromodels. Test fluids, i.e., Varsol™ (dyed red), deionized water (dyed blue) and air, were delivered to the injection ports of a micromodel under a constant pressure to perform the waterflood and GAGD processes. A precision pump (Quizix 20K) was used to produce fluids with constant rates (flowrate resolution: ± 0.1%) from the production port of the micromodel. All experiments were performed at a temperature of 24°C and a pressure of 4 bars. The interfacial tensions between fluids under corresponding test conditions were measured using the VINCI IFT 700 apparatus, and results are presented in Table 5-1. The experimental conditions resulted in an immiscible displacement of fluids without an appreciable swelling and evaporation of oil and water.

Figure 5-1. GAGD experimental setup.

Table 5-1. The interfacial tensions between test fluids (air, blue dyed water and red dyed Varsol™) measured at 24°C and 4.0 bars.

Bulk Fluid	Drop Fluid	IFT (mN/m)
Air	Water	71.5 ± 1.2
Air	Varsol	24.8 ± 0.4
Varsol	Water	31.5 ± 0.8

A pore network micromodel with improved capillary continuity was fabricated for the pore level study of GAGD in a transparent porous medium. The micromodel contains two networks of coarse and fine capillaries. The coarse pore network (Figure 5-2(a)) of the micromodel was formed with the repeat a smaller pattern that was designed based on a magnified image of a thin sand section as shown in Figure 5-2(b). The injection of gas was from the top port, and fluids were produced from the bottom port as shown in Figure 2a. Large heterogeneities (1 mm wide channels) were added in central regions of the micromodel to resemble a region containing matrices surrounded by fractures, where the displacement of oil and water in the gas-front is affected by the reduction of associated capillary pressures in wide channels. The coarse pore network was etched with a CO_2 laser device on the surface of an acrylic plate. The pore sizes (width) of the pattern were in the range of 0.15 mm to 1.3 mm, and the average depth of pores was approximately 0.15 mm.

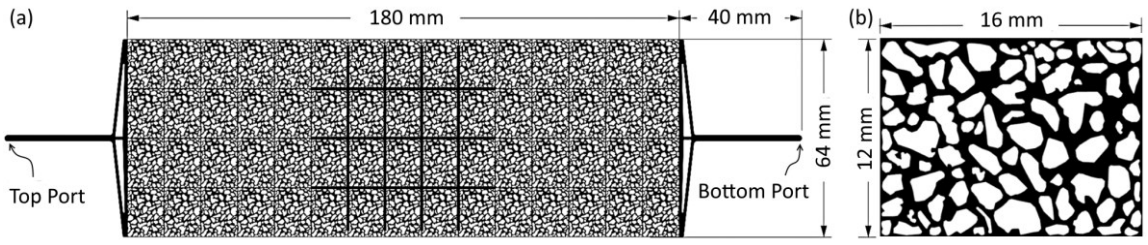

Figure 5-2. (a): Coarse pore network of micromodel. (b): Repeated pattern in the coarse pore network.

The etched plate of the micromodel was thermally bonded to another acrylic plate containing fine capillaries. The fine capillaries were created from the top port to the bottom port using a grit 60 sandpaper, so fine path remains opened after the thermal bonding process. The average depth and width of scratches were 30 μm and 80 μm, respectively. These fine capillaries retain films of a wetting phase where coarse pores are occupied by a non-wetting phase. Therefore, the wetting phase in the micromodel can flow in the form of thick films between bypassed zones. The pore volume (PV) of the fabricated micromodel was measured to be 0.850 ± 0.005 ml comparing weights of a dry and water-saturated micromodel. The permeability of micromodel was 24 Darcy based on the flow area of 64 mm × 0.16 mm (pattern width × maximum pore depth). The two-dimensional porosity of the designed pattern is 0.48. The GAGD experiments were also repeated in a duplicate of the micromodel.

The wettability of micromodels was varied from a strongly oil-wet condition to a strongly water-wet condition. The oil-wet condition was prepared by aging a clean micromodel with a transparent oil (e.g., Varsol™) for at least 1 hr. To prepare water-wet conditions, a solution containing nano-silica gel[43, 44] was flooded into a clean micromodel and then removed with the flow of compressed air to cure a thin layer of hydrophilic material on the surface of pores. The visibility and permeability of the micromodel were unaffected by the state of wettability. Figure 5-3 shows the wettability of acrylic under (a): oil-wet and (b): water-wet conditions with the sessile drop method (contact angles ~ 3°). No variation of the contact angle was observed between drops and solid surface with the

extension of the residence time up to 12 hrs, which confirms the stability of the wettability states.

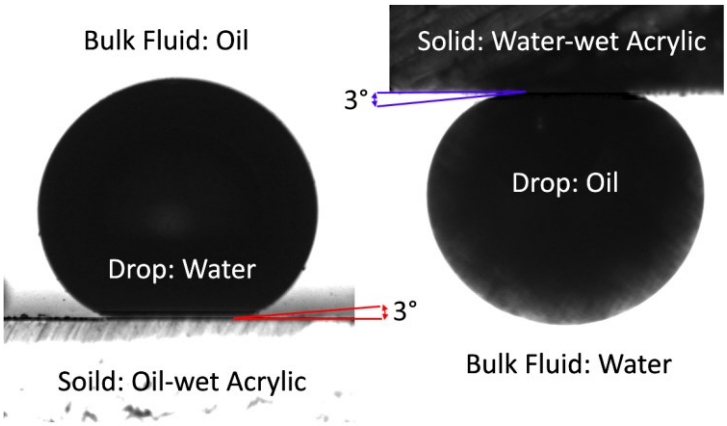

Figure 5-3. (a): A droplet of water on the surface of the oil-wet acrylic. (b): a droplet of oil on the surface of the water-wet acrylic.

The magnified images of a region in the oil-wet and water-wet micromodels containing red-dyed Varsol™ (oil) and blue dyed deionized water are shown in Figure 5-4. Films of wetting fluids in fine capillaries passing below solid grains can be observed in unprocessed images (Figure 5-4(a) & (c)). The micromodel images during GAGD experiments were recorded with a high-resolution imaging system (Canon 6D camera with EF 100 mm F/2.8 macro USM lens). A custom image analysis program was developed in-house to quantify the two-dimensional saturation of fluids by evaluating the colour of pixels in the micromodel images (Figure 5-4(b) & (d)). The parameters of an image processing program were calibrated based on the volumetric data measured with a precision pump. The uncertainty associated with the calculated saturations is ± 0.02 PV. The image processing and micromodel fabrication methodologies were described elsewhere.[16]

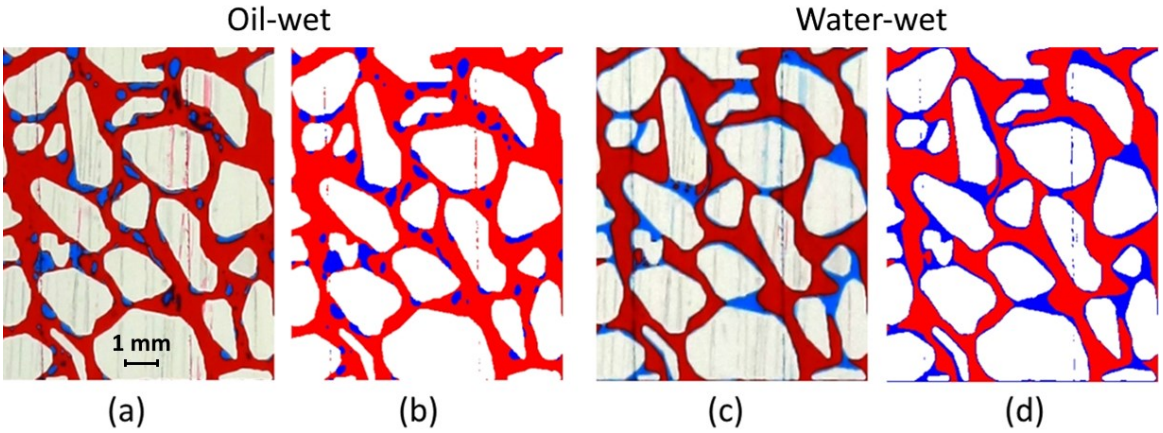

Figure 5-4. (a & b): Original and processed images of a region in the oil-wet micromodel at the residual water saturation, (c & d): original and processed images of the same region in the water-wet micromodel at the residual oil saturation, (red: oil, blue: water, white: grains, size of the region: 6.5×8.6 mm).

Micromodels containing oil at irreducible water saturations were prepared for the waterflood process. Under oil-wet conditions, the initial oil saturation was established by injecting 10 PV of water into a fully oil-saturated micromodel at 7.5 ml/min followed by injecting 10 PV of oil at 7.5 ml/min in the reverse direction. For water-wet conditions, the initial oil saturation was established by injecting 10 PV of oil at 7.5 ml/min into a fully water-saturated micromodel to establish an irreducible water saturation. The implementation of a high injection rate and injected pore volume ensures the reduction of the displaced fluid to an irreducible level. The injection of oil was from the top port of the micromodel, and the injection of water was from the bottom port of the micromodel (gravity stabilized) based on the design of piping in the experimental setup.[16] Waterflooding was performed at the injection rate of 2.0 ml/hr, and it was terminated at the time of water-breakthrough. Post-waterflood GAGD was initiated by injecting air at a

constant pressure of 4 bars and producing fluids with a constant rate (0.2 ml/hr in low rate tests and 2.0 ml/hr in high rate tests). The post-waterflood GAGD experiment at the low rate of production was repeated to examine the reproducibility of data. In addition, two-phase (air-water) GAGD tests were conducted to evaluate the stability of the gas-front at the production rates of 0.2 ml/hr and 2.0 ml/hr.

5.3. Result and Discussion

5.3.1. Two-Phase GAGD

Images of the two-phase GAGD experiments performed at production rates of 0.2 ml/hr and 2.0 ml/hr are shown in Figure 5-5(a) & (b). The images indicate that the stability of the gas-front under two-phase conditions above the fractured zone is approximately unaffected by increasing the drainage rate. However, Figure 5-5(c) & (d) show that increasing the production rate increased the size of the bypassed water in the central zones of the micromodel containing large heterogeneities. Therefore, the influence of the drainage rate on the performance of the gas-front depends on porous medium heterogeneities. This interaction is schematically explained in Figure 5-6(a) & (b) with a simple heterogeneity configuration. During a parallel displacement of the gas-water interfaces (with a controlled flowrate), the gas-front forms a leading zone in the large tube (1) and a trailing zone in the smaller tube (2). In Figure 5-6(a), the distance between these two zones *(H)* is determined by the balance between the gas-water capillary pressures in these zones ($P_{cgw}{}^{T}$ & $P_{cgw}{}^{L}$), gas-water differential density ($\Delta\rho_{gw}$), and viscous pressure drops of fluids in the tube 1 & 2 ($P_{vis\text{-}1}$ & $P_{vis\text{-}2}$). This balance can be shown by Eq. 5.1 if

the distance between leading and trailing zones is fixed, and the viscous pressure drop of the gas flow in the large tube is negligible. The former assumption is valid when the capillary and gravitational forces dominate viscous forces, thus stabilizing the gas-front.

$$H = \frac{P_{cgw}^{T} - P_{cgw}^{L} + P_{vis\text{-}2} - P_{vis\text{-}1}}{\Delta\rho_{gw} g}. \tag{5.1}$$

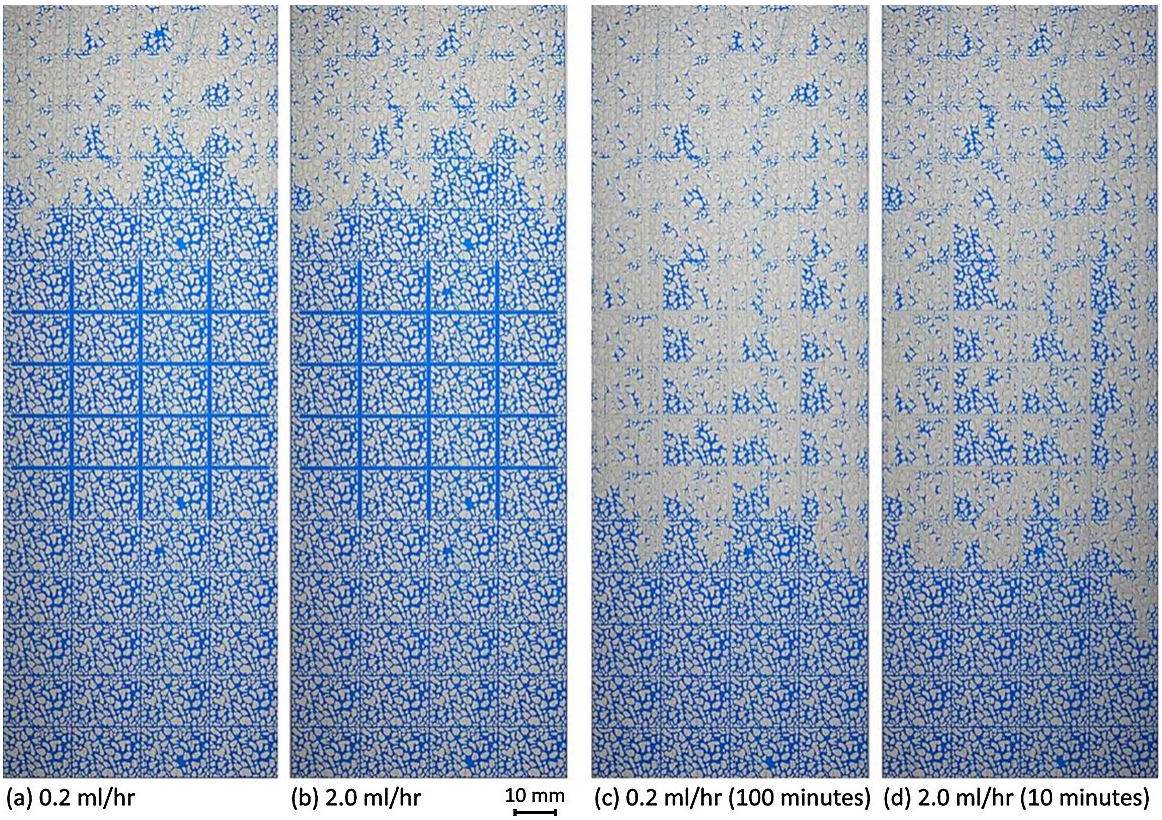

Figure 5-5. The stability of gas-front during two-phase GAGD tests with water (blue) and air performed at low (0.2 ml/hr) and high (2.0 ml/hr) rates of production (unprocessed images).

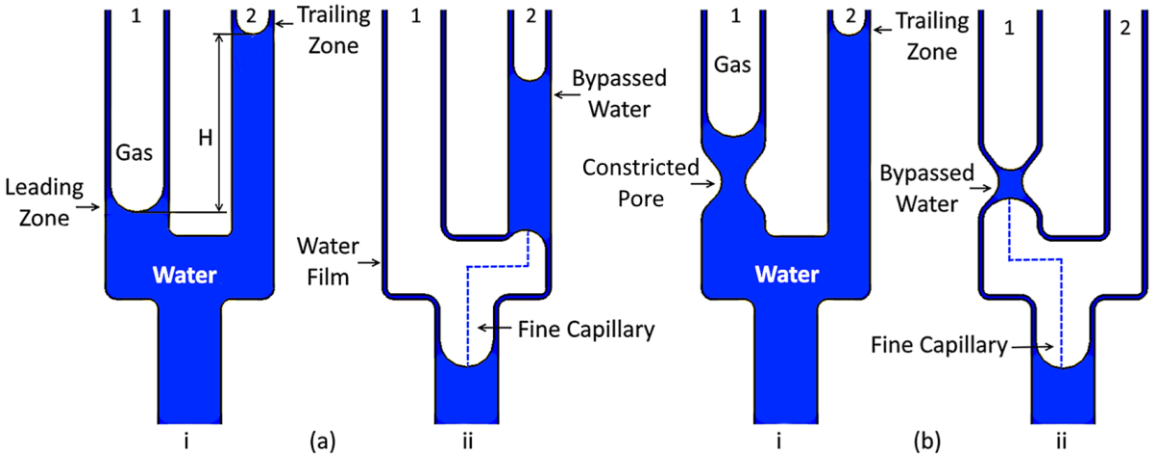

Figure 5-6. Schematic two-phase drainage process in a simple pore geometry. (a): bypass of the wetting phase in the small pore, (b): fluctuation of the gas-water capillary pressure in the gas-front.

Eq. 5.1 implies that the size of the bypassed water in tube 2 is larger when the viscous pressure drop ($P_{vis\text{-}2}$) and gas-water capillary pressure ($P_{cgw}{}^{T}$) associated with the flow of water in tube 2 are greater. Therefore, the bypassed volume increases when the drainage rate is higher and the size of tube 2 is smaller. A similar situation may occur in porous media containing smaller pores surrounded by larger pores (or matrices surrounded by fractures). In Figure 5-6(b), the leading zone of the gas-front (in tube 1) faces with a constriction on its path. The variation of pore sizes in the leading zone of the gas-front (in tube 1) promotes the gas-water capillary pressure. The increase of the capillary pressure in the leading zone collaborates with gravity to displace water from the trailing zone (in tube 2). A complete drainage of water from tube 2 can occur for a range of drainage rates depending on the increase of the frontal gas-water capillary pressure in the constricted pore. This happens when the gas-water capillary pressure and viscous pressure drop of water in the trailing zone are overcome effectively with the elevation of the frontal capillary pressures. Therefore, the stability of the gas-front in Figure 5-5(a) & (b) was

unaffected by the increase of the production rate as the viscous forces for both rates (0.2 & 2.0 ml/hr) were dominated by capillary and gravitational forces. In the performed two-phase GAGD experiments, the range of the air-water capillary pressure based on the micromodel pore sizes was approximately from 500 to 1000 Pa. The gradients of viscous pressure drop based on the micromodel permeability (24 Darcy) for linear velocities of 100 mm/hr and 1000 mm/hr (corresponding to drainage rates of 0.2 and 2.0 ml/hr) are approximately 1 and 10 Pa/mm.

The capillary number, N_{CA}, which shows the relative intensity of viscous to capillary forces,[6, 9] is calculated based on Eq. 5.2:

$$N_{CA} = \frac{\mu_w v}{\sigma_{gw}} \tag{2}$$

where μ_w is the water viscosity, v is the average velocity of the gas-front, and σ_{gw} is the gas-water interfacial tension. The capillary numbers corresponding to the low and high production rates are 3.8×10^{-7} and 38.5×10^{-6}, respectively. Stable gas-fronts with the domination of the capillary fingering can be expected for such low capillary numbers.[6]

5.3.2. Waterflood

The displacement of oil-water interfaces during gravity stabilized waterflood was studied in micromodels. Figure 5-7(a) & (b) show processed images of oil-wet and water-wet micromodels during waterflood, respectively (tests 1 & 2 in Table 5-2). In addition, the stepwise displacement of oil by water in a region of micromodels are presented in Figure 5-8(a) & (b). Under oil-wet conditions, the injected water displaced oil through larger pores on its paths as normal in a drainage process. Although the residual oil in the coarse

pore network was surrounded by water, the hydraulic communication of oil between bypassed pores was maintained through fine capillaries of the micromodel. Under water-wet conditions, water displaced oil in small pores where the wetting phase pressure was lower due to higher capillary pressure. Subsequently, the saturation of water around solid grains swelled, and oil was bypassed with water in the body of larger pores as expected from an imbibition process. The waterflood terminated the continuity of the residual oil-blobs under water-wet conditions. The result of waterflood in micromodels is presented in Table 5-2. The average oil recovery factor (after waterflood) under oil-wet conditions was 55% compared to 48% under water-wet conditions.

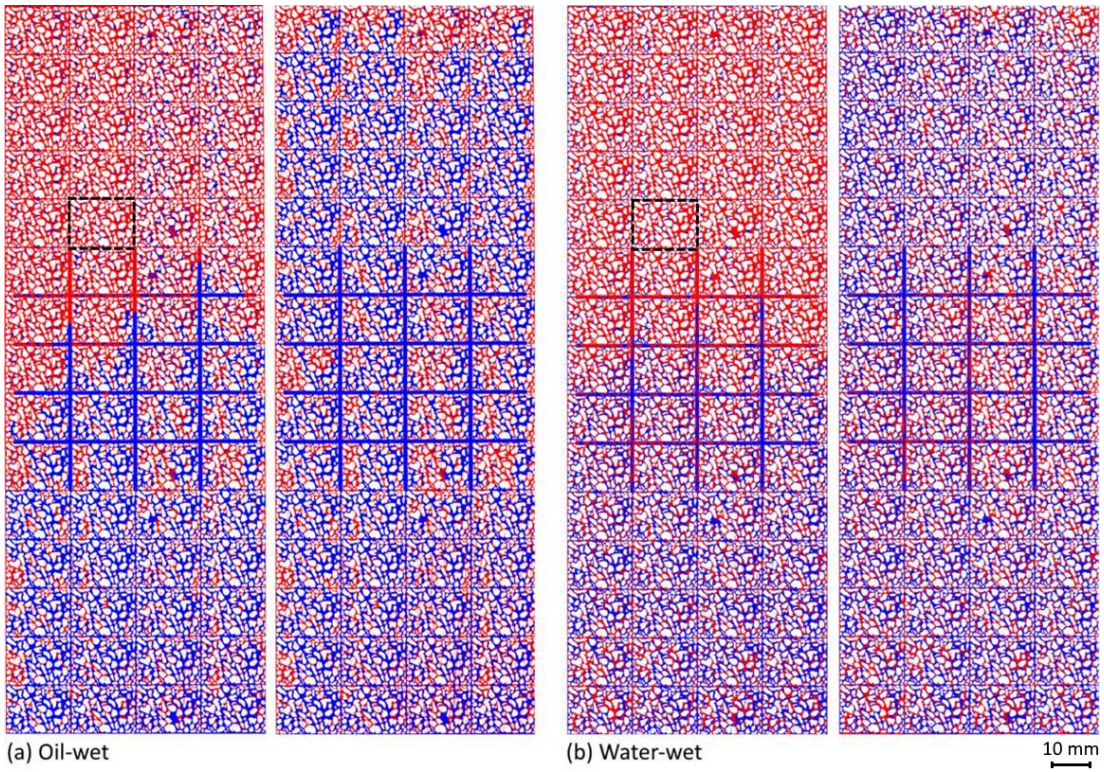

Figure 5-7. The waterflood process in (a) oil-wet and (b) water-wet micromodels performed with the production rate of 2.0 ml/hr (processed images, red: oil, blue: water, white: solid grains). Images of indicated zones during waterflood are shown in Figure 5-8.

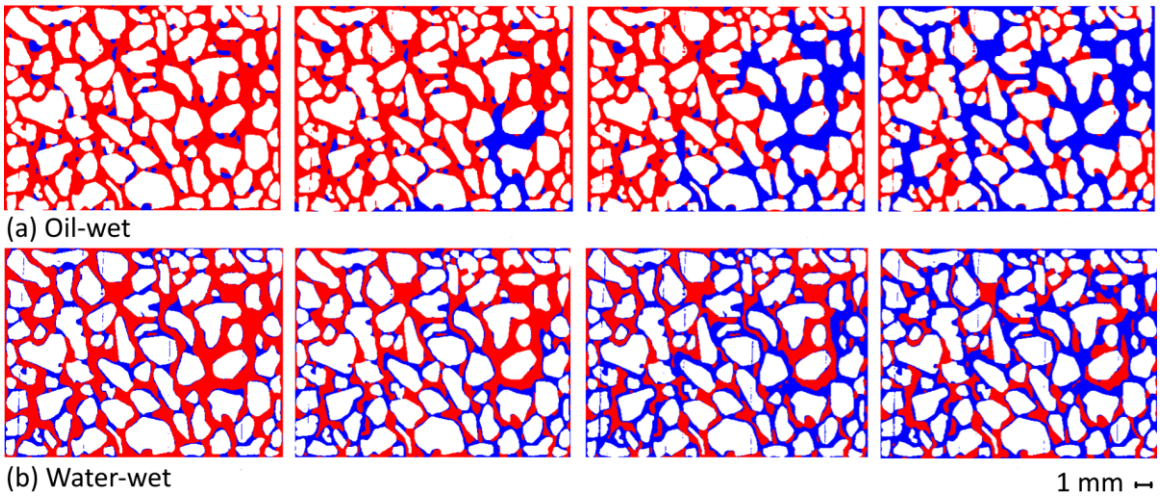

Figure 5-8. Mechanisms of oil displacements during waterflood in (a): oil-wet micromodel (b): water-wet micromodels (processed images, red: oil, blue: water, pattern size: 16×12 mm).

5.3.3. Post-waterflood GAGD

Results of post-waterflood GAGD experiments are summarized in Table 5-2. In addition, the variation of oil and water saturations during post-waterflood GAGD experiments performed in the same micromodel (tests 1-4) are shown in Figure 5-9 & Figure 5-10, respectively.

Results of post-waterflood GAGD experiments are summarized in Table 2. Tests 1-4 were conducted in the same micromodel varying the state of wettability and production rate. The variation of the oil and water saturations during tests 1-4 are shown in Figures 5-9 & 5-10, respectively. Under oil-wet conditions, the residual oil saturation dropped faster than the residual water saturation at early times after the gas-breakthrough. A similar trend can be observed for water under water-wet conditions indicating that the priority of the drainage after the gas-breakthrough is initially with the wetting phase. The variation of oil saturation in tests 2 & 4 in Figure 5-9 implies that a further drainage of oil

could be obtained upon the continuation of the process under water-wet conditions. It was also observed that increasing the production rate caused an early gas-breakthrough (breakthrough times are given in Table 2) without any remarkable recovery of oil under both wettability conditions (tests 3 & 4). The result of post-waterflood GAGD conducted with the low production rate was reproduced in the repeated experiments (tests 5 & 6), and the corresponding micromodel images are shown by Figures D-1 & D-2 in the Appendix D.

Table 5-2. Results of waterflood and post-waterflood GAGD experiments.

Wettability	Oil-wet	Water-wet	Oil-wet	Water-wet	Oil-wet	Water-wet
Test ID	1	2	3	4	5	6
Production Rate	0.2 ml/hr	0.2 ml/hr	2.0 ml/hr	2.0 ml/hr	0.2 ml/hr	0.2 ml/hr
Initial Oil Saturation (PV)	0.88	0.88	0.90	0.84	0.82	0.84
Oil Saturation after Waterflood (PV)	0.41	0.46	0.39	0.47	0.38	0.41
Waterflood Oil Recovery (% IOIP)	53%	48%	57%	44%	54%	51%
Oil Saturation at Gas-breakthrough (PV)	0.27	0.45	0.38	0.47	0.21	0.40
Water Saturation at Gas-breakthrough (PV)	0.36	0.29	0.36	0.40	0.38	0.24
Time to Gas-breakthrough	1 hr. & 34 min.	1 hr. & 11 min.	6 min.	3 min.	1 hrs. & 55 min.	1 hr. & 41 min.
Oil Saturation after 20 hrs. (PV)	0.14	0.32	0.20	0.37	0.14	-
Water Saturation after 20 hrs. (PV)	0.26	0.18	0.32	0.20	0.33	-
Oil Recovery after 20 hrs. (% IOIP)	84%	64%	78%	56%	83%	-
Oil Saturation after 47 hrs. (PV)	-	0.19	-	-	-	-
Water Saturation after 47 hrs. (PV)	-	0.14	-	-	-	-

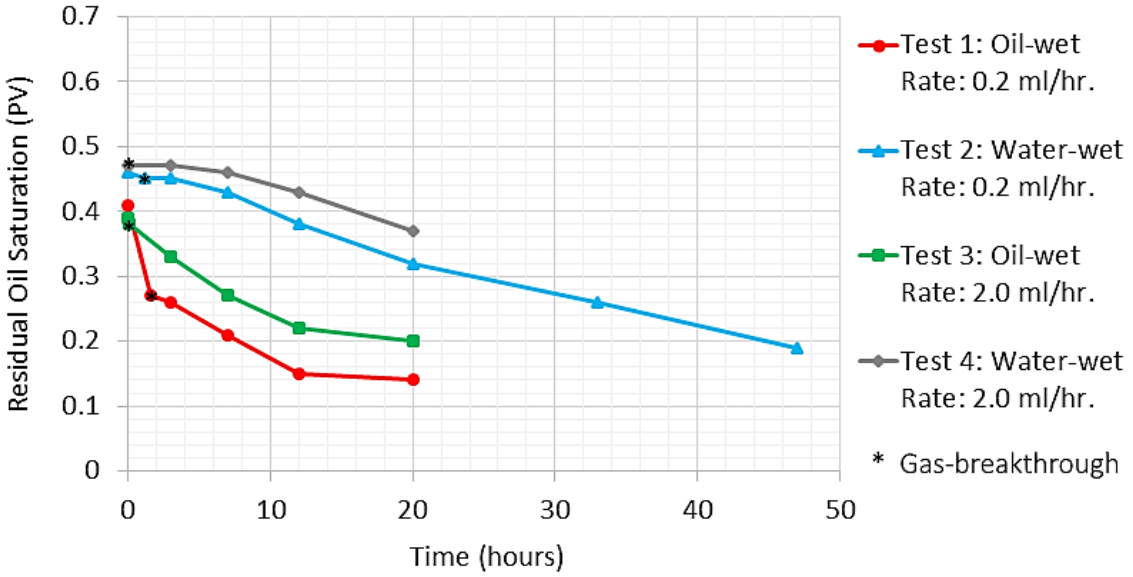

Figure 5-9. Variation of the oil saturation during post-waterflood GAGD tests. The drainage of oil at early times after gas-breakthrough was faster under oil-wet conditions (tests 1 & 3) compared to water-wet conditions (tests 2 & 4).

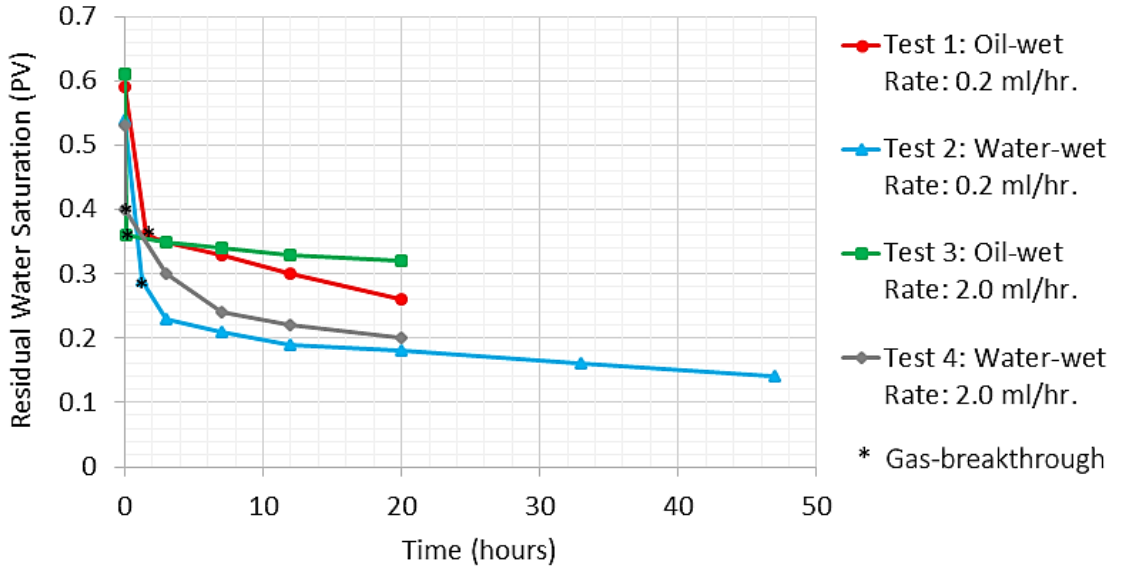

Figure 5-10. Variation of the water saturation during post-waterflood GAGD tests. The drainage of water at early times after gas-breakthrough was faster under water-wet conditions (tests 2 & 4) compared to oil-wet conditions (tests 1 & 3).

Images of the oil-wet micromodel during post-waterflood GAGD performed at the low production rate (0.2 ml/hr) are shown in Figure 5-11 (test 1 in Table 5-2). In addition, Figure 5-12 shows the stepwise displacement of fluids in a region of the oil-wet micromodel, as indicated in Figure 5-11: ii. The unprocessed images of the micromodel corresponding to Figure 5-12 are also presented in Appendix D (Figures D-3 to D-5). The inconsistency in the appearances of fine capillaries in different images was due to a variation in the autofocus of the imaging system.

Under oil-wet conditions, the production of water from the outlet of the micromodel allowed the entry of gas in top regions. Subsequently, gas displaced oil (drainage) and oil displaced water (imbibition) simultaneously. An oil-bank was formed ahead of the gas-front, where the oil saturation was increased with the displacement of water (Figure 5-11: i). The imbibition of oil ahead of the oil-bank resulted in the rupture of continuous water and isolation of water-blobs in the body of larger pores (Figures 5-12: ii-iii). The size of the oil-bank ahead of the gas-front grew until it reached the bottom of the micromodel.

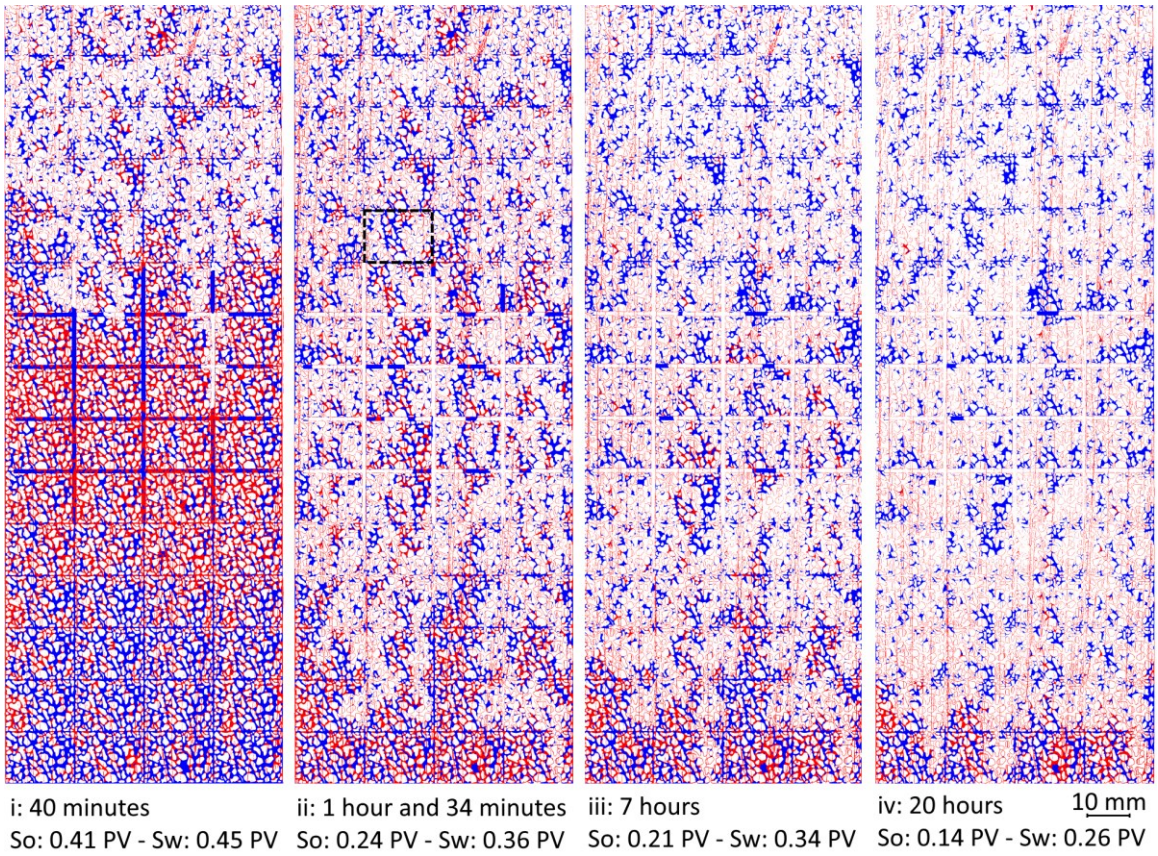

Figure 5-11. Processed images of the oil-wet micromodel during post-waterflood GAGD at the low production rate: 0.2 ml/hr. i: Development of oil-bank ahead of the gas-front, ii: gas-breakthrough, iii-iv: drainage of oil and water with film flow. (red: oil, blue: water, So: oil saturation, Sw: water saturation). Images of the indicated zone during the experiment are shown in Figure 5-12.

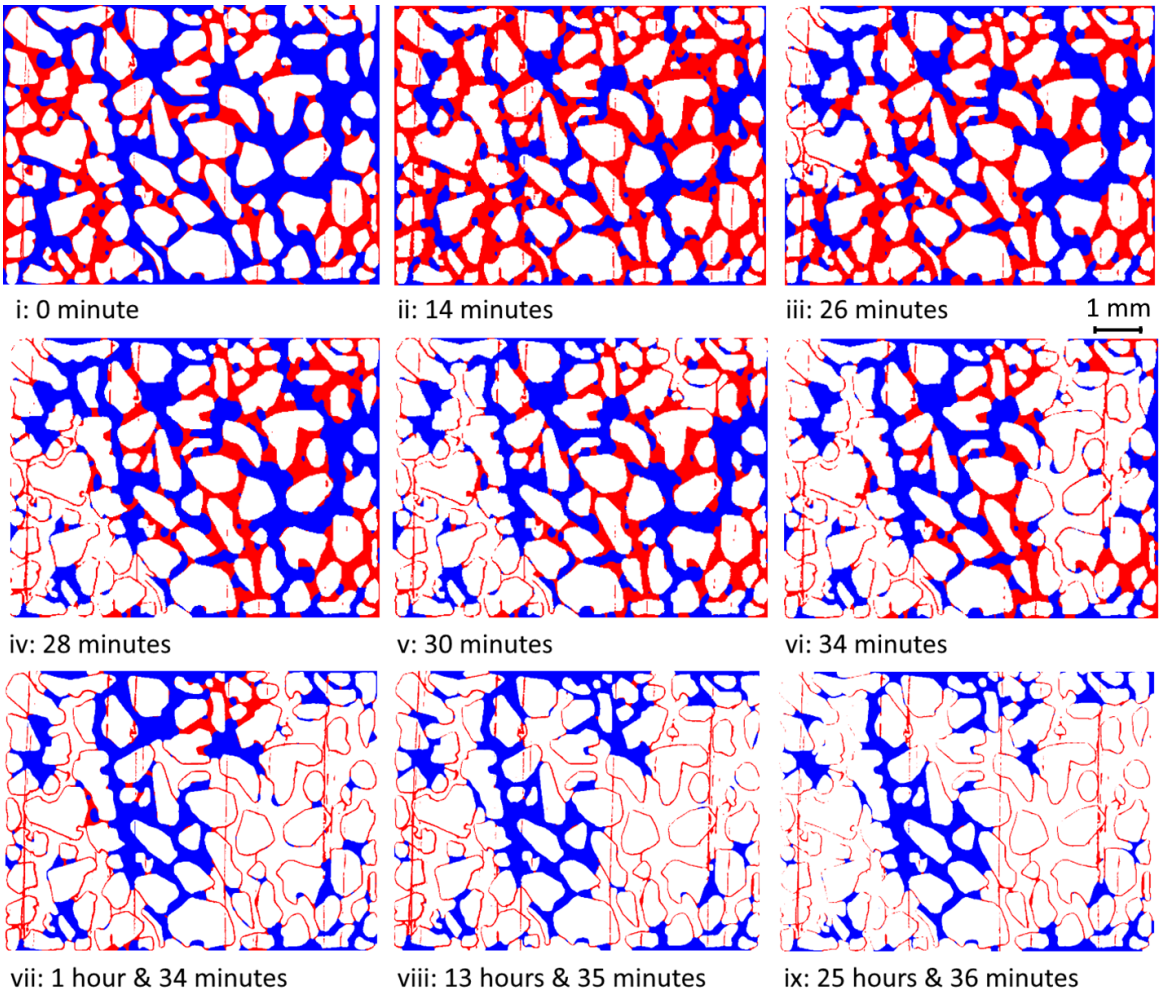

Figure 5-12. Stepwise displacement of fluids' interfaces in the oil-wet micromodel during post-waterflood GAGD at the production rate of 0.2 ml/hr. (i-vi): displacement of oil and water ahead of the gas-front, (vii): gas-breakthrough time, (viii-ix): drainage of oil and water through film-flow post gas-breakthrough. (red: oil, water: blue, pattern size: 16×12 mm). The corresponding micromodel images are shown in Appendix D, Figures D-3 to D-5.

In the oil-wet micromodel, leading zones of the gas-front were formed mainly in larger pores where the displacement of oil and water-blobs was accompanied with a lower effort compared to smaller pores. However, the growth of these capillary fingers was controlled by the effect of gravity on the gas-oil differential density, as well as the promotion of the

fluids' capillary pressures in leading zones of the gas-front due to the fluctuation of pore sizes in the breakthrough path. Figures 5-12: iii-vi show the subsequent displacement of oil and water in the trailing zones of the gas-front. However, heterogeneities of the porous medium caused the gas-front to bypass oil and water-blobs mainly in smaller pores. In addition, the presence of large heterogeneities in central regions of the micromodel caused the gas-front to follow the vertical channels (Figure 5-11: i). The presence of isolated water-blobs in horizontal channels prevented a complete bypass of oil with gas in matrices. This effect may no longer occur varying the orientation of fractures. The drainage of the bypassed oil continued after a gas-breakthrough (Figures 5-12: vii-viii) via a downward film flow through fine capillaries. The water-blobs also used any available space in fine capillaries to flow downward (Figures 5-11: ii-iv and Figures 5-12: viii-ix). The residual oil saturation after 20 hours of production was 0.14 PV that was mainly retained around solid grains and regions near the bottom of the pattern.

Images of the water-wet micromodel during the post-waterflood GAGD performed at the low production rate (0.2 ml/hr) are shown in Figure 5-13 (test 2 in Table 5-2). In addition, Figure 5-14 shows the displacement of fluid's interfaces in a region of the water-wet micromodel (as indicated in Figure 5-13) during the experiment. The original micromodel images corresponding to Figure 5-14 are shown in the Appendix D (Figures D-6 to D-8).

The GAGD process started by producing of water from the outlet port of the micromodel. The waterflooded residual oil in upper regions of the micromodel could flow and reconnect upon the displacement of their surrounding water. Subsequently, an oil-bank zone containing oil and residual water (in smaller pores) was developed ahead of the gas-

front (Figure 5-13: i and Figure 5-14: i-iv). Therefore, the displacement of gas-oil interfaces ahead of the gas-front and oil-water interfaces ahead of the oil-bank occurred simultaneously (dual drainage). The heterogeneities of the porous medium caused the gas-front to form leading zones in paths where gas-oil and oil-water interfaces were displaced with a lower capillary resistance.

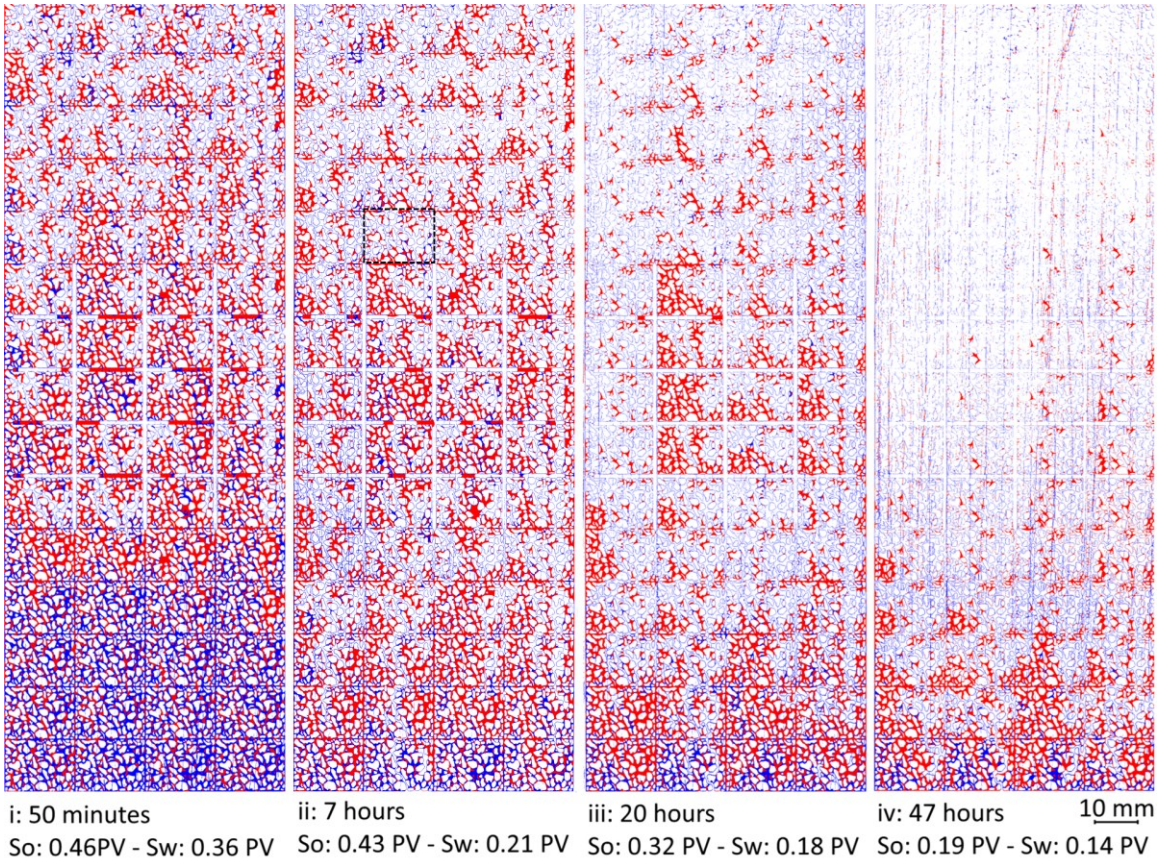

Figure 5-13. Processed images of the water-wet micromodel during post-waterflood GAGD at the low production rate: 0.2 ml/hr. i: Development of oil-bank ahead of the gas-front, ii-iv: drainage of oil and water with film flow. (red: oil, blue: water, So: oil saturation, Sw: water saturation). Images of the indicated zone during the experiment are shown in Figure 5-14.

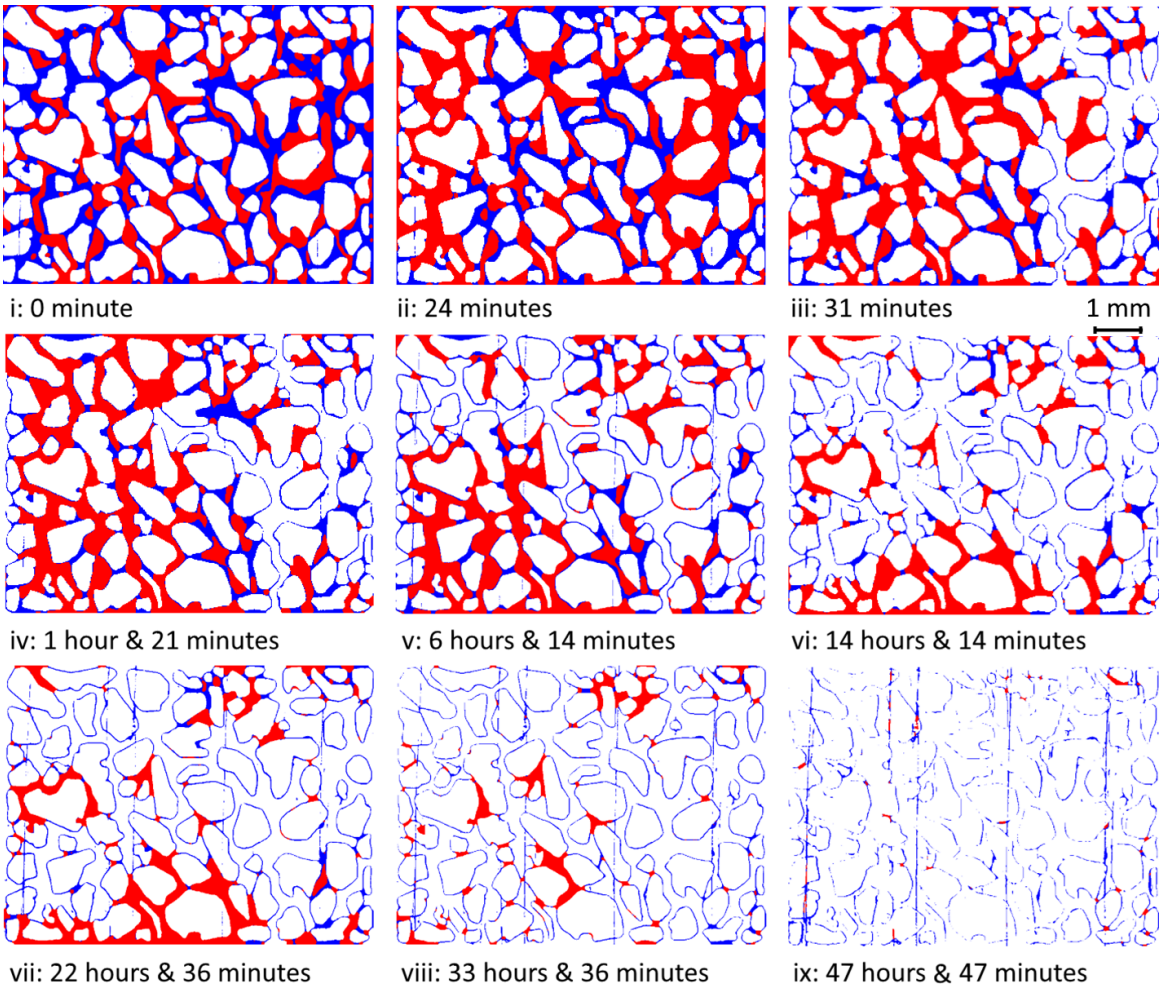

Figure 5-14. Stepwise displacement of oil and water in the water-wet micromodel during post-waterflood GAGD performed with the production rate of 0.2 ml/hr. (i): After waterflood, (ii): development of the oil-bank, (iii): entry of gas, (iv-vi): reduction of the residual water saturation, (vii-ix): reduction of the residual oil saturation (red: oil, water: blue). The corresponding micromodel images are shown in Appendix D, Figures D-6 to D-8.

Under water-wet conditions, the distance between leading and trailing zones of the gas-front was higher than oil-wet conditions, and oil-occupied zones containing residual water in small to medium sized pores were retained above the gas-front (Figure 5-13: i and Figure 5-14: iii). The distance between leading and trailing zones of the gas-front was

further increased in the fractured region of the micromodel where the displacement of interfaces was accompanied by lower frontal capillary pressures in wide channels. The recovery of oil started after the gas-breakthrough as the displaced oil (in the oil-bank) was mostly retained at the bottom of the micromodel. The drainage of the water through fine paths after the gas-breakthrough (Figures 5-13: iii-vi) resulted in the redistribution of the oil saturation through the coarse pore network. The reduction of the water saturation also promoted the film flow of oil through fine paths. The residual oil saturation after 20 hours of production was 0.32 PV and after 47 hours of production was 0.19 PV. Figure 5-13: iv and Figure 5-14: ix show that a very low residual oil was retained in top regions of the micromodel when the duration of the experiment was extended to 47 hrs. Figure 5-15 also shows an unprocessed image of the water-wet micromodel after 60 hrs. It can be observed that the continuation of the process resulted in a further drainage of oil and water. In addition, the absence of any dried colours around solid grains in top regions of the micromodel confirms that a complete drainage of oil and water at the end of the experiment was due to a film flow process, and the contribution of evaporation was unremarkable. The evaporation of a fluid leads to a deposition of a dried colour as shown in Figure D-9 in Appendix D.

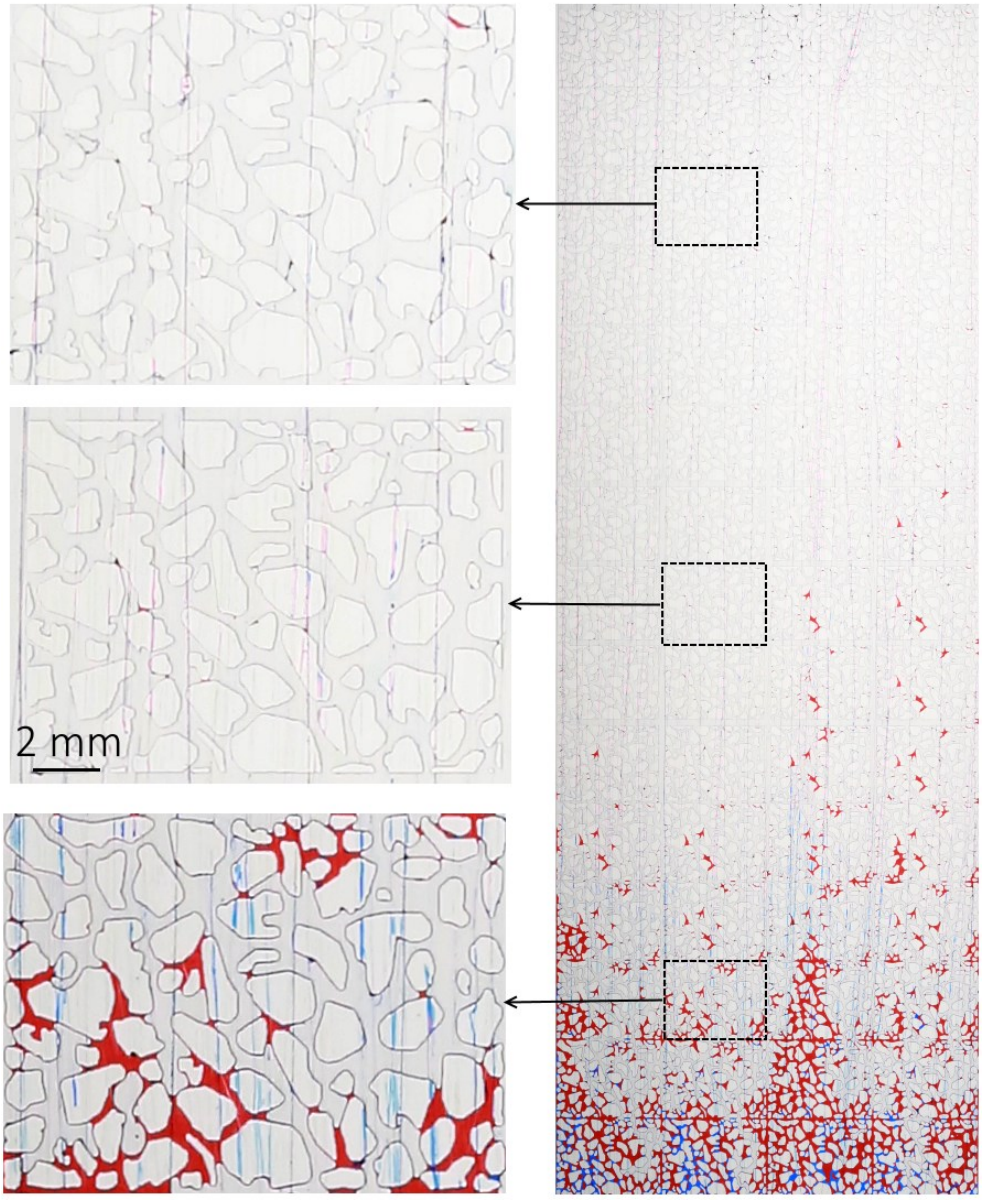

Figure 5-15. Image of the water-wet micromodel before the termination of test 2 (after 60 hrs) shows a complete drainage of oil and water in top regions upon continuation of GAGD process.

The displacement of fluids ahead of the gas-front under both wettability conditions was affected by the presence of residual water. Under oil-wet conditions, isolated water-blobs were formed in larger pores of the oil-bank. These water-blobs created a barrier for the flow of gas through larger pores. The displacement of a water-blob from a large pore into

a small pore is possible when the oil-water capillary pressure ahead of the water-blob is sufficiently increased. This happens with the reduction of the oil pressure upon the production of fluids from the outlet port of the micromodel. The reduction of the oil pressure enhanced the gas-oil capillary pressure in regions above the gas-front, thus helping with the drainage of oil from trailing zones and bypassed regions. Under water-wet conditions, larger pores were occupied by oil through which the entry of the gas-front was accompanied by a lower capillary pressure. The presence of the residual water in fine capillaries and small pores restricted the oil flow between trailing and leading zones of the gas-front. Consequently, the continuity of oil between higher and lower elevations was only through a limited number unblocked pores, as well as oil-films formed on the surface of water and around solid grains. The thickness of these oil-films was often low, and the drainage rate of oil prior to a gas-breakthrough from higher to lower elevations was insufficient to create a thick oil-bank under water-wet conditions.

For a better interpretation of data, images of the oil-wet and water-wet micromodels during tests 1 & 2 (at the low production rate: 0.2 ml/hr) were divided vertically into 15 equal sections (64×12 mm), and the saturation of the residual oil in each division was calculated. Figures 5-16 & 5-17 show the residual oil saturation with respect to the distance between centers of divisions from the bottom of the pattern under oil-wet and water-wet conditions, respectively. In Figure 5-16, the oil saturation profile after 40 minutes (before gas-breakthrough) shows an oil-bank region was formed in the gas-front. However, in Figure 5-16, the oil saturation profile after 50 minutes (before gas-breakthrough) implies that the size of the oil-bank under water-wet conditions was

smaller compared to oil-wet conditions. It should be noted that a reduction in the production rate could increase the thickness of the oil-bank under water-wet conditions, as a greater time is available for an effective drainage of oil and water from higher to lower elevations.

Figures 5-16 & 5-17 also indicate that the final residual oil saturation in top regions of the micromodel, which is far from the capillary end effect, is lowest under water-wet conditions. The average saturations of the residual oil and water (after 47 hrs) above the fractured zone of the water-wet micromodel are 0.02 PV and 0.08 PV, respectively. The residual oil and water saturations (after 20 hrs) in the same region of the oil-wet micromodel are 0.09 PV and 0.23 PV, respectively. The experimental data indicate that post-waterflood GAGD at early stages results in higher oil production with a lower water production under oil-wet conditions. In water-wet reservoirs, a very low residual oil saturation can be expected upon a sufficient extension of the process time.

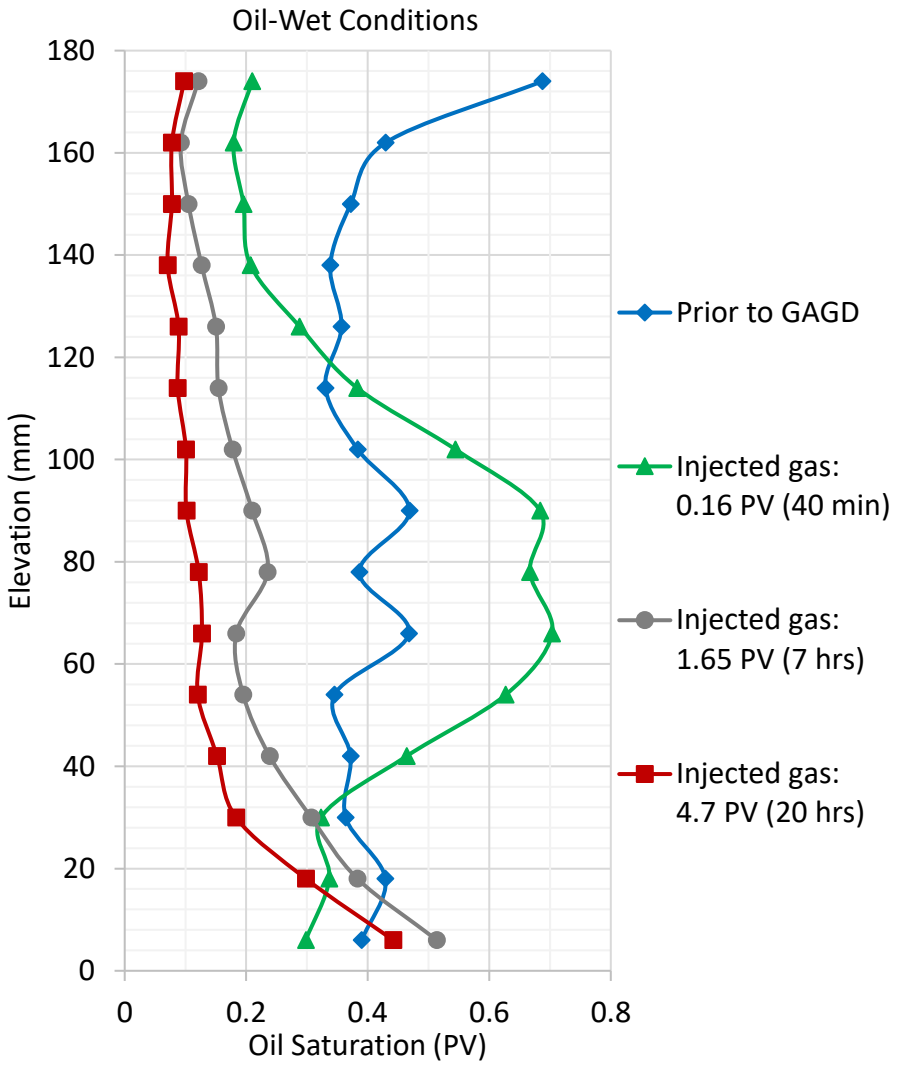

Figure 5-16. The variation of oil saturation profile in the oil-wet micromodel during post-waterflood GAGD in test 1.

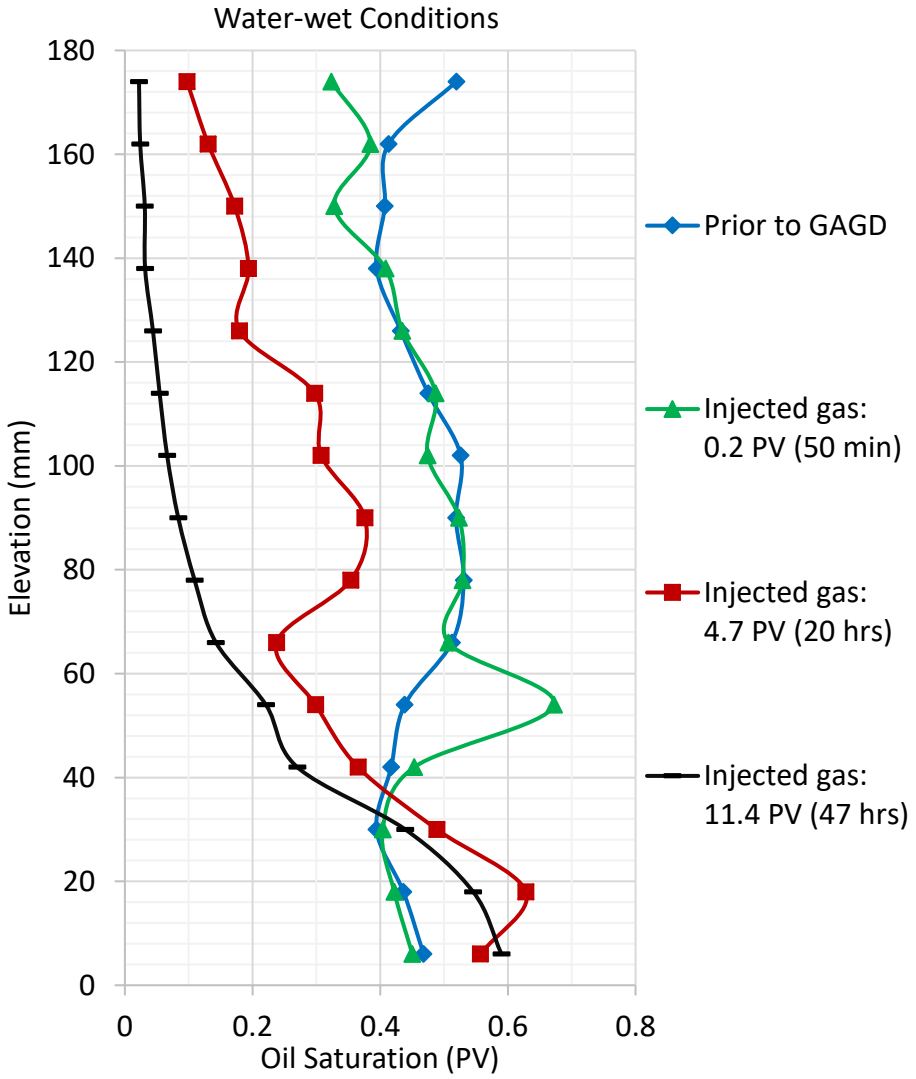

Figure 5-17. The variation of oil saturation profile in the water-wet micromodel during post-waterflood GAGD in test 2.

Images of the oil-wet and water-wet micromodels during post-waterflood GAGD performed with the high production rate (2.0 ml/hr) are shown in Figures 5-18 & 5-19, respectively. Under oil-wet conditions, increasing the production rate resulted in an unstable displacement of oil and water (Figure 5-18: ii), and the gas-breakthrough occurred after 6 minutes. Although an oil-bank was initially formed on top of the

micromodel, the leading zone of the gas-front penetrated this oil-bank through larger pores displacing oil and water-blobs not only downward but also latterly. The flowrate of oil in smaller pores and fine capillaries, because of the increased viscous pressure drops, was insufficient to create an oil-bank ahead of the gas-front (Figure 5-18: ii). Consequently, a gas-breakthrough occurred rapidly without any remarkable oil recovery. An additional recovery of oil was obtained after gas-breakthrough with a film flow in fine capillaries (Figures 5-18: iii-iv). The final residual oil saturation after 20 hours of production was 0.20 PV.

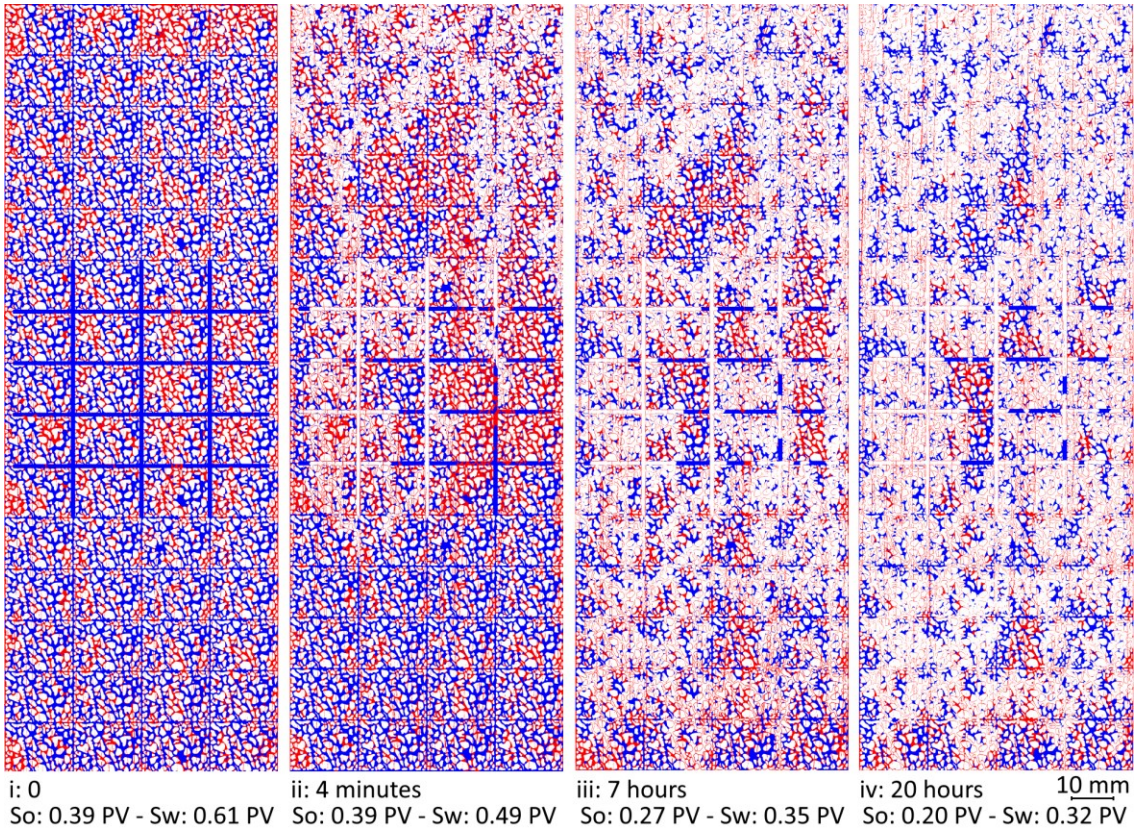

Figure 5-18. Processed images of the oil-wet micromodel during post-waterflood GAGD, which resulted in an unstable displacement of oil and water (test: 3) at the high production rate of 2.0 ml/hr. (i): Prior to GAGD. (ii): Prior to a gas-breakthrough. (iii-iv): Reduction of the residual oil saturation after the gas-breakthrough (red: oil, blue: water).

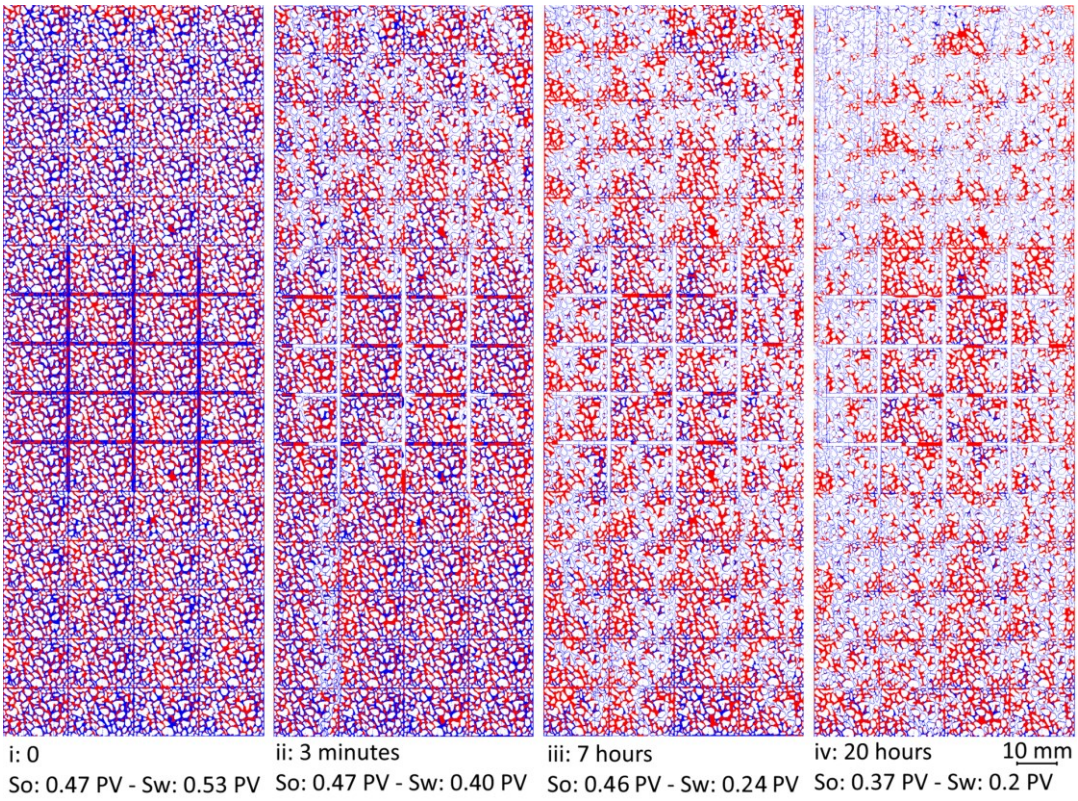

Figure 5-19. Processed images of the water-wet micromodel during post-waterflood GAGD, which resulted in an unstable displacement of oil and water (test: 4) at the high production rate of 2.0 ml/hr. (i): Prior to GAGD. (ii): Gas-breakthrough. (iii-iv): Reduction of residual oil and water saturations after the gas-breakthrough (red: oil, blue: water).

The post-waterflood GAGD at the high production rate (2.0 ml/hr) resulted in an instability of the gas-front under water-wet conditions as well. Increasing the production rate caused the gas-front to form capillary fingers that grew rapidly without developing an oil-bank. Therefore, both oil and water were retained at high saturations in trailing zones of the gas-front (Figure 5-19: ii), and no oil was recovered at a gas-breakthrough. The viscous and capillary pressures associated with the flow of oil and water from trailing zones to leading zones of the gas-front prevented an effective drainage of oil and water.

However, the continuation of GAGD resulted in the additional recovery of residual oil and water after gas-breakthrough flowing through fine paths (Figures 5-19: iii-iv).

It has been found that the capillary continuity of a porous medium is an important parameter affecting the flow of wetting and intermediate-wetting fluids, particularly at low residual saturations. Therefore, GAGD performance in macromodels made from smooth glass beads[45] is affected by the hydraulic discontinuity of wetting and intermediate-wetting fluids between regions occupied by a non-wetting phase, and gravity may hardly contribute to the film flow of the intermediate-wetting phase in such porous media. It is also to be noted that the morphology and geometry of coarse pores and fine capillaries in permeable rocks are more complex compared to pore network micromodels that are designed based on a small section of a rock. In addition, the morphology and geometry of coarse pores and fine capillaries in permeable rocks are more complex compared to a pore network micromodel that is designed based on a small section of a rock. Furthermore, the difference in the stability of gas-fronts between two-phase and three-phase GAGD experiments implies that three-phase processes may hardly be characterized only with data obtained from two-phase processes. Therefore, future research should include experiments in real-rock porous media to study the influence of gravity, viscous pressure drops and fluids' capillary pressures on the stability of the gas-front in reservoir rocks. High resolution computed tomography technologies can be employed for calculating the saturation of fluids and tracking their positions. The fluids' recovery, three-phase relative permeability, and three-phase capillary pressure curves can also be produced under corresponding conditions for optimizing a GAGD process.

5.4. Chapter Conclusions

Post-waterflood GAGD experiments were performed in oil-wet and water-wet micromodels at low and high production rates. Under both wettability conditions, an oil-bank was formed ahead of the gas-front when the production rate was low (0.2 ml/hr). In oil-wet micromodels, the oil-bank grew ahead of the gas-front, and the recovery of oil was initiated prior to the gas-breakthrough. In water-wet micromodels, an oil-bank was formed ahead of the gas-front upon the drainage of water. However, the flow of oil from trailing zones toward leading zones of the gas-front was restricted by the presence of the residual water in fine paths and smaller pores. Consequently, the size of oil-bank under water-wet conditions was smaller than oil-wet conditions, and the recovery of oil prior to a gas-breakthrough was negligible. However, a very low residual oil saturation was obtained under water-wet conditions when the process duration was extended. In addition, increasing the production rate resulted in the instability of the gas-front under both wettability conditions. Additional oil recovery was obtained after a gas-breakthrough via the film flow of oil and water through fine paths of the porous medium. The experimental result implies that both oil-wet and water-wet reservoirs are excellent candidates for post-waterflood GAGD. The former wettability state results in a faster drainage of oil (wetting phase) at early stages of the process, and the latter leads to a lower residual oil saturation (intermediate-wetting phase) upon an effective reduction of the water saturation.

Chapter References

15. Rao, D. N.; Ayirala, S. C.; Kulkarni, M. M.; Sharma, A. P., In *Development of gas assisted gravity drainage (GAGD) process for improved light oil recovery*, Proceeding of the SPE/DOE Symposium on Improved Oil Recovery, April 17-21, 2004; Society of Petroleum Engineers: Tulsa, Oklahoma, USA, 2004.
16. Thomas, B., Proposed screening criteria for gas injection evaluation. *Journal of Canadian Petroleum Technology* **1998,** *37*, (11).
17. Kulkarni, M. M.; Rao, D. N., In *Characterization of operative mechanisms in gravity drainage field projects through dimensional analysis*, Proceeding of the SPE Annual Technical Conference and Exhibition, September 24-27, 2006; Society of Petroleum Engineers: San Antonio, Texas, USA, 2006.
18. Løvoll, G.; Méheust, Y.; Måløy, K. J.; Aker, E.; Schmittbuhl, J., Competition of gravity, capillary and viscous forces during drainage in a two-dimensional porous medium, a pore scale study. *Energy* **2005,** 30, (6), 861-872.
19. Adamson, A. W.; Gast, A. P., Capillarity. In *Physical chemistry of surfaces*. 6th ed; John Wiley & Sons, Inc.: New York, USA, 1997; pp 4-43.
20. Dullien, F. A., Capillarity in Porous Media. In *Porous media: fluid transport and pore structure*, 2nd ed; Academic Press, Inc.: San Diego, Ca, USA, 1991; pp 118-232.
21. Tiab, D. and Donaldson, E. C., Capillary Pressure. In *Petrophysics: theory and practice of measuring reservoir rock and fluid transport properties*. 12th ed; Gulf Professional Publishing; Waltham, Ma, USA, 2015; pp 279-311.
22. Amyx, J. W.; Bass, D. M.; Whiting, R. L., Fundamental Properties of Fluid-Permeated Rocks. In *Petroleum reservoir engineering: physical properties*. McGraw-Hill College: 1960; Vol. 1. Pp 36-132.
23. Lenormand, R., Liquids in porous media. *Journal of Physics: Condensed Matter* **1990,** *2*, (S), SA79.

24. Khorshidian, H.; James, L. A.; Butt, S. D., In *Pore-Level Study of the Effect of Miscibility and Wettability on Oil Recovery during Gas Assisted Gravity Drainage*. Presented at Society of Core Analysts 31st Symposium, Vienna, Austria, August 27 – September 1, 2017.
25. Lenormand, R.; Zarcone, C.; Sarr, A., Mechanisms of the displacement of one fluid by another in a network of capillary ducts. *Journal of Fluid Mechanics* **1983,** *135*, 337-353.
26. Catalan, L. J.; Dullien, F. A.; Chatzis, I., The effects of wettability and heterogeneities on the recovery of waterflood the residual oil with low pressure inert gas injection assisted by gravity drainage. *SPE Advanced Technology Series* **1994,** *2*, (02), 140-149.
27. Zendehboudi, S.; Mohammadzadeh, O.; Chatzis, I., Experimental study of controlled gravity drainage in fractured porous media. *Journal of Canadian Petroleum Technology* **2009,** *50,* (02).
28. Dullien, F. A.; Zarcone, C.; Macdonald, I. F.; Collins, A.; Bochard, R. D., The effects of surface roughness on the capillary pressure curves and the heights of capillary rise in glass bead packs. *Journal of Colloid and Interface Science* **1989,** *127*, (2), 362-372.
29. Dong, M.; Chatzis, I., The imbibition and flow of a wetting liquid along the corners of a square capillary tube. *Journal of colloid and interface science* **1995,** *172*, (2), 278-288.
30. Khorshidian, H.; James, L. A.; Butt, S. D., Demonstrating the effect of hydraulic continuity of the wetting phase on the performance of pore network micromodels during gas assisted gravity drainage. *Journal of Petroleum Science and Engineering* **2017**.
31. Piri, M.; Blunt, M. J., Three-phase threshold capillary pressures in noncircular capillary tubes with different wettabilities including contact angle hysteresis. *Physical Review E* **2004,** *70*, (6), 061603.

32. Chatzis, I.; Ayatollahi, S., *In The effect of gas injection rate on the recovery of waterflood the residual oil under gravity assisted inert gas injection*, Proceeding of the Technical Meeting/Petroleum Conference of The South Saskatchewan Section, October 18 – 20, 1993; Petroleum Society of Canada: Regina, Canada, 1993.
33. Kantzas, A.; Nikakhtar, B.; De Wit, P.; Pow, M.; Jha, K. N., Design of a gravity assisted immiscible gas injection program for application in a vuggy fractured reef. *Journal of Canadian Petroleum Technology* **1993**, 32, (10).
34. Øren, P.; Pinczewski, W., Fluid distribution and pore-scale displacement mechanisms in drainage dominated three-phase flow. *Transport in Porous Media* **1995,** *20*, (1-2), 105-133.
35. Dong, M.; Dullien, F. A.; Chatzis, I., Imbibition of oil in film form over water present in edges of capillaries with an angular cross section. *Journal of colloid and interface science* **1995,** *172*, (1), 21-36.
36. Blunt, M.; Zhou, D.; Fenwick, D., Three-phase flow and gravity drainage in porous media. *Transport in porous media* **1995,** *20*, (1-2), 77-103.
37. Dong, M.; Chatzis, I., Oil layer flow along the corners of non-circular capillaries by gravity drainage. *Journal of Canadian Petroleum Technology* **2003,** *42*, (02).
38. Oren, P.; Billiotte, J.; Pinczewski, W., Mobilization of waterflood the residual oil by gas injection for water-wet conditions. *SPE Formation Evaluation* **1992,** *7*, (01), 70-78.
39. Dumore, J.; Schols, R., Drainage capillary-pressure functions and the influence of connate water. *Society of Petroleum Engineers Journal* **1974,** *14*, (05), 437-444.
40. Vizika, O.; Lombard, J., Wettability and spreading: two key parameters in oil recovery with three-phase gravity drainage. *SPE Reservoir Engineering* **1996,** *11*, (01), 54-60.
41. Grattoni, C.; Jing, X.; Dawe, R., Dimensionless groups for three-phase gravity drainage flow in porous media. *Journal of Petroleum Science and Engineering* **2001,** *29*, (1), 53-65.

42. Paidin, W. R.; Rao, D. N. In Physical Model Experiments to Evaluate the Effect of Wettability and Fractures on the Performance of the Gas-assisted Gravity Drainage (GAGD) Process. Presented the Society of Core Analysts 21st Symposium, September 10-12, 2007; Calgary, Canada, 2007.
43. Maroufi, P.; Rahmanifard, H.; Al-Hadrami, H. K.; Escrochi, M.; Ayatollahi, S.; Jahanmiri, A., Experimental investigation of wettability effect and drainage rate on tertiary oil recovery from fractured media. *Journal of Porous Media* **2012**, 15(12).
44. Kantzas, A.; Chatzis, I.; Dullien, F. In *Enhanced oil recovery by inert gas injection*, Proceeding of the SPE Enhanced Oil Recovery Symposium, April 16-21, 1988; Society of Petroleum Engineers: Tulsa, Oklahoma, USA, 1988.
45. Parsaei, R.; Chatzis, I., Experimental investigation of production characteristics of the gravity-assisted inert gas injection (GAIGI) process for recovery of waterflood the residual oil: effects of wettability heterogeneity. *Energy & Fuels* **2011,** *25*, (5), 2089-2099.
46. Kantzas, A.; Chatzis, I.; Dullien, F. In *Mechanisms of capillary displacement of the residual oil by gravity-assisted inert gas injection*, Proceeding of the SPE Rocky Mountain Regional Meeting, May 11-13, 1988; Casper, Wyoming, USA, 1988.
47. Chatzis, I.; Kantzas, A.; Dullien, F. In On the investigation of gravity-assisted inert gas injection using micromodels, long berea sandstone cores, and computer-assisted tomography, Proceeding of the SPE Annual Technical Conference and Exhibition, October 2-5, 1988; Society of Petroleum Engineers: Houston, Texas, USA, 1988.
48. Dullien, F.; Lai, F. S.; Macdonald, I., Hydraulic continuity of residual wetting phase in porous media. *Journal of colloid and interface science* **1986,** *109*, (1), 201-218.
49. Meszaros, G.; Chakma, A.; Jha, K.; Islam, M. In Scaled model studies and numerical simulation of inert gas injection with horizontal wells, SPE Annual Technical Conference and Exhibition, September 23-26, 1990; Society of Petroleum Engineers: New Orleans, Louisiana, USA, 1990.
50. Terwilliger, P.; Wilsey, L.; Hall, H. N.; Bridges, P.; Morse, R., An experimental and theoretical investigation of gravity drainage performance. *Journal of Petroleum Technology* **1951,** *3*, (11), 285-296.

51. Chatzis, I.; Morrow, N. R.; Lim, H. T., Magnitude and detailed structure of residual oil saturation. *Society of Petroleum Engineers Journal* **1983,** *23*, (02), 311-326.
52. Lenormand, R.; Zacone, C., Physics of blob displacement in a two-dimensional porous medium. *SPE formation evaluation* **1988,** *3*, (01), 271-275.
53. Jerauld, G.; Salter, S., The effect of pore-structure on hysteresis in relative permeability and capillary pressure: pore-level modeling. *Transport in porous media* **1990,** *5*, (2), 103-151.
54. Vizika, O.; Avraam, D.; Payatakes, A., On the role of the viscosity ratio during low-capillary-number forced imbibition in porous media. *Journal of colloid and interface science* **1994**, *165*, (2), 386-401.
55. Oren, P. E.; Pinczewski, W. V., The effect of wettability and spreading coefficients on the recovery of waterflood residual oil by miscible gasflooding. *SPE Formation Evaluation* **1994,** *9*, (02), 149-156.
56. Keller, A. A.; Blunt, M. J.; Roberts, A. P. V., Micromodel observation of the role of oil layers in three-phase flow. *Transport in Porous Media* **1997,** *26*, (3), 277-297.
57. Golshokooh, S.; Khoramian, R.; SA, A. R., Using Hybrid Silica Nanoparticles-Copolymer with Novel Micro-Model for Enhanced Oil Recovery. Article in Press: *Scientia Iranica* **2017**.
58. Hydrophil. http://lotusleafcoatings.com. (access date: January 22, 2017).
59. Golshokooh, S.; Khoramian, R.; SA, A. R., Methods for fabricating porous media with controllable characteristics. U.S. Patent Application No. 15/135,191. 2016.

Chapter 6 : Conclusions

The performance of the GAGD process has been studied at the pore-level under various conditions. GAGD experiments were conducted at irreducible water saturations and post-waterfloods. The main studied parameters in GAGD tests performed at irreducible water saturations are:

- the state of wettability (oil-wet and water-wet);
- the hydraulic continuity of residual wetting phase in porous media;
- the porous medium heterogeneities; and
- the miscibility of gas with oil.

The studied parameters in post-waterflood GAGD experiments are:

- the state of wettability;
- the porous medium heterogeneities; and
- the production rate.

A new pore network micromodel containing a heterogeneous coarse pore network covered by fine capillaries was designed and constructed to perform experiments in transparent porous media representing characteristics of reservoir rocks. The new micromodel effectively reflected phenomena affecting GAGD performance, such as the interaction between capillary, gravitational and viscous forces. An experimental setup was developed in the Hibernia EOR lab at Memorial University to perform GAGD experiments. In addition, a custom image processing program was developed to quantify saturations of fluids from micromodel images captured during experiments.

Results of GAGD tests at irreducible water saturation indicate that:

- The displacement of interfaces between a wetting phase and a non-wetting phase occurred through paths of the least resistance, such as larger pores where capillary pressures between fluids were lower to overcome. Therefore, the wetting phase in smaller pores surrounded by larger pores was often bypassed with the non-wetting phase.
- The hydraulic continuity of the residual wetting phase played an important role in the interaction between capillary and gravitational forces. The presence of fine capillaries passing over the coarse pore network of a porous medium caused a wetting phase (e.g. oil) to maintain its hydraulic continuity between regions bypassed with a non-wetting phase (e.g. gas). In GAGD, an enhancement of the gas-oil capillary pressure could be obtained at higher elevations due to the effect of gravity on the gas-oil differential density. Therefore, the flow of oil from higher toward lower elevations was possible with the film flow through fine capillaries. In reservoir rocks, these fine paths are formed by the irregularities existing on surfaces of connected solid grains.
- Under water-wet conditions, the continuity of oil between bypassed regions can be arrested by the presence of residual water. Therefore, the increase of the gas-oil capillary pressure due to a reduction in the hydrostatic pressure of oil at higher elevations was limited. This may result in the retention of the residual oil (as the inetrmediate-wetting phase) with a higher saturation compared to oil-wet conditions.

- Under oil-wet conditions, fine capillaries provided oil with paths where oil can directly flow from higher toward lower elevations. The geometry and continuity of these paths determine the highest gas-oil capillary pressure that can be obtained at greater elevations. Therefore, the residual oil may be retained in smaller pores and around solid grain where the hydraulic continuity of oil to lower elevations was terminated due to the geometric constraints of fine capillaries.
- During GAGD, the variation of gas-oil capillary pressure in small and large pores caused the gas-front to form leading and trailing zones. The leading zones may bypass trailing zones because of heterogeneities. Lowering the gas-oil interfacial tension may reduce the size of trailing zones, thus reducing the saturation of the bypassed oil, specially when oil is the intermediate-wetting phase. The development of a miscible contact between oil and gas eliminates the capillarity in porous media and results in a complete recovery of oil.

Results of post-waterflood GAGD experiments indicate that:

- The waterflood process under oil-wet conditions resulted in the displacement of oil through larger pores as normal during a drainage process. The waterflood under water-wet conditions, which was an imbibition process, resulted in the flow of water through smaller pores, and residual oil was surrounded by water in larger pores.
- Under oil-wet conditions, a growing oil-bank was developed in the gas-front when post-waterflood GAGD was performed with a low production rate. The displaced oil in the gas-front used fine paths and small pores to flow in zones ahead of the

gas-front. Conseuently, isolated water-blobs were created in larger pores during an imbibition process at interfaces between oil and water.

- Under oil-wet conditions, the residual oil remained in pores with smaller sizes and pores with entries blocked by residual water-blobs. Although, the presence of fine paths helped with the film flow and recovery of the residual oil after a gas-breakthrough, the residual oil was finally retained around solid grains after 20 hrs.
- Under water-wet conditions, an oil-bank was also developed upon the displacement of water and the reconnection of oil-blobs. However, the growth of the oil bank was limited as the flow of oil and water between the trailing and leading zones of the gas-front was slow.
- The size of an oil-bank under oil-wet conditions was larger than water-wet conditions. This resulted in a higher recovery of oil prior to a gas-breakthrough. In addition, the film flow of the residual oil under oil-wet conditions was faster than water-wet conditions, as fine paths and small pores under water-wet conditions were initialy occupied by water.
- The continuation of the GAGD process under water-wet conditions resulted in a high recovery of oil upon an effective drainage of water with the extension of the process duration. The drainage of water opened spaces in coarse pores and fine paths for the drainage of oil from higher to lower elevations.
- The capillary forces and viscous pressure drops in the trailing zone of the gas-front contributed to an unstable displacement of oil and water by gas. However,

the fluctuation of capillary pressure in the leading zones of the gas-front and gravity could help with the stability of gas-front.

- The presence of large scale heterogeneities caused the gas-front to follow fractures instead of matrices, as the capillary pressures associated with the displacement of fluids' interfaces are lower in wider paths. Consequently, oil and water were bypassed and retained at higher saturations in matrices.
- Increasing the production rate increased the distance between leading and trailing zones of the gas-front, and a gas-breakthrough occurred rapidly without an appreciable oil recovery. However, the recovery of oil after a gas-breakthrough was obtained with the film flow through fine paths.

In this research, Gas Assisted Gravity Drainage was studied in the new micromodel to reflect the influence of effective forces that control the displacement of fluids. These forces are capillary, gravitational and viscous forces. Micromodel experiments provided useful information that can be used to characterize the performance of GAGD operations at reservoir scale. Similar to the porous medium of a micromodel, reservoir heterogeneities cause the injected gas to follow least resistant paths on its front, thus bypassing wetting and intermediate-wetting phase in regions where a higher capillary pressure must be overcome compared to neighbouring zones. Therefore, the gas-front tends to follow paths containing fractures and high permeable zones. We have also demonstrated that the hydraulic continuity of a fluid plays an important role in the interplay of these forces. The wetting phase keeps a strong hydraulic continuity though fine paths and smaller pores of a porous medium. When the saturation of the wetting

phase is higher, the associated viscous pressure drop in these paths is lower. Therefore, any increase of the capillary pressure in the gas-front, as well as the reduction of fluids' hydrostatic pressure (due to effect of gravity on fluids' differential densities) help with the subsequent drainage of the residual wetting phase. The gas-front capillary pressure can be promoted facing with low permeable zones on its front. The drainage rate of the wetting phase becomes lower with an increase of the retaining forces upon a reduction of its saturation. The retaining forces are viscous pressure drop and capillary pressures that must be overcome for a further reduction of the fluids saturation in zones containing smaller pores. The retaining forces are lower when the injected gas dissolves in oil, thus reducing oil viscosity and gas-oil interfacial tension. The intermediate-wetting phase is normally found in medium to large size pores, compared to residual wetting phase that occupies smaller pores. Therefore, the drainage of oil as the intermediate wetting phase can lead to high recovery factors when the wetting phase saturation is low.

The research outcomes suggest that:

1. GAGD performance is better when the gas-oil differential pressure is promoted in th gas-front. This can be obtained by directing the breakthrough path perpendicular with the bedding of low permeable formations. The placement of the injection and production wells influences the direction of the breakthrough path.
2. The three-phase capillary pressure curve/model is an important parameter of fluid flow in porous media that must be included in reservoir simulations, and it should

be extracted/validated conducting real-rock microfluidic experiments with the assistance of tomography techniques.

3. Mechanisms that minimizes viscous pressure drops associated with the drainage of oil from the bypassed regions should be considered in any gravity drainage process.

The future work should include:

- the fabrication of scaled micromodels based on pore size distribution of a real-rock porous medium;
- adding wettability heterogeneities to micromodels, thus preparing more realistic conditions for studying multi-phase flow in porous media;
- the fabrication of real-rock porous medium utilized with tomography techniques to calculate three-phase capillary pressure and relative permeability curves against saturation of fluids under three-phase conditions;
- the investigation of dimensionless numbers in order to model pore-scale phenomena under three-phase flow conditions as a function of the interplay between capillary and gravitational and viscous forces, as well as the heterogeneity characteristics.
- and, the mathematical modeling of three-phase flow and the validation of models with representative micromodels for generating relative permeability and capillary pressure curves to be used in reservoir simulations for different oil recovery processes.

Appendix A

Figure A-1 shows the micromodel pattern used for the preliminary GAGD experiments in Chapter 2. The presence of a smaller pore network at the bottom of the pattern (in the outlet zone) played the role of a capillary barrier, which contributed to the attenuation of the capillary end effect during GAGD. In addition, the original (unprocessed) images of micromodels (corresponding to experimental results in Chapter 2) are presented to compare residual oil and water under oil-wet (Figure A-2) and water-wet conditions (Figure A-3).

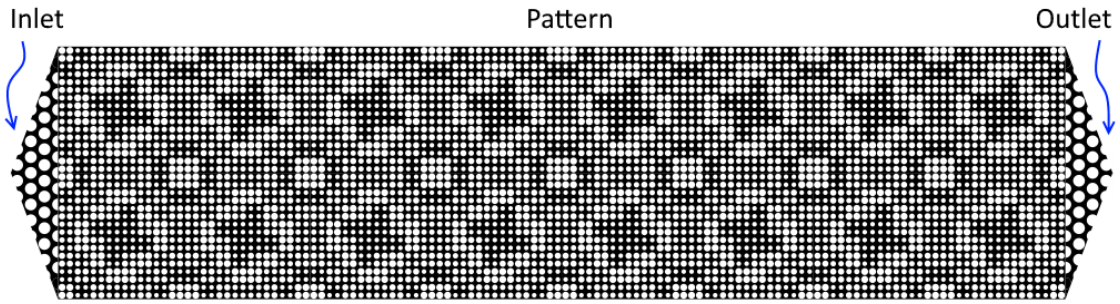

Figure A-1. Micromodel pattern designed for the preliminary GAGD experiments in Chapter 2.

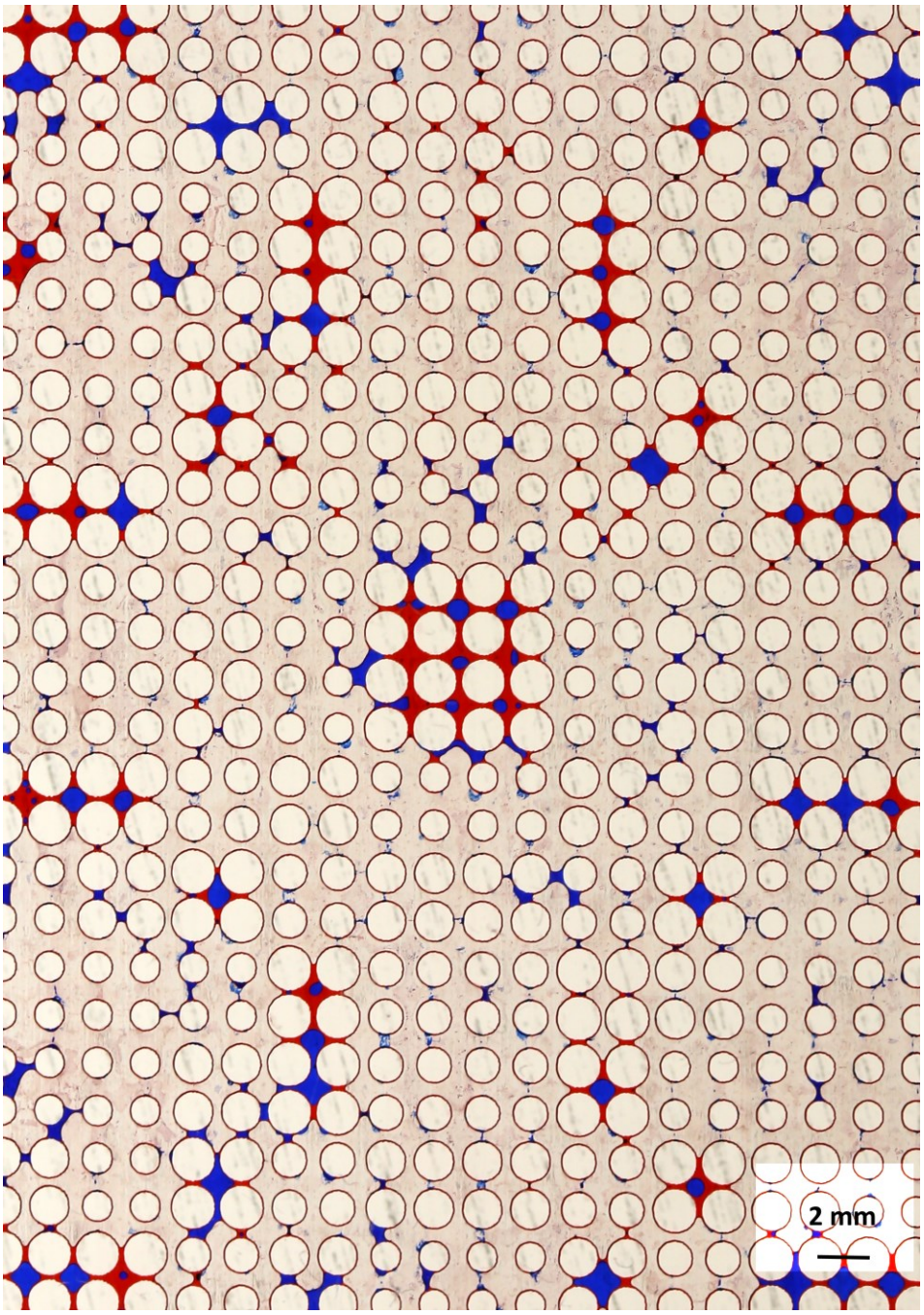

Figure A-2. Image of the central region in the oil-wet micromodel showing the final state of the residual oil (red) and water (blue) after 68 hrs.

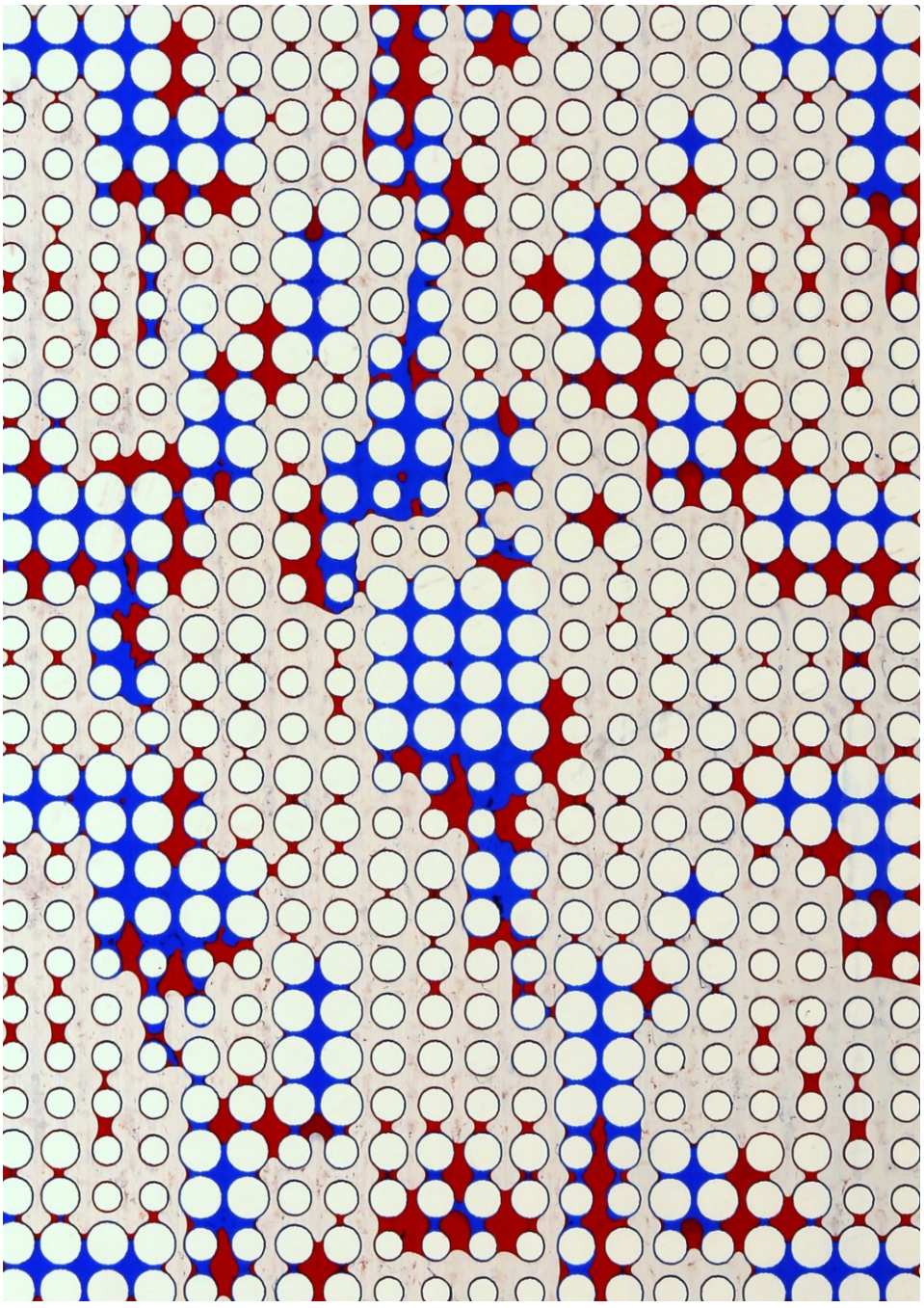

Figure A-3. Image of the central region in the water-wet micromodel showing the final state of the residual oil (red) and water (blue) after 67 hrs.

Table A-1 present the mutual solubility of water-CO_2 simulated with the Peng-Robinson equation of state using the PVT-sim software (lincensed by Faculty of Engineering and Applied Science at Memorial University).

Table A-1: Mutual solubility of water-CO_2 system at 1.7 bars and 25°C simulated with Peng-Robinson equation of state.

Components	Liquid Composition (Mole%)	Vapour Composition (Mole%)
CO2	0.14	99.08
Water	99.86	0.92

Based on the calculated equilibrium ratios, the volume of the injected CO_2 afetr 68 hrs is 6.8 ml (production rate: 0.1 ml/hr) that is approximately equivalent with 0.52×10^{-3} moles of CO_2 under corresponding experimental conditions (1.7 bars & 24°C). Therefore, the volume of the evaporated water is approximately 9×10^{-5} ml which negiligible compared to the micromodel pore volume (1.25 ml).

The solubility of water in CO_2 was experimentally[1] measured at 2.7 mole% under corresponding experimental conditions (1.7 bar & 25°C). Although the experimental measurement shows that the volume of the evaporated water can be as high as 3×10^{-4} ml, this volume is still negligible compared to micromodel pore volume (0.0002 PV).

Table A-2 also presents the mutual solubility of Varsol components in CO_2 under corresponding experimental conditions. The summation of the evaporated volumes of Varsol components is only 5×10^{-7} ml. This volume compared to the micromodel pore volume (1.25 ml) is unremarkable as well. The micromodel images also shows no sign of

an oil evaporation at the end of GAGD experiments. Therefore, the drainage was the main mechanism in the reduction of both the wetting and intermediate-wetting phase in the conducted experiments.

Table A-2: Mutual evaporation of Varsol components and CO_2 at 1.7 bars and 25°C simulated with Peng-Robinson equation of state

Components	Composition	Liquid Composition (Mole%)	Vapour Composition (Mole%)	Molar Volume of Alkanes	Evaporated Volume of Alkane
CO2	0.909	4.8785	99.9082	-	-
C9	0.007	7.4101	0.0278	178	1.45E-07
C10	0.025	25.5611	0.0382	195	1.99E-07
C11	0.035	36.2795	0.0218	211	1.13E-07
C12	0.023	23.9531	0.004	214	2.08E-08
C13	0.002	1.9184	0	232	-

Reference

1. Spycher, N.; Pruess, K.; Ennis-King, J., CO_2-H2O mixtures in the geological sequestration of CO_2. I. Assessment and calculation of mutual solubilities from 12 to 100°C and up to 600 bar. *Geochimica et cosmochimica acta* **2003,** 67, (16), 3015-3031.

Appendix B

B.1. Image Analysis Methodology

The processing of computerized images has been used in many applications from an image quality enhancement to the segmentation of a region of interest.[1] The evaluation of the perfromance and robustness of the developed processing algorithms can be tested qualitatively or quantitatively. Mahmoodi et al.[2] used the IMAQ vision module of LabVIEW program for quantifying saturations of fluids during a multiphase flow process in a pore network micromodel. In their program, the monochrome plane is first extracted, and an image enhancement step was introduced. Then the regions occupied by oil, water and gas were recognized via a particle analysis technique. They evaluated the uncertainty of their image processing program with the material balance comparing calculated data with measured volumes by a precision pump. The error associated with the calculated saturation of fluids was found to be as high as ± 2.5%.

We developed an image analysis program with the MATLAB[†] software to quantify two-dimensional saturations of fluids in micromodel images that were cropped precisely to contain the area of interest. Figure B-1 shows the image analysis process. The program counts the total number of pixels (N_T) in an uploaded image and evaluates the red (R), green (G) and blue (B) components of all pixels. Every pixel has R, G and B values ranging from 0 to 255.

[†]Software license was provided by the Faculty of Engineering and Applied Science at Memorial University of Newfoundland.

The green component of the white backlight was filtered by the red colour of oil and blue colour of water. Therefore, pixels with a higher intensity of R and B components have a lower G value. The white pixels, which are the solid grains and gas invaded zones, have a higher value of the green component (G). Therefore, a threshold value (T_G) was defined for the green component of each pixel ($0 < T_G < 255$) to categorize the pixel as white or red and blue. The red and blue pixels can then be determined by comparing the R and B components of pixels which were not identified as white. When the illuminated backlight contains an unequal intensity of red and blue colours, an adjusting parameter (X) can be used to calibrate the detection of red and blue pixels. Therefore, where $R \geq B + X$, the pixel is defined as red, and where $R < B + X$, the pixel is defined as blue. Ultimately, a processed image that only contains pure white (255, 255, 255), pure red (255, 0, 0) and pure blue (0, 0, 255) pixels is generated. The micromodel porosity (Φ) can be defined by dividing the total number of red and blue pixels (N_R+N_B) by the total number of pixels (N_T) for the image of a micromodel fully saturated with oil and water. The saturation of oil (So), gas (Sg) and water (Sw) can be calculated knowing the number of red, blue and white pixels in an image of micromodel containing oil, gas and water.

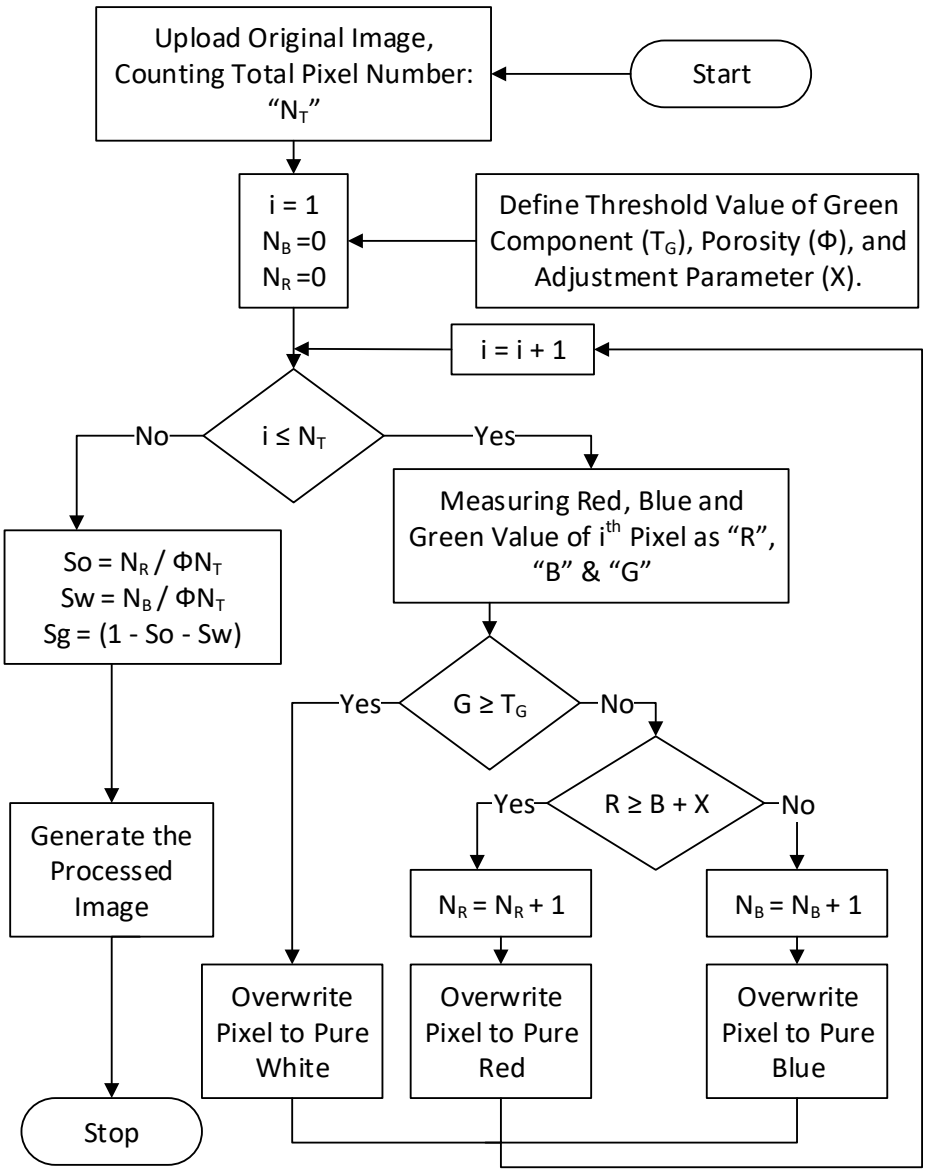

Figure B-1. The image analysis algorithm developed to calculate saturation of fluids in micromodel containing red dyed oil and blue dyed water.

In order to determine the appropriate settings for T_G and X parameters, the original image and analysed image can be compared visually. The image analysis tool, with the appropriate setting of parameters, produces a processed image with fluids boundaries similar to the original image. Figures B-2(a) & B-2(b) show the magnified images of a

region in a micromodel before and after processing with a T_G value of 120 and X value of 5.

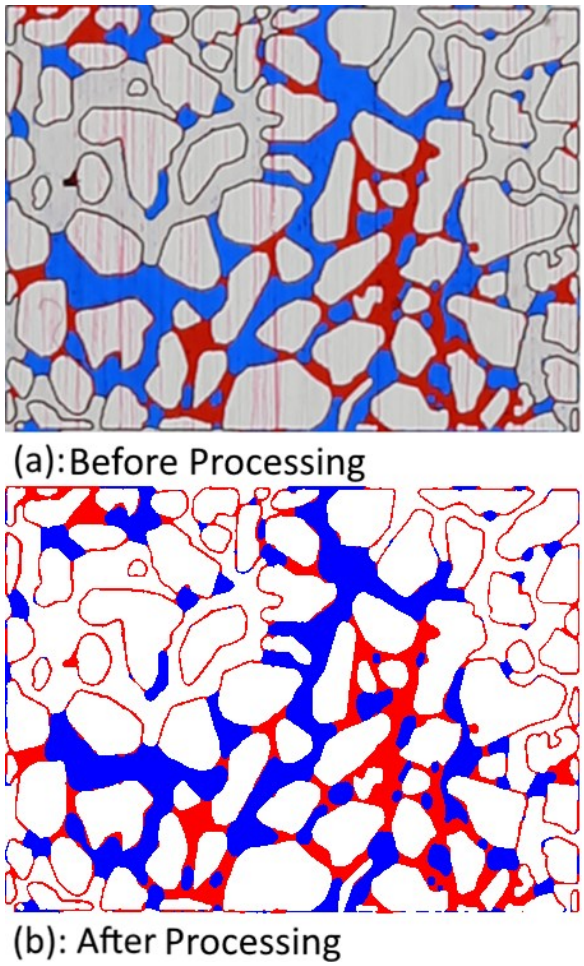

Figure B-2. Image of a zone in micromodel before and after image processing.

The error of the calculated fluid saturations, in comparison with volumetric data, is affected by the quality of the image, overlap of fluids at their interfaces, unequal backlight intensity in different regions of the micromodel, focus of the imaging system, variations in pore depths, colour of fluids, and the surface quality of the micromodel

plate. However, proper thresholding of the image analysis tool in detection of white, blue and red pixels can minimize the error of the calculated saturations.

The calculated saturations of fluids in images were compared with the measured volume of produced fluids during three separate GAGD experiments to evaluate the error of the image analysis data. Experiments were conducted at irreducible water saturations, so the variation of oil saturation was equal with the variation of the gas saturation prior to a gas-breakthrough. The saturations of fluids during experiments were calculated with the image processing program. In addition, a precision pump (flowrate resolution: ± 0.1%) measured the corresponding volume of the produced oil. Figure B-3 shows the average of the calculated gas volume against the measured volume of produced oil. The calculated gas saturation was multiplied by the pore volume of micromodels to calculate the volume of the injected gas. The uncertanty of data was calculated as the ratio of the 'difference between the calculated and measured volumes' to 'the measured volume'. The associated uncertainties with the calculated gas volumes in all comparison points were smaller than ± 2%. Based on the result of calibration experiments, it can be concluded that the maximum uncertainty associated with the calculated volume of a fluid can be ± 0.02 PV. The main source of this error is the resolution of the imaging system in the detection of boundaries between fluids. The highest error belongs to the wetting phase at a residual saturation when it forms maximum number of interfaces with other fluids. This error is smaller than ± 0.02 PV when the imaging system parameters are calibrated based on available volumetric data during an experiment.

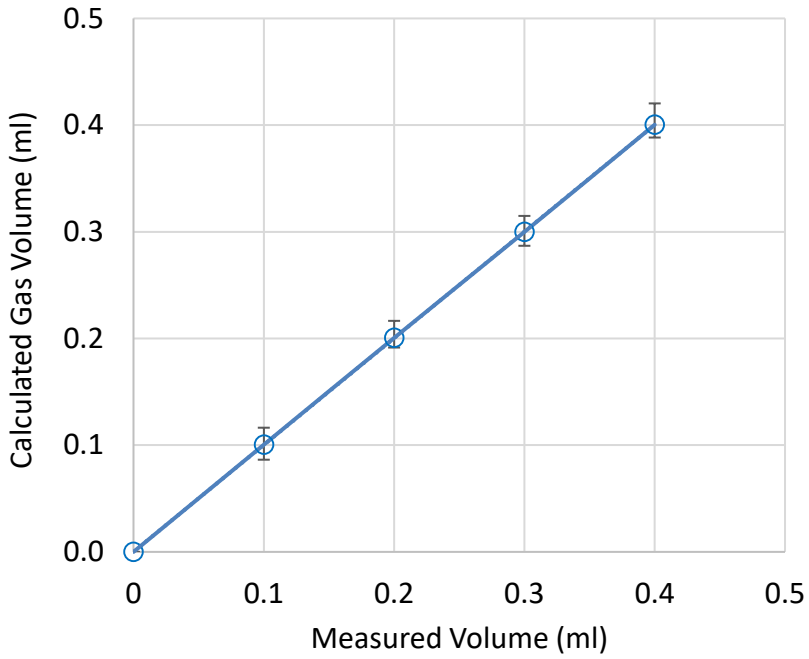

Figure B-3. Average gas volume calculated with the image analysis tool vs. produced volume of fluids measured with a precision pump during three GAGD experiments (bars show the maximum and minimum uncertainties of the calculated gas volume).

B.2. Image Analysis MATLAB Code

```
A=imread('1.png');                          Uploding cropped image;
B=A, a=size(A,1), b=size(A,2),              Defining the number of pixels in the image;
R1=1:a, C1=1:b;
C2=repmat(C1,1,a), R2=[];                   Converting two-dimentional array of pixels
for i=1:a                                   to one-dimensional array for the ease of
R2=[R2 ones(1,b)*i];                        mathematical operations;
end
pixels=impixel(A,C2,R2);                    Defining each individual pixel in the image;
p=pixels,
white=0,                                    Initialization;
red=0,
blue=0,
TG=120,                                     Defining threshold for the G component;
X=5;                                        Defining threshold between R & B;
for i=1:length(p)                           Beginning of the white pixel delineation;
if p(i,2)>TG
p(i,:)=0255, white=white+1;                 Counting White pixels;
elseif p(i,1)>=p(i,3)+X                     Red pixel delineation;
p(i,1)=255, p(i,2:3)=0, red=red+1;          Counting Red pixels;
elseif p(i,1)<p(i,3)+X                      Blue pixel delineation;
p(i,1:2)=0, p(i,3)=255, blue=blue+1;        Blue pixel counting;
end
end
for i=1:a
for j=1:b
k=k+1, B(i,j,1:3)=p(k,:);                   Counting total pixels;
end
end
imwrite(B,'2.png');                         Generating the processed image.
```

References

1. Wirth, M.; Fraschini, M.; Masek, M.; Bruynooghe, M., Performance evaluation in image processing. *EURASIP journal on Applied signal processing* **2006,** 2006, 211-211.
2. Mahmoudi, M.; James, L. A.; Johansson, T., Advanced Image Processing for Micromodel Flow Experiments: An Application Using LabVIEW. Paper submitted for review and publication to the Journal of Petroleum Science and Engineering 2017.

Appendix C

Images of repeated experiments in chapter 4 are given in this section. Figures C-1 and C-2 show the GAGD perfromed with CO_2 at 4 bars under oil-wet and water-wet conditions, respectively. Figures C-3 and C-4 show GAGD perfromed with C_3H_8 at 4 bars under oil-wet and water-wet conditions, respectively. Figure C-5 shows a chamber used for the evaluation of the oil and water swelling and evaporation in contact with gas.

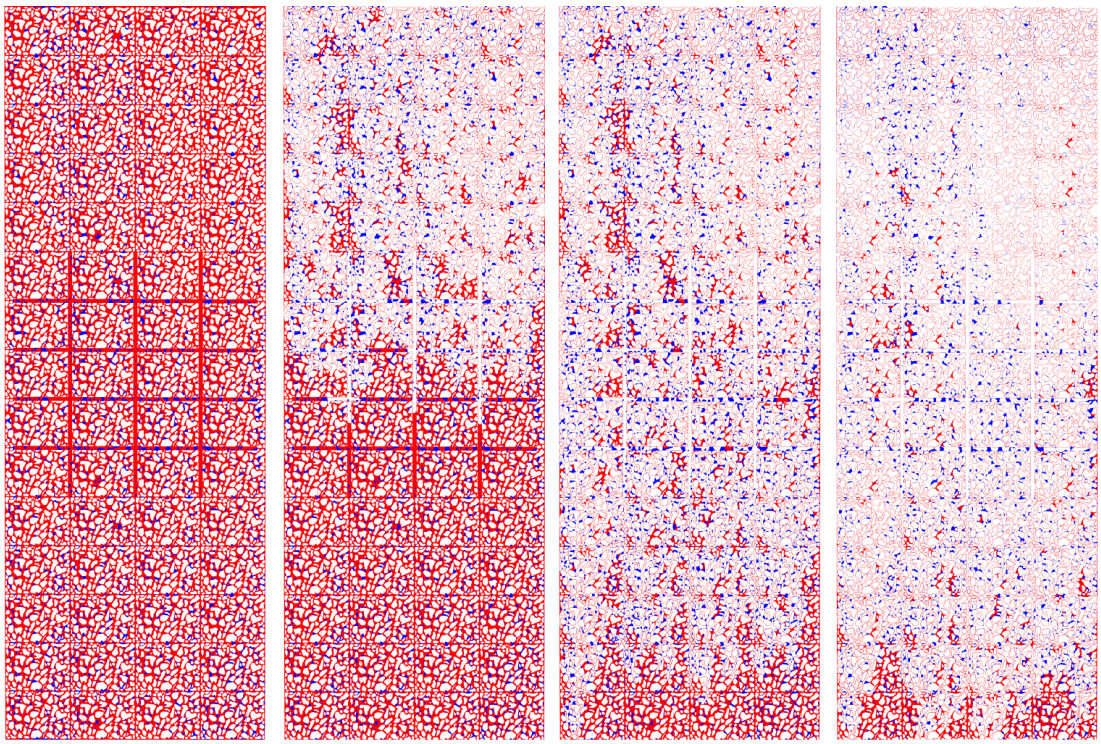

Figure C-1. Immiscible GAGD experiment performed with CO2 (pressure: 4 bars) under oil-wet conditions (processed images, red: oil – blue: water, So: oil saturation, Sw: water saturation, pattern size: 64×185 mm).

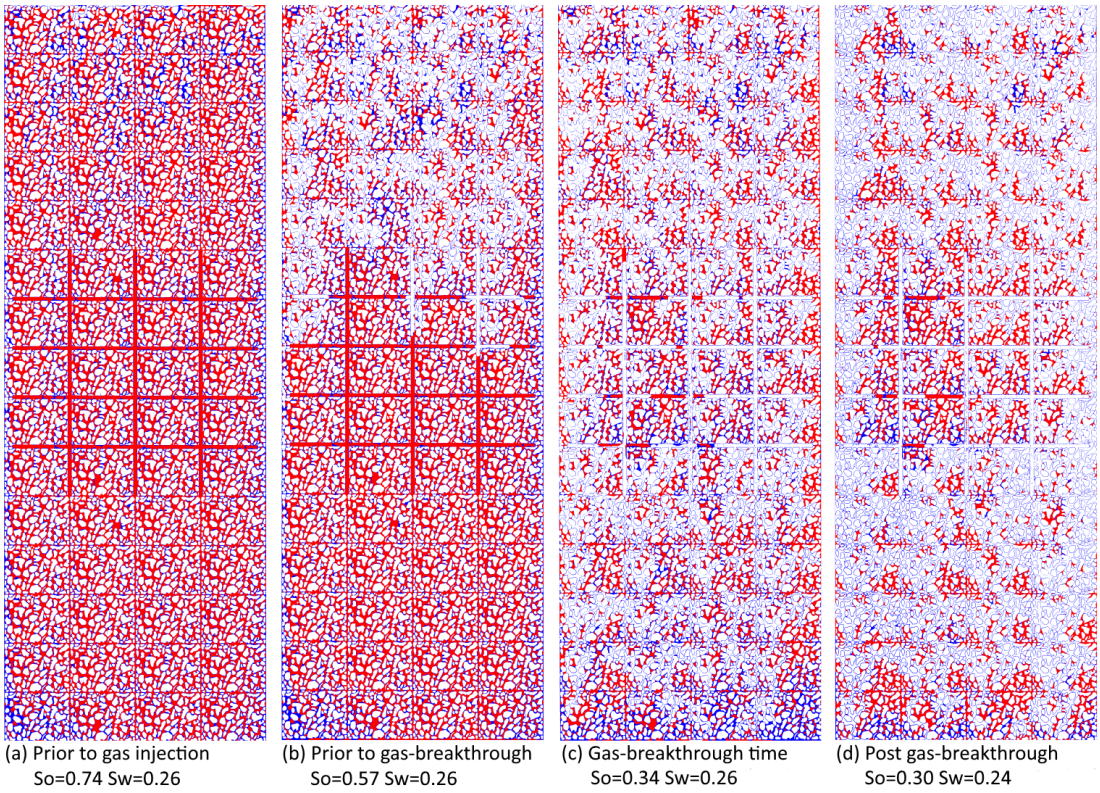

Figure C-2. Immiscible GAGD experiment performed with CO_2 (pressure: 4 bars) under water-wet conditions (processed images, red: oil – blue: water, So: oil saturation, Sw: water saturation, pattern size: 64×185 mm).

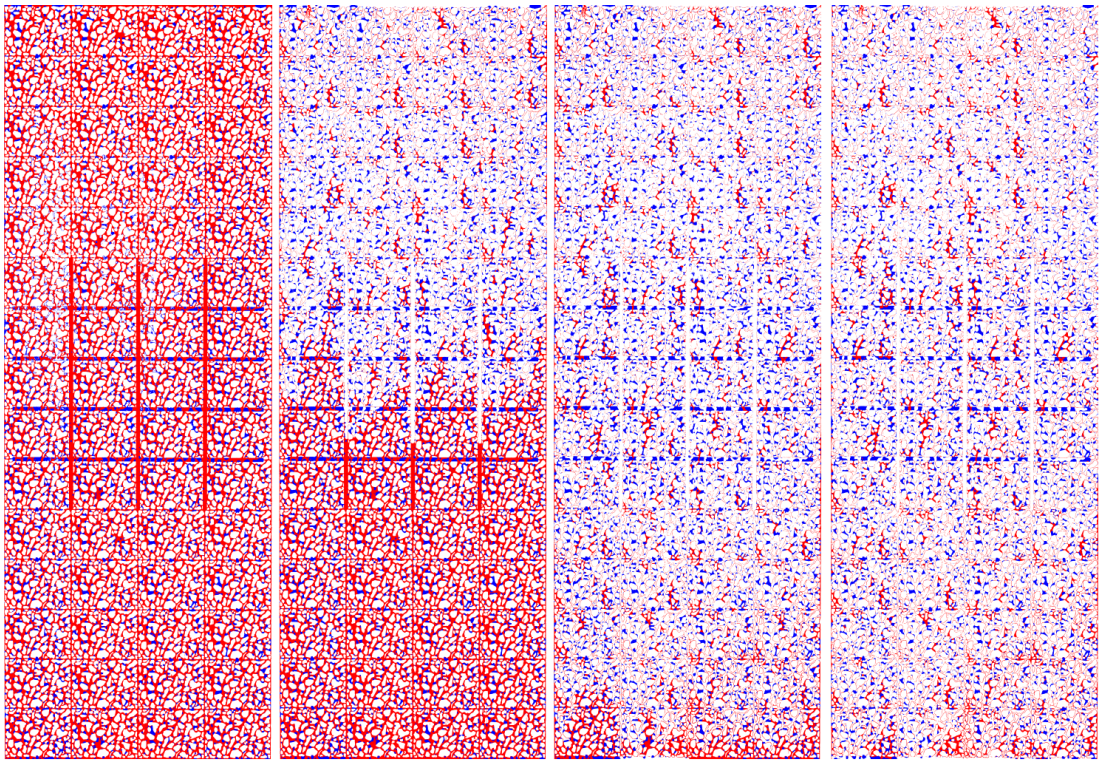

Figure C-3. Immiscible GAGD experiment performed with C_3H_8 (pressure: 4 bars) under oil-wet conditions (processed images, red: oil – blue: water, So: oil saturation, Sw: water saturation, pattern size: 64×185 mm).

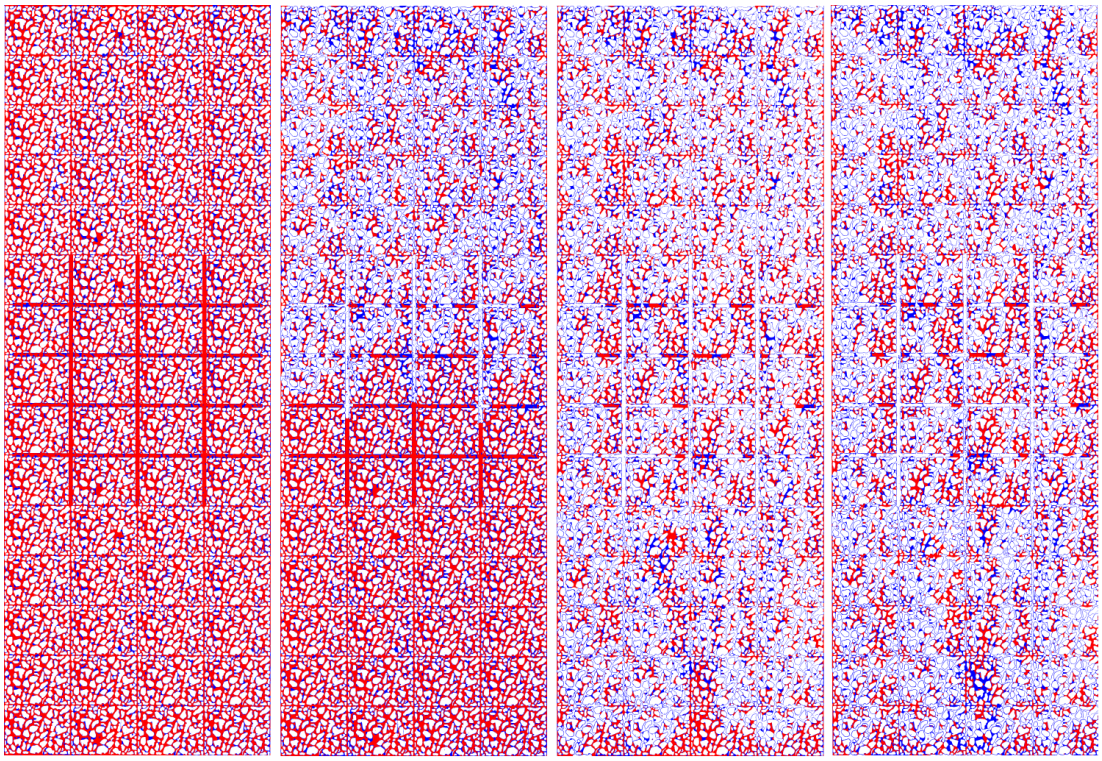

Figure C-4. Immiscible GAGD experiment performed with C_3H_8 (pressure: 4 bars) under water-wet conditions (processed images, red: oil – blue: water, So: oil saturation, Sw: water saturation, pattern size: 64×185 mm).

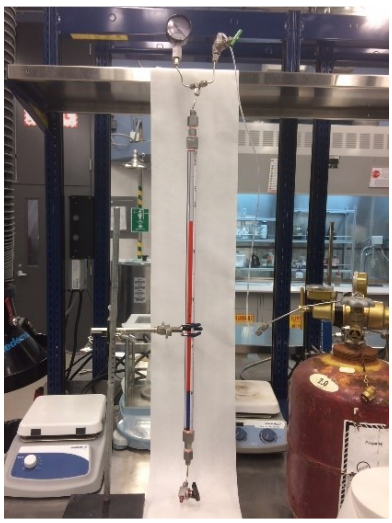

Figure C-5. Three-phase chamber developed in Hibernia EOR Lab for measuring the variation of oil and water volumes in contact with gas.

Appendix D

Images of repeated post-waterflood GAGD experiments (tests 5 & 6) are presented in Figures D-1 & D-2. In addition, original images of micromodel (without processing) corresponding to tests 1 & 2 are presented in Figures D-3 to D-8.

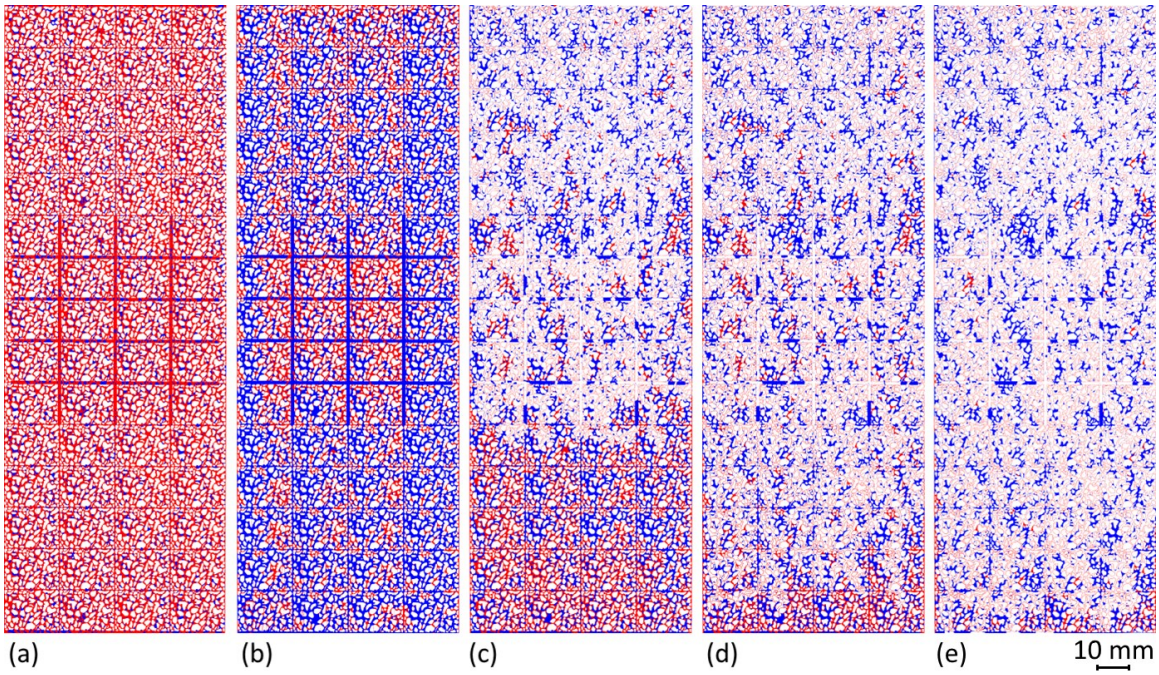

Figure D-1. Processed images of the oil-wet micromodel during test 5 in Table 5-2. (a): prior to waterflood, (b): post-waterflood, (c): prior to gas-breakthrough, (d): gas-breakthrough after 1 hour and 55 minutes, (e): after 20 hours of production. (red: oil, blue: water).

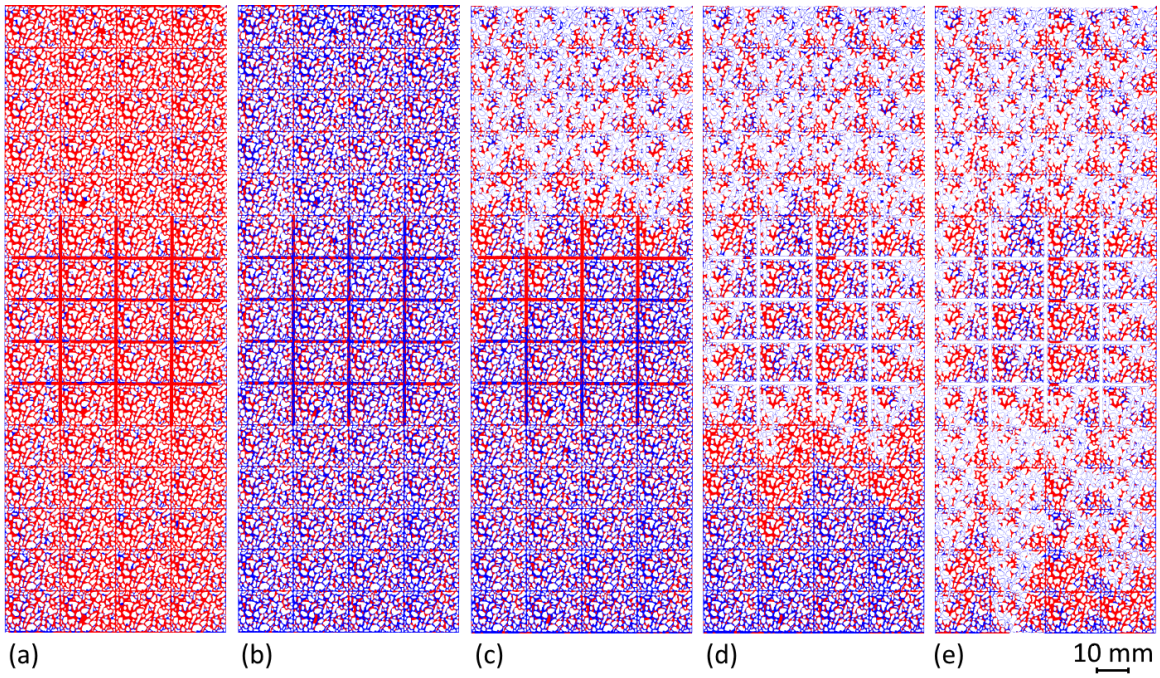

Figure D-2. Processed images of the water-wet micromodel during test 6 in Table 5-2, (a): prior to waterflood, (b): post-waterflood, (c): development of oil-bank, (d): developed oil-bank prior to gas-breakthrough, (e): gas breakthrough after 1 hour and 41 minutes. (red: oil, blue: water).

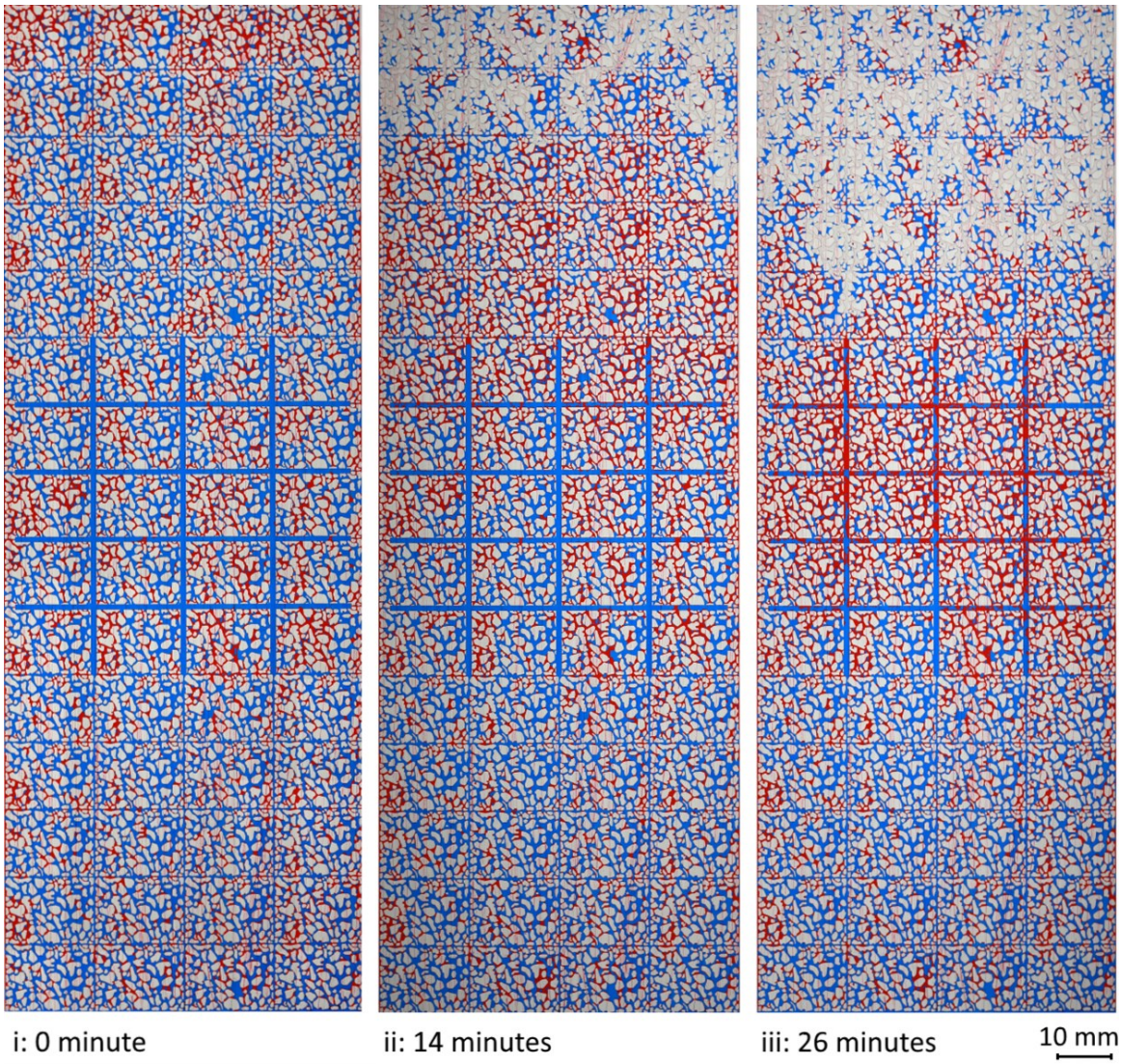

Figure D-3. Unprocessed images of micromodel during post-waterflood GAGD under oil-wet condition (test 1 in Table 5-2, red: oil, blue: water, i: prior to entry of gas, ii & iii: development of the oil-bank ahead of the gas-front).

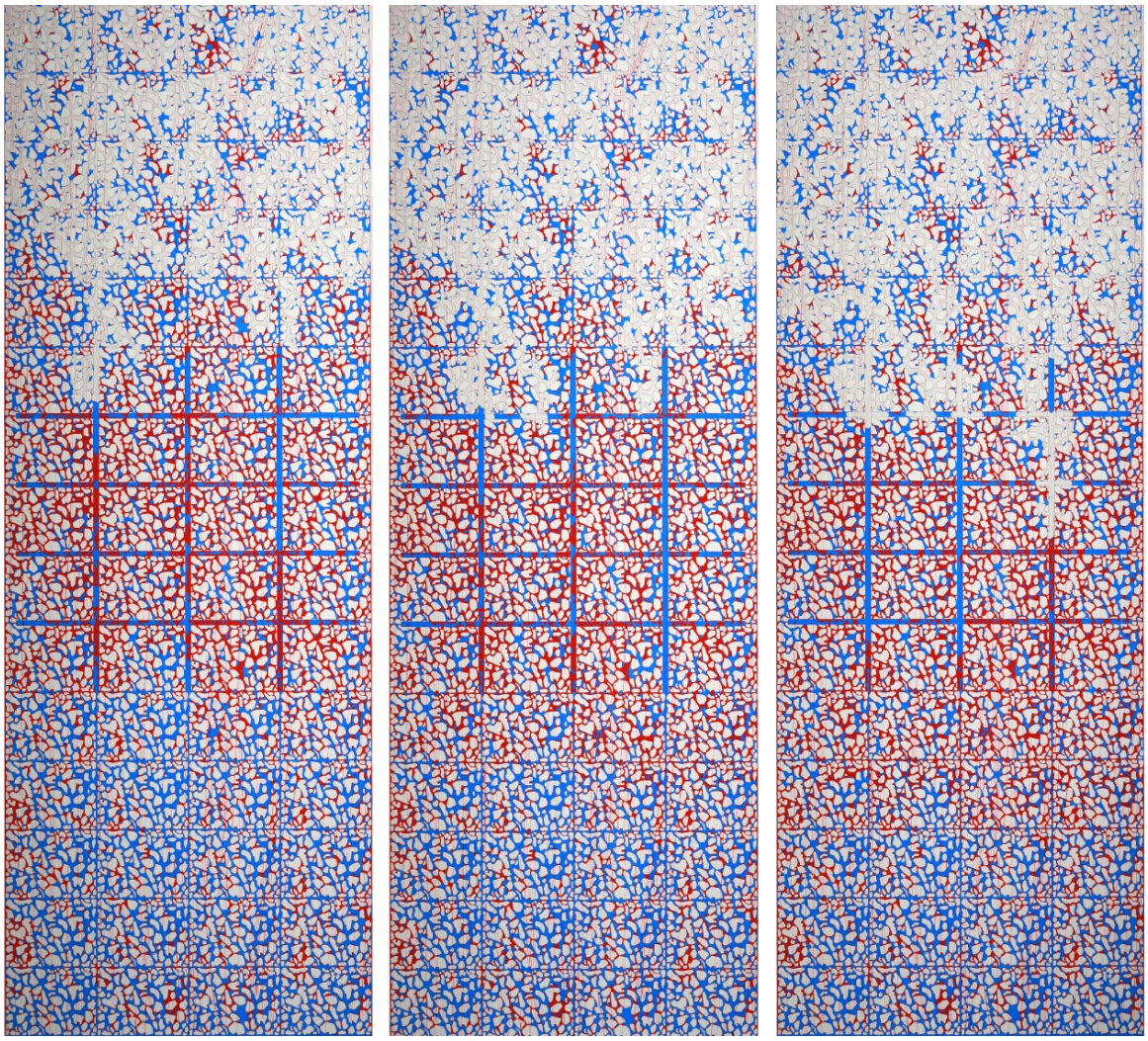

Figure D-4. Micromodel images during post-waterflood GAGD under oil-wet condition (red: oil, blue: water, iv-vi: development and grow of oil-bank ahead of the gas-front).

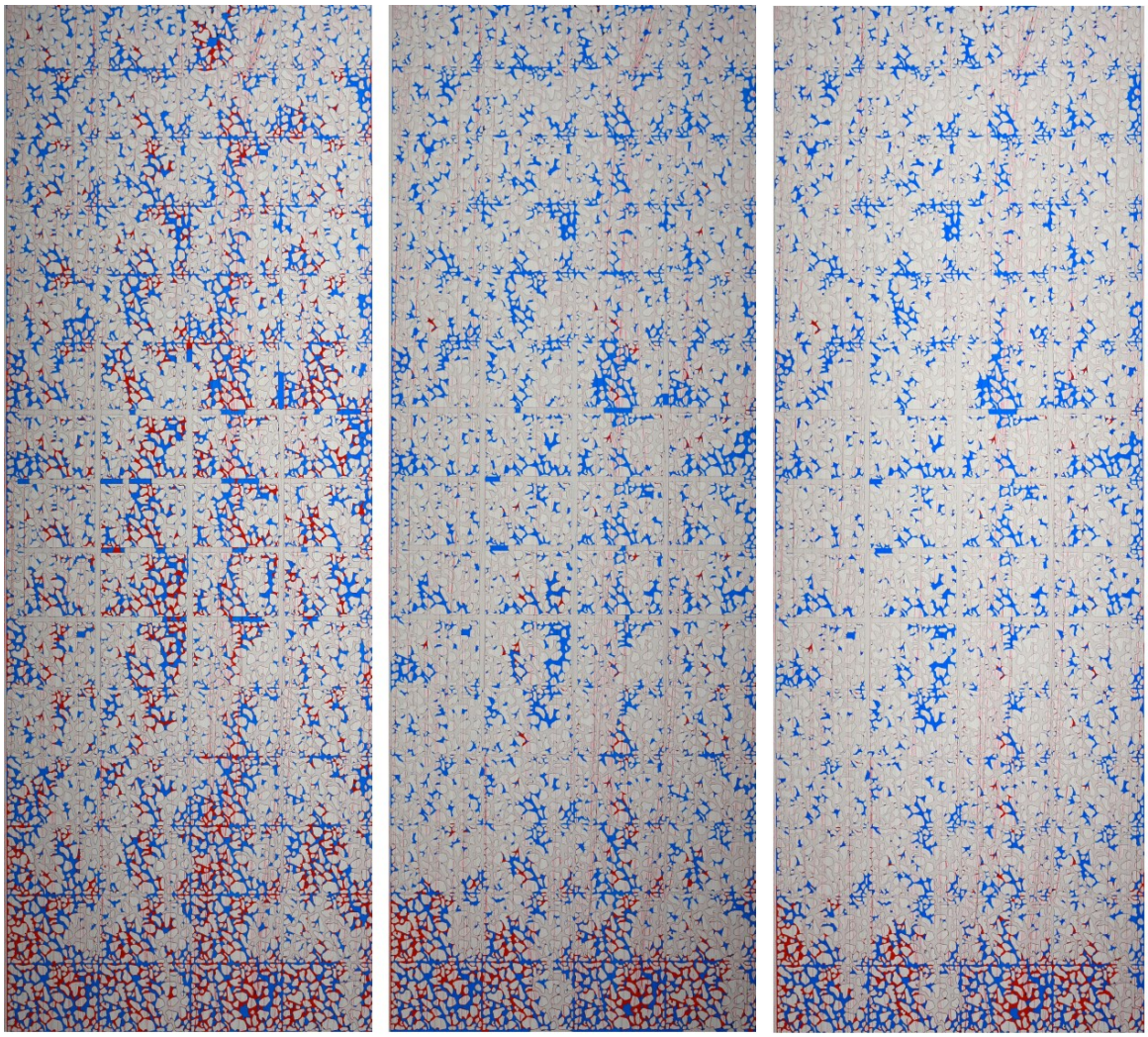

vii: 1 hour & 34 minutes viii: 13 hours & 35 minutes ix: 25 hours & 36 minutes

Figure D-5. Micromodel images during post-waterflood GAGD under oil-wet condition (red: oil, blue: water, vii: time of gas-breakthrough, viii and ix: production of oil and water through the film-flow mechanism).

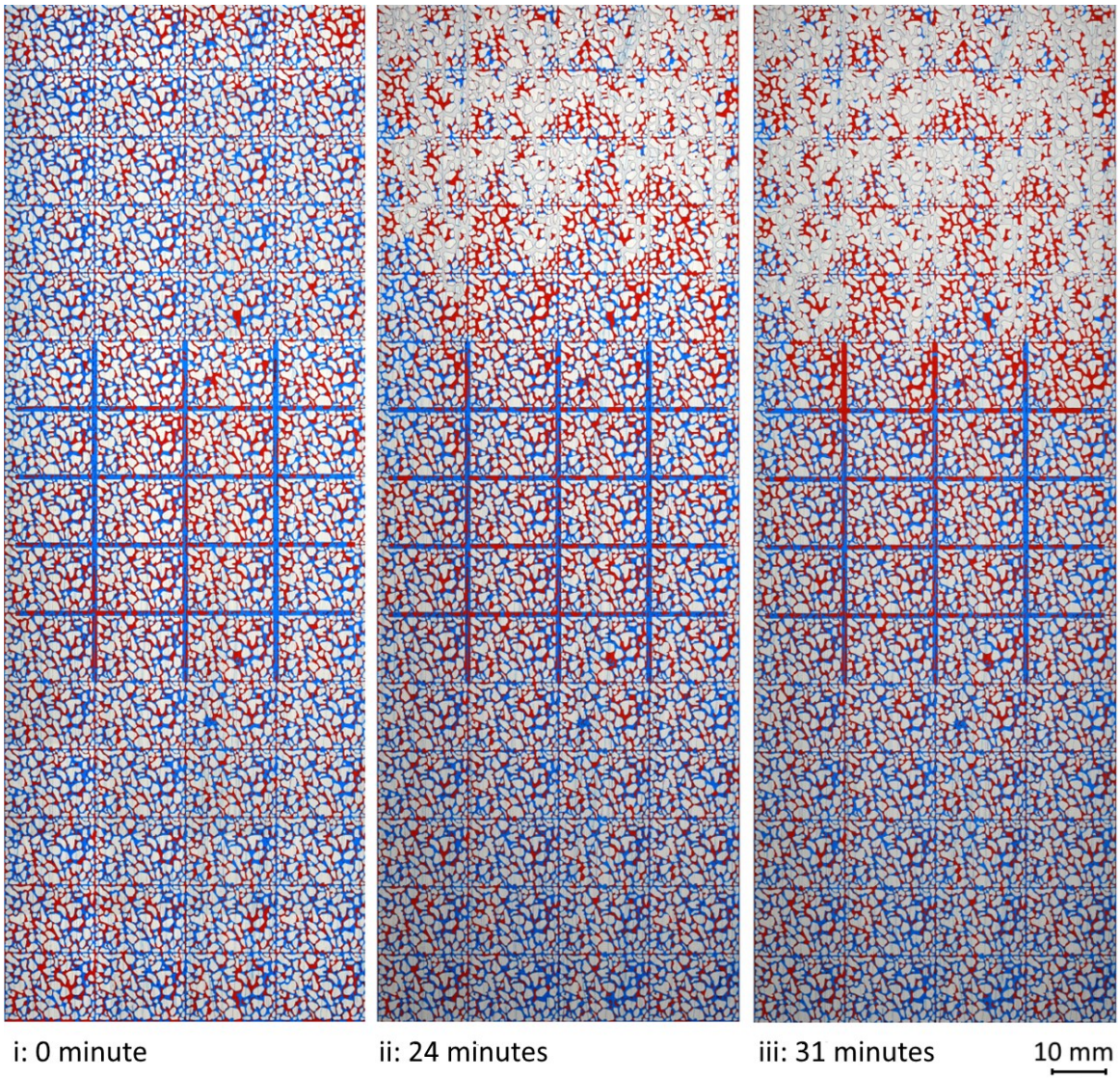

Figure D-6. Unprocessed images of micromodel during post-waterflood GAGD under water-wet condition (test 2 in Table 5-2, red: oil, blue: water, i: prior to entry of gas, ii & iii: development of oil-bank ahead of the gas-front and the displacement of water.

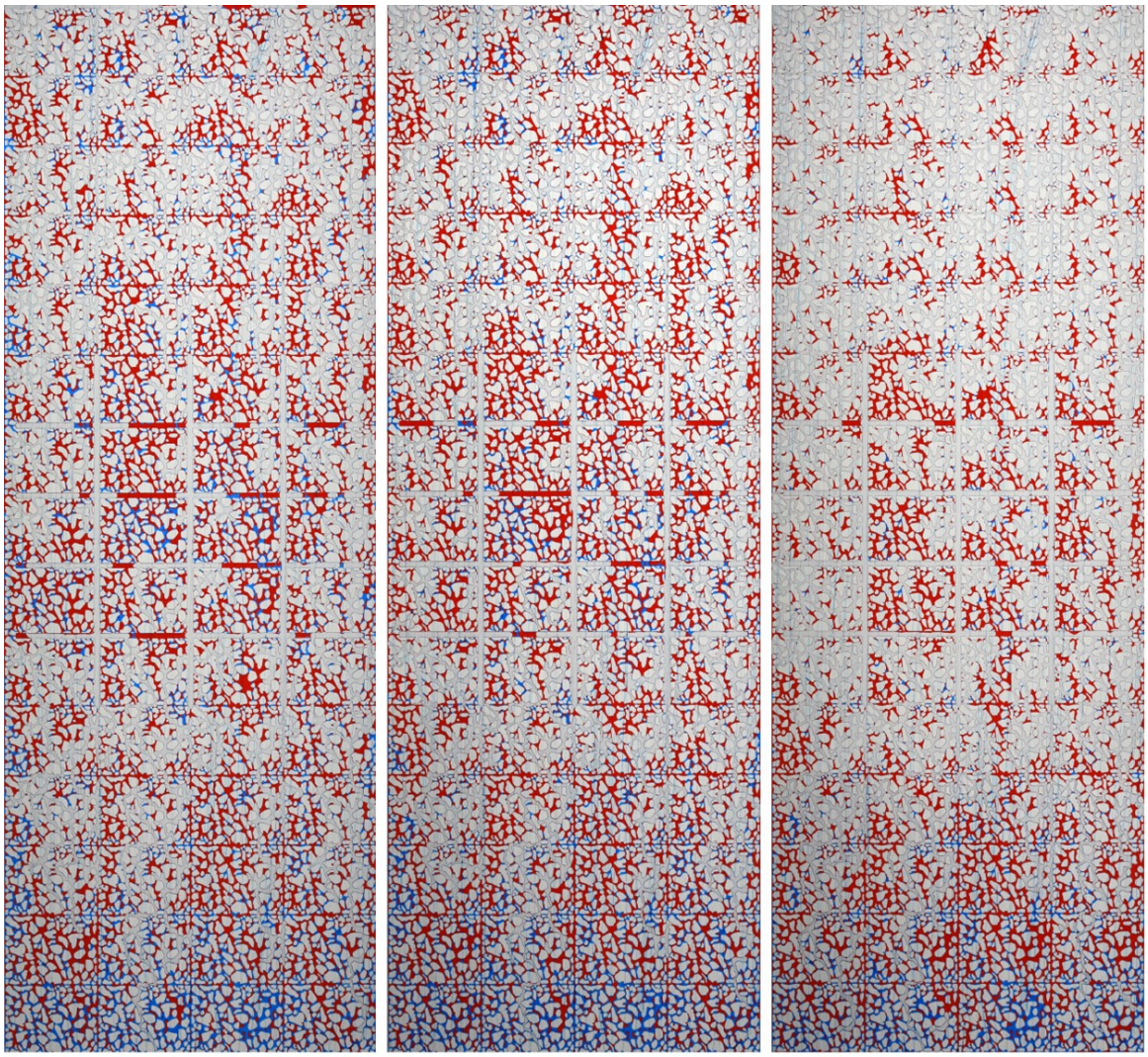

Figure D-7. Micromodel images during post-waterflood GAGD under water-wet condition (red: oil, blue: water, iv-vi: gas-breakthrough and drainage of water after a gas-breakthrough).

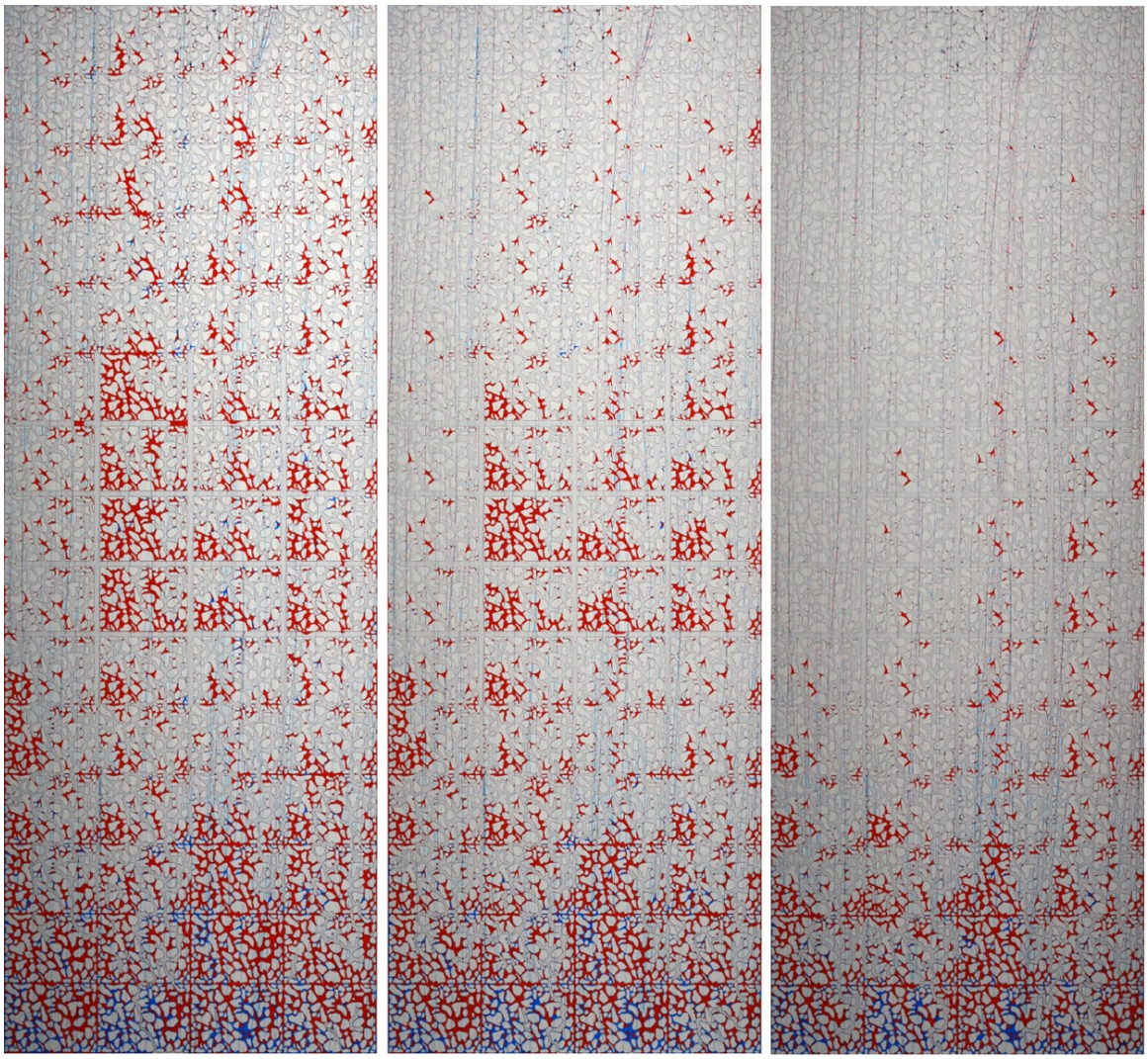

Figure D-8. Micromodel images during post-waterflood GAGD under water-wet condition (red: oil, blue: water, vii-ix: drainage of oil upon the drainage of water).

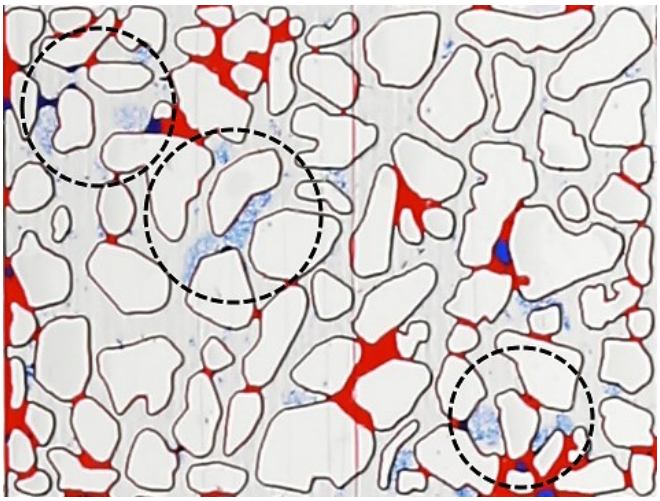

Figure D-9. An example of water evaporation in a GAGD test conducted under ambient conditions that resulted in the deposition of dried blue colour. The dried colour could be cleaned flushing the micromodel with warm water after the completion of an experiment.